Computational Design of Random Rough Surfaces in Thin-film Solar Cells by Stochastic Gradient Methods

by

Qiang Li

A dissertation submitted to the Graduate Faculty of
Auburn University
in partial fulfillment of the
requirements for the Degree of
Doctor of Philosophy

Auburn, Alabama
August 7, 2021

Keywords: Helmholtz equation, optimal design, random rough surface, solar cell, stochastic gradient descent

Approved by

Junshan Lin, Chair, Associate Professor of Mathematics and Statistics of Auburn University
Yanzhao Cao, Professor of Mathematics and Statistics of Auburn University
Hans-Werner Van Wyk, Assistant Professor of Mathematics and Statistics of Auburn University
Xiaoying Han, Professor of Mathematics and Statistics of Auburn University
Thi Thao Phuong Hoang, Assistant Professor of Mathematics and Statistics of Auburn University

Abstract

We present an efficient numerical algorithm to solve for the optimal random structure in maximizing the absorptance for thin-film solar cells. Random rough texture can increase the absorbing efficiency of solar cells by trapping the optical light and increasing the optical path of photons. The thim-film solar cells consist of several different layers. The interfaces separating the layers are modeled as random profiles. The Karhunen-Loève Expansion is used to represent the random profiles. Two parameters, the root mean square to the average height and the correlation length, delicate the shape of the random interface statistically with the help of Karhunen-Loéve Expansion. In maximizing the absorptance, we formulate the design problem as a optimization problem with PDE constraint to solve for the optimal parameters. The stochastic gradient method is applied to solve the random optimization problem, which leads to significant savings in computational cost compared to the full gradient method. The adjoint state method is employed to calculate the gradient of the objective function at each sample. The convergency of the stochastic gradient method in optimizing the proposed objective function is proved. Numerical examples are performed which demonstrate the accuracy and convergence of the algorithm. It is shown that the optimally obtained random textures yield absorption enhancement of the solar cells. In addition, the computational cost is reduced dramatically compared to the full gradient method.

Acknowledgments

I am immensely grateful for everyone who has been a part of my educational experience throughout the years. I would especially like to thank my advisor Dr. Yanzhao Cao and Dr. Junshan Lin for all of their guidance, encouragement, and support. You both have taught me so much and have been incredibly kind. I am beyond thankful for you both. I would also like to thank my committee members for their kind advices.

Thank you for all the kind people who have ever helped me in Auburn!

Table of Contents

List of Figures

List of Tables

Chapter 1

Introduction

1.1 Background

Thin-film silicon solar cell technology is one of the promising photovoltaic [31, 32, 36, 39] technologies for delivering low-cost solar electricity. Until recently, amorphous silicon (a-Si) thin-film solar cells have dominated the development of thin-film modules and demonstrated the potential for lower cost production than can be achieved for crystalline silicon (c-Si). A typical a-Si thin film solar cell is coated with p-i-n semiconductor film on the transparent conductive oxide film under the glass surface, and an electrode plate is plated on the back. Thin-film solar cells consume less materials, which need tens of nanometers to hundreds of nanometers in thickness to achieve photoelectric conversion. However, the thin-film solar cells have lower efficiency. A typical a-Si cell structure is shown in Figure 1.1.

Since the first report on practical microcrystalline cells in 1994 [43], much research effort has been made worldwide into the development of both fundamental knowledge and technological skills that are needed to improve thin-film silicon multijunction solar cells. In addition, an efficient trapping structure can be designed to make amorphous silicon films absorb and utilize sunlight as much as possible. The absorption of more photons also provides a guarantee for improving the photoelectric conversion efficiency of thin-film cells. There are many ways to increase the absorption efficiency of solar cells. The commonly used trapping techniques are surface velvet, antireflection film, surface plasmon, reflector on the back of the battery, etc [2, 5, 7, 8, 9, 24].

Another way to increase the efficiency is by using randomly textured interfaces to trap the optical light [1, 4, 41, 46]. When the random interface is introduced into the contact surface

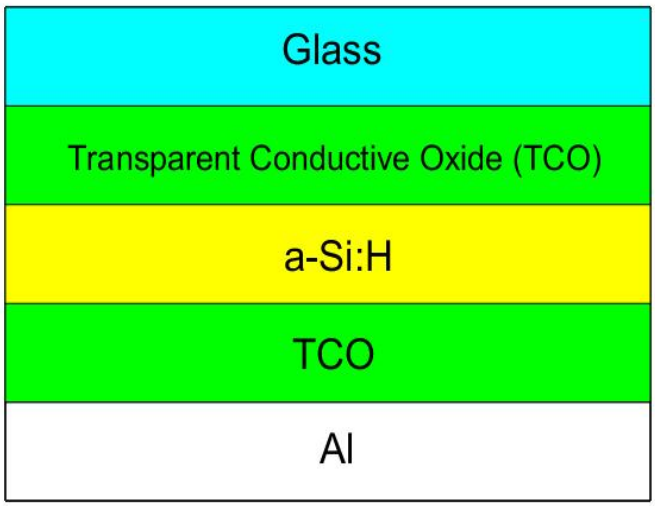

Figure 1.1: A schematic plot of thin-film solar cells.

of the solar cell, the light is reflected into the cell for many times to increase the optical path. In this way, the optical thickness of the thin-film cell can be increased as much as possible without changing the physical thickness of the thin-film cell. The existing solar cells of this kind include Asahi-U substrate, the Jülich substrate, and the Neuchătel substrate. Here we refer to some deterministic texture optimization designs [16, 19, 20, 21, 33], as well as the following deterministic shape optimization problems [11, 12, 13, 14, 26, 44, 45] in physics and engineering. Most of the previous research on random texture optimization are based on certain ad hoc schemes. Mainly by calculating the absorption of several selected statistical parameters to select the parameter values that produce the maximum absorptivity. The optimal solution obtained in this way depends to a largely depends on the selected set of statistical parameters. If the optimal parameters are not in the set, we will not be able to find the corresponding parameter values of the optimal solution. A gradient-based method is also used to solve the optimization problem [6]. The Monte-Carlo method was used for sampling the probability space and to calculate the expectation of the reflectivity. However the computational cost of the gradient is very high.

In this thesis, we formulate the optimal design of random surface textures as a random PDE-constrained optimization problem. The stochastic gradient method is applied to solve the random optimization problem for obtaining the statistical parameters of the optimal random textures. The stochastic gradient method uses the gradient of one sample to approximate the

gradient of cost function in each iteration, which reduces the computational cost dramatically. It is demonstrated that new random textures gives rise to significant absorption enhancement and higher photon absorptance.

1.2 Outline

The rest of the thesis is organized as follows. Chapter 2 describes the mathematical model for the optical wave scattering in solar cells, including the governing partial differential equations, the outgoing wave condition, and the modeling of the random surfaces. In Chapter 3, we formulate the design problem as a random PDE-constrained optimization problem. Chapter 4 presents the numerical algorithm to solve the optimization problem, we also derive the gradient of the cost function and show the convergency of the algorithm. Several numerical experiments are presented in Chapter 5 to demonstrate the efficiency of the numerical method. It is showed that the optimally obtained random textures yield an absorption enhancement of solar cells. The computational cost is reduced dramatically compared to the full gradient method.

Chapter 2

The Mathematical model

2.1 Maxwell's equations and continuity conditions

In this section, we consider the Maxwell's equations and the continuity conditions. The differential form of Maxwell's equations is

$$\begin{cases} \nabla \times E = -\dfrac{\partial B}{\partial t}, \\ \nabla \times H = \dfrac{\partial D}{\partial t} + J, \\ \nabla \cdot D = \rho, \\ \nabla \cdot B = 0, \end{cases} \tag{2.1}$$

where $E,\ H$ denote the electric and magnetic fields respectively, $D,\ B$ denote the electric and magnetic fluxes respectively, J is electric current density and ρ is electric charge density.

The following constitutive hold:

$$D = \varepsilon E,$$

$$B = \mu H,$$

$$J = \sigma E,$$

where ε denotes the electric permittivity, μ denotes magnetic permeability which is usually is a constant, and σ denotes the conductivity.

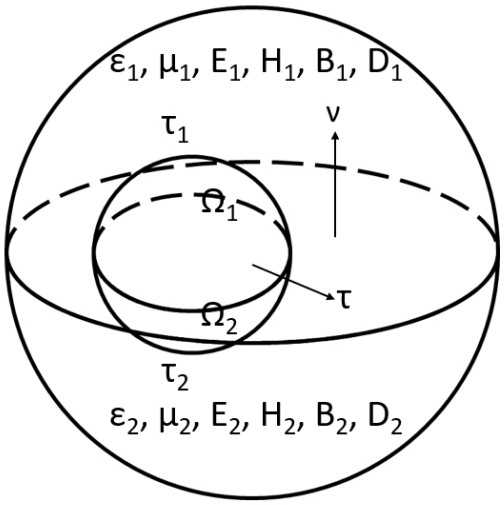

Figure 2.1: The reflectivity value $\tilde{R}(\boldsymbol{\alpha})$ during the stochastic gradient iterations of the structure with five layers for Problem(I).

Suppose that $\varepsilon,\ \mu$ are independent of time variable t, we get

$$\begin{cases} \nabla \times E = -\mu \dfrac{\partial H}{\partial t}, \\ \nabla \times H = \varepsilon \dfrac{\partial D}{\partial t} + \sigma E. \end{cases} \tag{2.2}$$

Suppose the whole domain Ω consists two parts Ω_1 and Ω_2. Denote $\Omega = \Omega_1 \cup \Omega_2$, see Figure 2.1. For source free problem with $\rho = 0$, we know that $\nabla \cdot D = 0$ on Ω from Maxwell's equations. Thus the integral over Ω is also zero, that is,

$$0 = \int_{\Omega} \nabla \cdot D d\Omega.$$

By the divergence theorem, it yields

$$0 = \int_{\Omega} \nabla \cdot D d\Omega = \int_{\partial\Omega} D \cdot \nu ds = \int_{\tau_1} D_1 \cdot \nu ds + \int_{\tau_2} D_2 \cdot \nu ds, \tag{2.3}$$

and

$$\begin{aligned} 0 &= \int_{\Omega} \nabla \cdot D d\Omega \\ &= \int_{\Omega_1} \nabla \cdot D_1 d\Omega + \int_{\Omega_2} \nabla \cdot D_2 d\Omega \\ &= \int_{\tau_1 \cup \tau} D_1 \cdot \nu ds + \int_{\tau_2 \cup \tau} D_2 \cdot \nu ds \\ &= \int_{\tau_1} D_1 \cdot \nu ds + \int_{\tau_2} D_2 \cdot \nu ds + \int_{\tau} (-D_1 + D_2) \cdot \nu_{12} ds, \end{aligned} \tag{2.4}$$

where τ_{12} is the unit normal vector form domain Ω_1 to domain Ω_2. From (2.3) and (2.4), we have

$$\int_{\tau} D_1 \cdot \nu_{12} ds = \int_{\tau} D_2 \cdot \nu_{12} ds$$

which implies

$$\tau \cdot (D_1 - D_2) = 0. \tag{2.5}$$

Since $\nabla \cdot B = 0$, the integral over Ω is also zero, that is,

$$0 = \int_{\Omega} \nabla \cdot B d\Omega.$$

By the divergence theorem, it yields

$$0 = \int_{\Omega} \nabla \cdot B d\Omega = \int_{\partial\Omega} B \cdot \nu ds = \int_{\tau_1} B_1 \cdot \nu ds + \int_{\tau_2} B_2 \cdot \nu ds, \tag{2.6}$$

and

$$\begin{aligned} 0 &= \int_{\Omega} \nabla \cdot B d\Omega \\ &= \int_{\Omega_1} \nabla \cdot B_1 d\Omega + \int_{\Omega_2} \nabla \cdot B_2 d\Omega \\ &= \int_{\tau_1 \cup \tau} B_1 \cdot \nu ds + \int_{\tau_2 \cup \tau} B_2 \cdot \nu ds \\ &= \int_{\tau_1} B_1 \cdot \nu ds + \int_{\tau_2} B_2 \cdot \nu ds + \int_{\tau} (-B_1 + B_2) \cdot \nu_{12} ds, \end{aligned} \tag{2.7}$$

where τ_{12} is the unit normal vector form domain Ω_1 to domain Ω_2. From (2.6) and (2.7), we have

$$\int_\tau B_1 \cdot \nu_{12} ds = \int_\tau B_2 \cdot \nu_{12} ds$$

which implies

$$\tau \cdot (B_1 - B_2) = 0. \tag{2.8}$$

From equation (2.1), we have $\nabla \times E = -\dfrac{\partial B}{\partial t}$. Take the integral of this equation on both sides over surface $\tau_1 \cup \tau_2$, we get

$$\int_{\tau_1 \cup \tau_2} (\nabla \times E) \cdot ds = -\int_{\tau_1 \cup \tau_2} \frac{\partial B}{\partial t} \cdot ds = -\frac{\partial}{\partial t} \int_{\tau_1 \cup \tau_2} B \cdot ds. \tag{2.9}$$

By the divergence theorem, we have

$$\int_{\tau_1 \cup \tau_2} B \cdot ds = \int_{\Omega_1 \cup \Omega_2} \nabla \cdot B d\Omega,$$

and from equations (2.1), we know that $\nabla \cdot B = 0$, thus

$$\int_{\tau_1 \cup \tau_2} (\nabla \times E) \cdot ds = 0.$$

By stokes theorem, we obtain that

$$\begin{aligned} 0 &= \int_{\tau_1 \cup \tau_2} (\nabla \times E) \cdot ds \\ &= \int_{\tau_1} (\nabla \times E_1) \cdot ds + \int_{\tau_2} (\nabla \times E) \cdot ds \\ &= \int_c E_1 \cdot dr - \int_c E_2 \cdot dr, \end{aligned} \tag{2.10}$$

which lead to $\nu \times (E_1 - E_2) = 0$.

For electric current free problem with $J = 0$ and source free problem with $\nabla \cdot D = 0$, we have $\nabla \times H = \dfrac{\partial D}{\partial t}$.

Take the integral of this equation on both sides over surface $\tau_1 \cup \tau_2$, we get

$$\int_{\tau_1 \cup \tau_2} (\nabla \times H) \cdot ds = \int_{\tau_1 \cup \tau_2} \frac{\partial D}{\partial t} \cdot ds = \frac{\partial}{\partial t} \int_{\tau_1 \cup \tau_2} D \cdot ds. \tag{2.11}$$

By the divergence theorem, we have

$$\int_{\tau_1 \cup \tau_2} D \cdot ds = \int_{\Omega_1 \cup \Omega_2} \nabla \cdot D d\Omega,$$

and from equations (2.1), we know that $\nabla \cdot D = 0$, thus

$$\int_{\tau_1 \cup \tau_2} (\nabla \times H) \cdot ds = 0.$$

By Stokes theorem, we obtain that

$$\begin{aligned} 0 &= \int_{\tau_1 \cup \tau_2} (\nabla \times H) \cdot ds \\ &= \int_{\tau_1} (\nabla \times H_1) \cdot ds + \int_{\tau_2} (\nabla \times H) \cdot ds \\ &= \int_c H_1 \cdot dr - \int_c H_2 \cdot dr, \end{aligned} \tag{2.12}$$

which lead to $\nu \times (H_1 - H_2) = 0$. That is for source free Maxwell's equation, we have

$$\nu \cdot (D_1 - D_2) = 0, \tag{2.13}$$

$$\nu \cdot (B_1 - B_2) = 0, \tag{2.14}$$

$$\nu \times (E_1 - E_2) = 0, \tag{2.15}$$

$$\nu \times (H_1 - H_2) = 0, \tag{2.16}$$

which means the normal components of D and B are continuous across the interface, the tangential components of E and H are continuous across the interface.

2.2 Time-harmonic Maxwell's equations and polarization

Consider the time-harmonic solution $E(x,t) = E(x)e^{-i\omega t}$ of Maxwell's equation without free electric charge

$$\begin{cases} \nabla \times E = i\omega\mu_0\mu_r H \\ \nabla \times H = -i\omega\varepsilon_0\varepsilon_r E \\ \nabla \cdot E = 0 \\ \nabla \cdot H = 0 \end{cases} \tag{2.17}$$

where E is electric field, H is magnetic field, ε_0 and μ_0 are the permittivity and permeability of free space. And $\varepsilon_r = \varepsilon_r(x)$ and $\mu_r = \mu_r(x)$ are the relative permittivity and permeability, respectively.

2.2.1 Transverse electric polarization

Let $E = \begin{bmatrix} 0 \\ 0 \\ u(x_1, x_2) \end{bmatrix}$ and $H = \begin{bmatrix} H_1 \\ H_2 \\ 0 \end{bmatrix}$, and take curl operator on both sides of the first equation of (2.17), we have

$$\nabla \times (\frac{1}{\mu_0\mu_r}(\nabla \times E)) = i\omega\nabla \times H = i\omega(-i\omega\varepsilon_0\varepsilon_r E) = \omega^2\varepsilon_0\varepsilon_r E. \tag{2.18}$$

By simple computation yields

$$\nabla E = \begin{bmatrix} \partial_{x_2} u \\ -\partial_{x_1} u \\ 0 \end{bmatrix},$$

$$\nabla \times (\frac{1}{\mu_0\mu_r}(\nabla \times E)) = \begin{bmatrix} \partial_{x_3}(\frac{1}{\mu_0\mu_r}\partial_{x_1}u) \\ -\partial_{x_3}(\frac{1}{\mu_0\mu_r}\partial_{x_2}u) \\ -\partial_{x_1}(\frac{1}{\mu_0\mu_r}\partial_{x_1}u) - \partial_{x_2}(\frac{1}{\mu_0\mu_r}\partial_{x_2}u) \end{bmatrix}$$
$$= \begin{bmatrix} 0 \\ 0 \\ -\partial_{x_1}(\frac{1}{\mu_0\mu_r}\partial_{x_1}u) - \partial_{x_2}(\frac{1}{\mu_0\mu_r}\partial_{x_2}u) \end{bmatrix},$$

which leads to

$$-\partial_{x_1}(\frac{1}{\mu_0\mu}\partial_{x_1}u) - \partial_{x_2}(\frac{1}{\mu_0\mu}\partial_{x_2}u) = \omega^2\varepsilon_0\varepsilon u,$$

It is equivalent to

$$\nabla \cdot (\frac{1}{\mu_0\mu_r}\nabla u) + \omega^2\varepsilon_0\varepsilon_r u = 0.$$

In case $\mu_r \equiv 1$, we have the Helmholtz equation

$$\triangle u + k_0^2\varepsilon_r u = 0,$$

where $k_0^2 = \omega^2\varepsilon_0\mu_0$ is the wave number in free space.

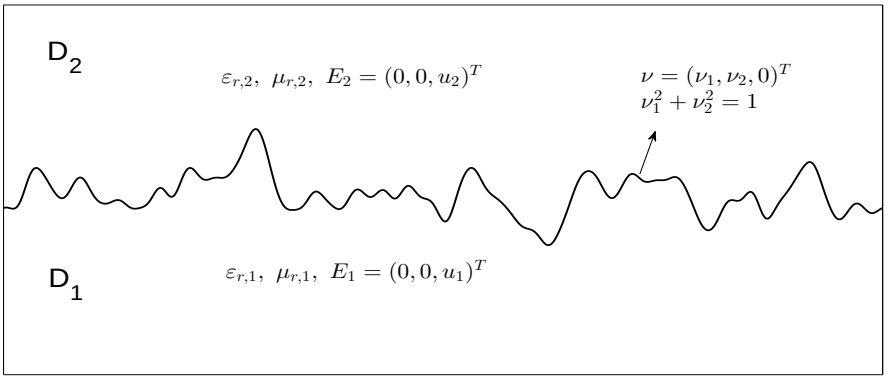

Figure 2.2: Continuous condition for transverse electric polarization.

For the continuous condition for transverse electric polarization, denote E_1 and E_2 as the electric field in D_1 and D_2, respectively as shown in Figure 2.2, we have

$$E_1 = \begin{bmatrix} 0 \\ 0 \\ u_1 \end{bmatrix} \text{ and } E_2 = \begin{bmatrix} 0 \\ 0 \\ u_2 \end{bmatrix},$$

By direct calculation,

$$\nu \times E_1 = \begin{bmatrix} \nu_2 u_1 \\ -\nu_1 u_1 \\ 0 \end{bmatrix} \text{ and } \nu \times E_2 = \begin{bmatrix} \nu_2 u_2 \\ -\nu_1 u_2 \\ 0 \end{bmatrix}$$

The continuity condition (2.15): $\nu \times E_1 = \nu \times E_2$ leads to

$$u_1 = u_2.$$

Since

$$H = (i\omega\mu_0\mu_r)^{-1}\nabla \times E,$$

we have

$$H = (i\omega\mu_0\mu_r)^{-1} \begin{bmatrix} \partial_{x_2} u \\ -\partial_{x_1} u \\ 0 \end{bmatrix},$$

thus

$$\nu \times H = \begin{bmatrix} 0 \\ 0 \\ -(i\omega\mu_0\mu_r)^{-1}(\nu_1\partial_{x_1}u + \nu_2\partial_{x_2}u) \end{bmatrix} = \begin{bmatrix} 0 \\ 0 \\ -(i\omega\mu_0\mu_r)^{-1}\dfrac{\partial u}{\partial \nu}. \end{bmatrix}$$

Therefore, from the continuous condition (2.16): $\nu \times H_1 = \nu \times H_2$, we get

$$-(i\omega\mu_0\mu_r)^{-1}\frac{\partial u_1}{\partial \nu} = -(i\omega\mu_0\mu_r)^{-1}\frac{\partial u_2}{\partial \nu},$$

which is

$$\frac{\partial u_1}{\partial \nu} = \frac{\partial u_2}{\partial \nu},$$

when $\mu_r \equiv 1$ and ν is the unit normal direction along the interface.

The perfect electrically conducting condition on a surface S is

$$\nu \times E = 0 \text{ on } S.$$

Denote $\nu = \begin{bmatrix} \nu_1 \\ \nu_2 \\ 0 \end{bmatrix}$, with $\nu_1^2 + \nu_2^2 = 1$. Thus

$$0 = \nu \times E = \begin{bmatrix} \nu_2 u \\ -\nu_1 u \\ 0 \end{bmatrix}.$$

Thus,

$$u = 0, \text{ on } S.$$

Therefore, we have the boundary value problem with Dirichlet boundary condition

$$\begin{cases} \Delta u + k_0^2 \varepsilon_r u = 0, \text{ in } D_1 \cup D_2, \\ \dfrac{\partial u_1}{\partial \nu} = \dfrac{\partial u_2}{\partial \nu} \text{ on interface}, \\ u = 0 \text{ on on boundary}. \end{cases} \tag{2.19}$$

2.2.2 Transverse magnetic Polarization

Let $H = \begin{bmatrix} 0 \\ 0 \\ u(x_1, x_2) \end{bmatrix}$ and $E = \begin{bmatrix} E_1 \\ E_2 \\ 0 \end{bmatrix}$, and take curl operator on both sides of the first equation of (2.17), we have

$$\nabla \times (\frac{1}{\varepsilon_0 \varepsilon_r}(\nabla \times H)) = i\omega \nabla \times E = i\omega(-i\omega\mu_0\mu_r H) = \omega^2 \mu_0 \mu_r H.$$

Similar calculation as in TE polarization yields

$$\nabla \cdot (\frac{1}{\varepsilon_0 \varepsilon_r} \nabla u) + \omega^2 \mu_0 \mu_r u = 0.$$

In case $\mu_r \equiv 1$, we have the generalized Helmholtz equation

$$\nabla \cdot (\varepsilon_r^{-1} \nabla u) + k_0^2 u = 0,$$

where $k_0^2 = \omega^2 \varepsilon_0 \mu_0$ is the wave number in free space.

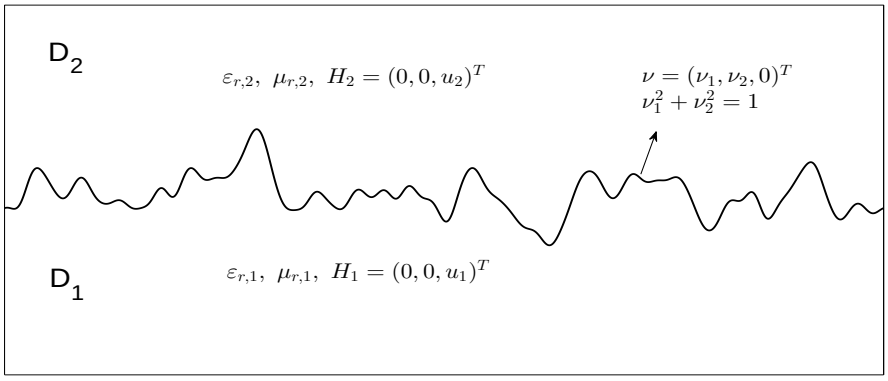

Figure 2.3: Continuous condition for transverse magnetic polarization.

For the continuous condition for transverse magnetic polarization, see Figure 2.3, we have

$$H_1 = \begin{bmatrix} 0 \\ 0 \\ u_1 \end{bmatrix} \text{ and } H_2 = \begin{bmatrix} 0 \\ 0 \\ u_2 \end{bmatrix},$$

By direct calculation,

$$\nu \times H_1 = \begin{bmatrix} \nu_2 u_1 \\ -\nu_1 u_1 \\ 0 \end{bmatrix} \text{ and } \nu \times H_2 = \begin{bmatrix} \nu_2 u_2 \\ -\nu_1 u_2 \\ 0 \end{bmatrix}$$

Continuous condition (2.15): $\nu \times E_1 = \nu \times E_2$ leads to

$$u_1 = u_2.$$

Since

$$E = (-i\omega\varepsilon_0\varepsilon_r)^{-1}\nabla \times H,$$

we have

$$E = (-i\omega\varepsilon_0\varepsilon_r)^{-1} \begin{bmatrix} \partial_{x_2} u \\ -\partial_{x_1} u \\ 0 \end{bmatrix},$$

thus

$$\nu \times E = \begin{bmatrix} 0 \\ 0 \\ -(i\omega\varepsilon_0\varepsilon_r)^{-1}(\nu_1\partial_{x_1}u + \nu_2\partial_{x_2}u) \end{bmatrix} = \begin{bmatrix} 0 \\ 0 \\ -(-i\omega\varepsilon_0\varepsilon_r)^{-1}\dfrac{\partial u}{\partial \nu}. \end{bmatrix}$$

Therefore, from continuous condition (2.15): $\nu \times E_1 = \nu \times E_2$, we get

$$(-i\omega\varepsilon_0\varepsilon_r)^{-1}\frac{\partial u_1}{\partial \nu} = (-i\omega\varepsilon_0\varepsilon_r)^{-1}\frac{\partial u_2}{\partial \nu},$$

which is

$$\frac{1}{\varepsilon_{r,1}}\frac{\partial u_1}{\partial \nu} = \frac{1}{\varepsilon_{r,2}}\frac{\partial u_1}{\partial \nu},$$

when $\mu_r \equiv 1$ and ν is the unit normal direction along the interface.

The perfect electrically conducting condition on a surface S is

$$\nu \times E = 0 \text{ on } S.$$

Denote $\nu = \begin{bmatrix} \nu_1 \\ \nu_2 \\ 0 \end{bmatrix}$, with $\nu_1^2 + \nu_2^2 = 1$. From the second equation of (2.17), we have $\nabla \times H = -i\omega\varepsilon_0\varepsilon_r E$, that is, $E = -\frac{1}{i\omega\varepsilon_0\varepsilon_r}(\nabla \times H)$. By direct calculation, it yields

$$\nabla \times H = \begin{bmatrix} \partial_{x_2} u \\ -\partial_{x_1} u \\ 0 \end{bmatrix},$$

$$0 = \nabla \times (\frac{1}{\varepsilon_0\varepsilon_r}(\nabla \times H)) = \begin{bmatrix} 0 \\ 0 \\ -\nu_1(-\frac{1}{\varepsilon_0\varepsilon_r})\partial_{x_1} u - \nu_2(-\frac{1}{\varepsilon_0\varepsilon_r})\partial_{x_2} u \end{bmatrix},$$

which leads to

$$\nu_1\partial_{x_1} + \nu_2\partial_{x_2} u = 0,$$

that is,

$$\nu \cdot \nabla u = 0 \Rightarrow \frac{\partial u}{\partial \nu} = 0.$$

Therefore, for TM polarization, we have problem with Neumann boundary condition

$$\begin{cases} \nabla \cdot (\varepsilon_r^{-1} \nabla u) + k_0^2 u = 0 \text{ on } D_1 \cup D_2, \\ \dfrac{1}{\varepsilon_{r,1}} \dfrac{\partial u_1}{\partial \nu} = \dfrac{1}{\varepsilon_{r,2}} \dfrac{\partial u_1}{\partial \nu} \text{ on the interface,} \\ \dfrac{\partial u}{\partial \nu} = 0 \text{ on the boundary .} \end{cases} \tag{2.20}$$

2.3 Mathematical model for scattering by multiple interfaces

We consider a two-dimensional model by assuming that the structure is invariant along the x_3 direction. The whole structure consists of several layers $D_1, D_2, \cdots, D_\ell$ and it is periodic with the period Λ. Let $\varepsilon_r(x) = \varepsilon_{r,j},\ x \in D_j,\ j = 1, \cdots, \ell$ be the relative permittivity in each layer. The bottom of the structure Γ_1 and the interface $\Gamma_j,\ j = 2, \cdots, \ell$ between the two layers

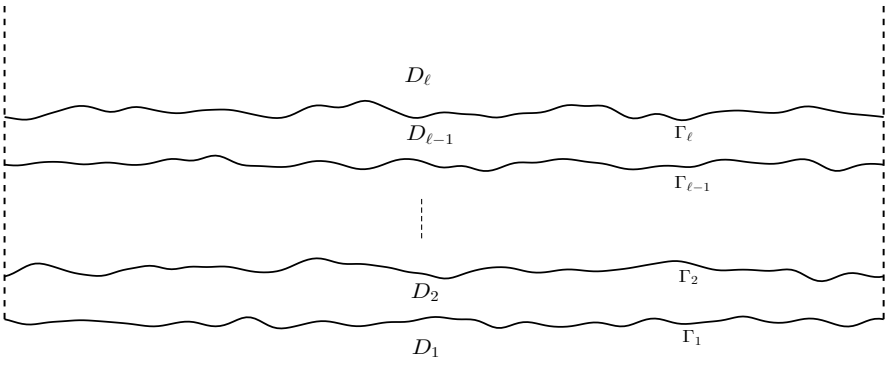

Figure 2.4: Schematic plot of the geometry.

D_{j-1} and D_j are textured in a random manner(see Figure 2.4). For each random sample ζ, the interface Γ_j is represented as $\Gamma_j(\zeta) := \{(x_1, x_2) \mid x_2 = f_j(\zeta; x_1)\}$, $j = 1, \cdots, \ell$. Let $D^\infty = \bigcup_{j=1}^{\ell} D_j$ be the whole domain, and $\Gamma = \bigcup_{j=1}^{\ell} \Gamma_j$ denote the union of the interfaces.

We first consider the transverse electric (TE) polarization, in which the electric field is of the form $E = (0, 0, u)$. Let k_0 the free-space wavenumber, $\theta \in (-\frac{\pi}{2}, \frac{\pi}{2})$ be the incident angle and $q_\ell := \sqrt{\varepsilon_{r,\ell}}$ be the refractive index of D_ℓ. When the random structure is illuminated by a time–harmonic incident plane wave $u^i = e^{ik_0 q_\ell (\sin\theta, -\cos\theta)\cdot x}$, the total field u after the

scattering consists of the incident wave u^i and the scattered wave u^s. We get the incident wave $u^i = e^{i(\tau x_1 - \rho x_2)}$ by denoting $\tau = k_0 q_\ell \sin\theta$ and $\rho = k_0 q_\ell \cos\theta$.

For each sample ζ, the total field u satisfies

$$\begin{cases} \Delta u(\zeta;\cdot) + k_0^2 \varepsilon_r u(\zeta;\cdot) = 0 \qquad \text{in } D^\infty(\zeta)\backslash\Gamma(\zeta) \\ u(\zeta;\Lambda,x_2) = e^{i\tau\Lambda} u(\zeta;0,x_2), \\ u(\zeta;x_1,f_1(x_1)) = 0, \quad 0 < x_1 < \Lambda. \end{cases} \tag{2.21}$$

Along the surfaces $\Gamma_j(\zeta),\ j = 2,\cdots,\ell$, the continuity of the electric field and magnetic field implies that

$$u_+(\zeta;x_1,f_j(\zeta,x_1)) = u_-(\zeta;x_1,f_j(\zeta,x_1)), \tag{2.22}$$

$$\partial_\nu u_+(\zeta;x_1,f_j(\zeta,x_1)) = \partial_\nu u_-(\zeta;x_1,f_j(\zeta,x_1)), \tag{2.23}$$

where ν denotes the unit normal vector along Γ_j pointing toward D_j, $u_\pm$ and $\partial_\nu u_\pm$ denote the limits of u and $\partial_\nu u$ from above and below the surface, respectively. In addition, the diffracted field u^s is outgoing in the domain $D_\ell(\zeta)$ that lies above the interface $\Gamma_\ell(\zeta)$ [5, 9].

To formulate the scattering problem in a bounded domain, we use $x_2 = b$ as an artificial upper boundary of the region, where $b > \max\limits_{0<x_1<\Lambda} f_\ell(x_1)$. By the Rayleigh expansion and the radiation condition [37, 42, 30] , the diffracted field in the region $D_\ell(\zeta) := \{(x_1,x_2) \mid x_1 \in (0,\Lambda), f_\ell(\zeta;x_1) < x_2 < b\}$ can be expressed as

$$u^s(\zeta;\cdot) = \sum_{n=-\infty}^{\infty} \hat{u}_n^s(\zeta;b)\, e^{i\kappa_n x_1 + i\eta_n(x_2-b)}, \tag{2.24}$$

where $\kappa_n := \tau + \dfrac{2\pi n}{\Lambda}$ for $n \in \mathbb{Z}$, and

$$\eta_n = \begin{cases} \sqrt{k_\ell^2 - \kappa_n^2}, & k_\ell > \kappa_n, \\ \\ i\sqrt{\kappa_n^2 - k_\ell^2}, & k_\ell < \kappa_n. \end{cases} \tag{2.25}$$

$\hat{u}_n^s(\zeta; b)$ are the Fourier coefficients of $u^s(\zeta; x_1, b)$ defined by

$$\hat{u}_n^s(\zeta; b) = \frac{1}{\Lambda} \int_0^\Lambda u^s(\zeta; x_1, b) e^{-i\kappa_n x_1} dx_1. \tag{2.26}$$

We assume $\kappa_n \neq k_\ell$ to exclude resonance. Then we have the Dirichlet-to-Neumann map T on the line $x_2 = b$,

$$\frac{\partial u^s}{\partial x_2}(\zeta; x_1, b) = \sum_{n=-\infty}^{\infty} i\eta_n \hat{u}_n^s(\zeta; b) e^{i\kappa_n x_1} =: T[u^s(\zeta; x_1, b)]. \tag{2.27}$$

Since $u = u^i + u^s$, we obtain

$$\frac{\partial u}{\partial x_2}(\zeta; x_1, b) = T(u(\zeta; x_1, b)) + g,$$

where $g = -2i\rho e^{i\tau x_1 - i\rho b}$. Therefore, for each sample ζ, the scattering problem can be formulated in a bounded domain (showed in Figure (2.5)) $D := \bigcup_{j=1}^{\ell} D_j$ as

$$\begin{cases} \Delta u(\zeta; \cdot) + k_0^2 \varepsilon_r u(\zeta; \cdot) = 0 & \text{in } D(\zeta) \setminus \Gamma(\zeta), \\ u(\zeta; \Lambda, x_2) = e^{i\tau\Lambda} u(\zeta; 0, x_2), & 0 < x_2 < b, \\ u(\zeta; x_1, f_1(x_1)) = 0, & 0 < x_1 < \Lambda \\ \dfrac{\partial u}{\partial x_2}(\zeta; x_1, b) = T(u(\zeta; x_1, b)) + g & 0 < x_1 < \Lambda. \end{cases} \tag{2.28}$$

Additionally, the continuity conditions (2.22), (2.23) are imposed along the interfaces $\Gamma_j,\ j = 2, \cdots, \ell - 1$.

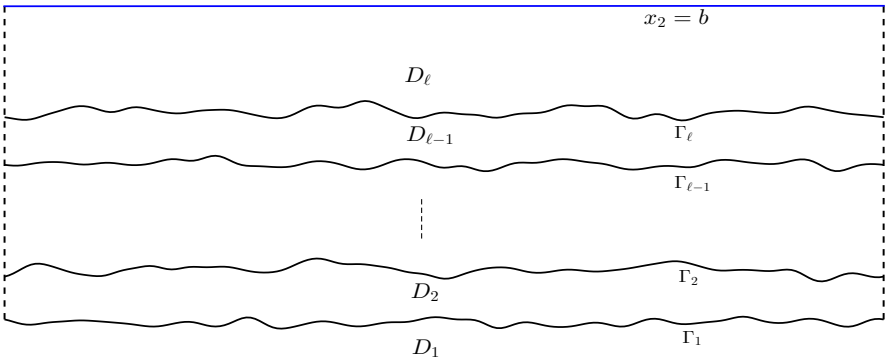

Figure 2.5: Schematic plot of the bounded domain.

The transverse magnetic (TM) polarization in which H is of the form of $(0, 0, u)$ works analogously with a small change in the boundary condition and continuous condition.

$$\begin{cases} \nabla \cdot (\varepsilon_r^{-1} \nabla u(\zeta; \cdot)) + k_0^2 u(\zeta; \cdot) = 0 \qquad \text{in } D(\zeta) \backslash \Gamma(\zeta), \\ u(\zeta; \Lambda, x_2) = e^{i\tau\Lambda} u(\zeta; 0, x_2), \qquad\qquad 0 < x_2 < b, \\ \partial_\nu u(\zeta; x, 0) = 0, \quad 0 < x < \Lambda, \\ \dfrac{\partial u}{\partial x_2}(\zeta; x_1, b) = T(u(\zeta; x_1, b)) + g \qquad\qquad 0 < x_1 < \Lambda. \end{cases} \tag{2.29}$$

In addition, the continuity conditions are satisfied along the interface $\Gamma_j,\ j = 2, \cdots, \ell - 1$ is given by

$$u_+(\zeta; x_1, f_j(\zeta, x_1)) = u_-(\zeta; x_1, f_j(\zeta, x_1)), \tag{2.30}$$

$$\varepsilon_{r,j}^{-1} \partial_\nu u_+(\zeta; x_1, f_j(\zeta, x_1)) = \varepsilon_{r,j-1}^{-1} \partial_\nu u_-(\zeta; x_1, f_j(\zeta, x_1)), \tag{2.31}$$

2.4 Representation of random surfaces

This section is dedicated to the modeling of the random surfaces that separate each layer. It is structured as follows. First, there will be a description of the Karhunen–Loève expansion which explains the expansion and where it originates. This description follows the lead of

[17, 18, 29, 28]. From there, the Karhunen–Loève expansion will be used to represent the random surfaces in our framework.

In what follows we consider a probability space $(\Omega, \mathcal{F}, P)$, where Ω is a sample space, $\mathcal{F}$ is σ-algebra on Ω and P is a probability measure. A real valued random variable X on $(\Omega, \mathcal{F}, P)$ is an $\mathcal{F}/\mathcal{B}(\mathcal{R})$-measurable mapping $X : (\Omega, \mathcal{F}, P) \to (R, \mathcal{B}(\mathcal{R}))$, where $\mathcal{R}$ is the real number set and $\mathcal{B}(\mathcal{R})$ is the Borel set on $\mathcal{R}$. The expectation and variance of a random variable X is denoted by,

$$E[X] := \int_\Omega X(\zeta) dP\zeta, \;\; Var[X] := E[(X - E[X])^2].$$

A stochastic process X_t is called centered if $E[X_t] = 0$. It is mean-square continuous if

$$\lim_{\delta \to 0} E[(X_{t+\delta} - X_t)^2] = 0.$$

A stochastic process $\{X_t\}_{t \in I}$ is mean square continuous if and only if its auto correlation function $c(s,t) := E[X_s X_t]$ is continuous.

Assume that $X : I \times \Omega \to \mathcal{R}$ is a centered mean square continuous stochastic process such that $X \in L^2(I \times \Omega)$. Define the integral operator $K : L^2(I) \to L^2(I)$ by

$$[K\varphi](s) := \int_I c(s,t)\varphi(t) dt, \;\; \varphi \in L^2(I),$$

Such defined K is compact, positive and self-adjoint. Therefore, K has a complete set of eigenvectors $\{e_i\}$ in $L^2(I)$ and real eigenvalues $\{\lambda_i\}$:

$$Ke_i = \lambda_i e_i.$$

The basis $\{e_i\}$ of $L^2(I)$ can be used to expand X_t as follows,

$$X_t = \sum_i x_i e_i(t), \;\; x_i = \int_I X_t e_i(t) dt.$$

Theorem 2.4.1 *(Karhunen–Loève expansion) Let that $X : I \times \Omega \to \mathcal{R}$ is a centered mean square continuous stochastic process such that $X \in L^2(I \times \Omega)$. There exist a basis $\{e_i\}$ of $L^2(I)$ such that for all $t \in I$,*

$$X_t = \sum_{i}^{\infty} x_i e_i(t), \text{ in } L^2(I),$$

where the coefficients x_i are given by $x_i(\zeta) = \int_I X_t(\zeta) e_i(t) dt$ and satisfy the following.

1. $E[x_i] = 0$,
2. $E[x_i x_j] = \delta_{ij}\lambda_j$,
3. $Var[x_i] = \lambda_i$

By letting $\xi_i = \dfrac{1}{\sqrt{\lambda_i}} x_i$ in above theorem, Karhunen–Loève expansion can be written as,

$$X_t(t, \zeta) = \sum_{i=1}^{\infty} \sqrt{\lambda_i}\xi_i(\zeta) e_i(t), \text{ in } L^2(I). \tag{2.32}$$

where ξ_i are centered mutually uncorrelated random variables with unit variance and are given by,

$$\xi_i(\zeta) = \frac{1}{\sqrt{\lambda_i}} \int_I X_t(\zeta) e_i(t) dt.$$

The Karhunen–Loève expansion of a Gaussian process has the further property that ξ_i are independent standard normal variables[29].

The random interfaces in Figure 2.4 are represented by

$$\Gamma_j(\zeta) = \{(x_1, x_2) \mid x_2 = f_j(\zeta; x_1)\}, \ j = 1, \cdots, \ell.$$

We assume that $f_j(\zeta; x_1)$ is a stationary random process with a continuous and bounded covariance function $C_j(x_1, \tilde{x}_1) = c_j(x_1 - \tilde{x}_1)$. The following covariance functions are widely used for the modeling of rough surfaces:

$$c_j(x_1 - \tilde{x}_1) = \left(\alpha_j^{(1)}\right)^2 \exp\left(-|x_1 - \tilde{x}_1|^p / \left(\alpha_j^{(2)}\right)^p\right), \ 0 < \alpha_j^{(2)} \ll \Lambda, \ p = 1, 2$$

where $\alpha_j^{(1)}$ is the root mean square and $\alpha_j^{(2)}$ is the correlation length of the surface $\Gamma_j(\zeta)$[35].

The root mean quare of the surface $\alpha_j^{(1)}$, and the correlation length $\alpha_j^{(2)}$ dictate the shape of the surface. As the value of $\alpha_j^{(1)}$ is increased, the size (in the x_2-direction) of the interface Γ_j will also increase, and vice versa. Figure 2.6 demonstrates the effect of increasing the value of the root mean quare of the surface Γ_j.

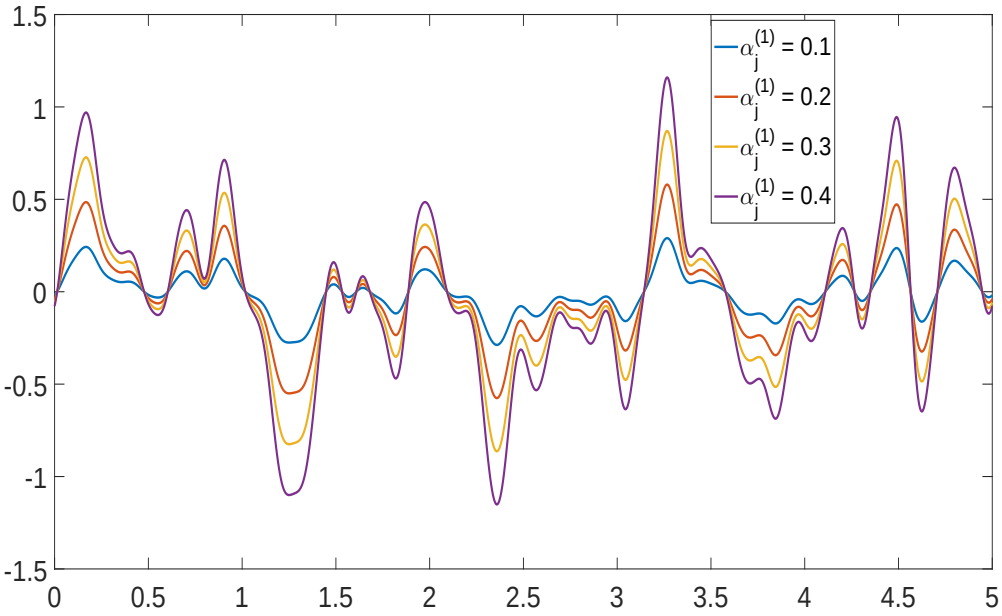

Figure 2.6: Sample surface represented by Karhunen Loéve expansion with varying root mean square of the surface

As the value of the correlation length $\alpha_j^{(2)}$ is increased, the interface shapes will become "smoother" (less rough or "choppy"). Figure 2.7 demonstrates the effect of increasing the correlation length of the surface Γ_j.

By the Karhunen–Loève expansion[27], the random process $f_j(\zeta; x_1)$ can be represented as

$$f_j(\zeta; x_1) = f_j^a + \sum_{m=1}^{\infty} \sqrt{\lambda_{jm}} \xi_{jm} \varphi_{jm}$$

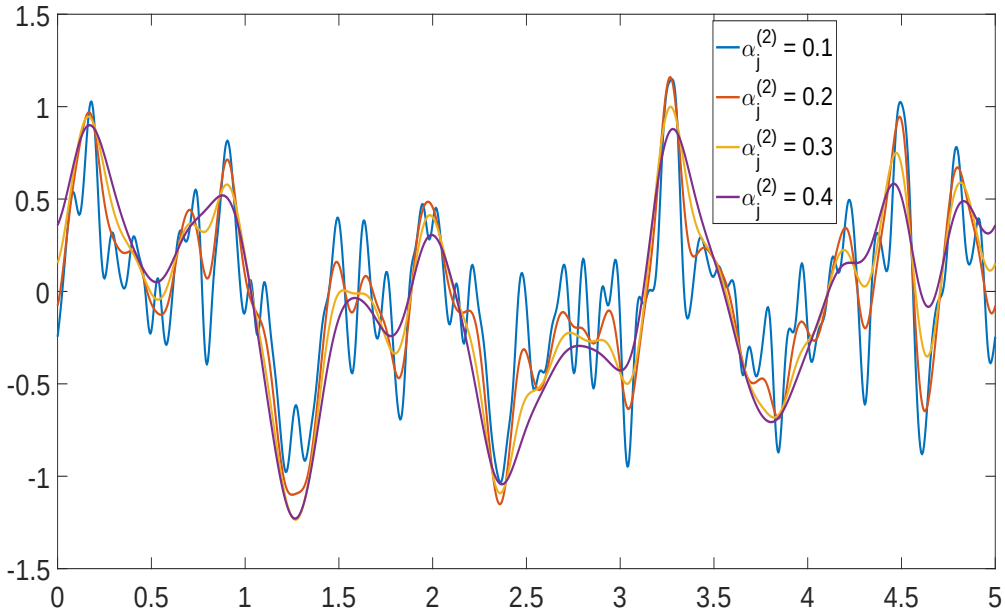

Figure 2.7: Sample surface represented by Karhunen Loéve expansion with varying correlation length of the surface

where f_j^a is the average height of f_j, ξ_{jm} are mutually uncorrelated with zero mean and unit covariance, λ_{jm} and φ_{jm}, $(m = 1, 2, \cdots,)$ are the eigenvalues and eigenfunctions of covariance operator $[K\varphi](x_1) := \int_0^\Lambda c_j(x_1 - \tilde{x}_1)\ \varphi(\tilde{x}_1) d\tilde{x}_1$, respectively.

Since $c_j(x_1)$ is even, we expand $c_j(x_j)$ as

$$c_j(x_1) = \left(\alpha_j^{(1)}\right)^2 \left[\frac{\widehat{c}_{j0}}{2} + \sum_{p=1}^{\infty} \widehat{c}_{jp} \cos\left(\frac{2p\pi x_1}{\Lambda}\right)\right],\ x_1 \in [0, \Lambda],$$

where $\widehat{c}_{j0}, \widehat{c}_{j1}, \widehat{c}_{j2}, \cdots,$ are the Fourier cosine expansion coefficients of the correlation function $c_j(x_1)$. The covariance operator $K\varphi(x_1) := \int_0^\Lambda c_j(x_1 - \tilde{x}_1)\ \varphi(\tilde{x}_1) d\tilde{x}_1$ attains the eigenvalues

$$\lambda_{jm} = \frac{\left(\alpha_j^{(1)}\right)^2 \Lambda \widehat{c}_{jm}}{2}, \quad m = 0, 1, 2, \cdots.$$

The corresponding eigenfunctions are

$$\varphi_{jm}(x_1) = \begin{cases} \sqrt{\dfrac{1}{\Lambda}}, & m = 0, \\ \sqrt{\dfrac{2}{\Lambda}} \cos\left(\dfrac{2j\pi x_1}{\Lambda}\right), & m > 1, \text{even} \\ \sqrt{\dfrac{2}{\Lambda}} \sin\left(\dfrac{2j\pi x_1}{\Lambda}\right), & m > 1, \text{odd}. \end{cases}$$

Hence Karhunen–Loève representation of the random process $f_j(\zeta; x_1)$ is given by

$$\begin{aligned} f_j(\zeta; x_1) =& f_j^a + \sqrt{\lambda_{j0}}\xi_{j0}(\zeta)\sqrt{\frac{1}{\Lambda}} \\ &+ \sum_{m=1}^{\infty} \sqrt{\lambda_{jm}} \left[\xi_{m,s}(\zeta)\sqrt{\frac{2}{\Lambda}} \sin\left(\frac{2m\pi x_1}{\Lambda}\right) + \xi_{m,c}(\zeta)\sqrt{\frac{2}{\Lambda}} \cos\left(\frac{2m\pi x_1}{\Lambda}\right) \right], \end{aligned} \tag{2.33}$$

where ξ_{j_0}, $\xi_{m,c}$ and $\xi_{m,s}$ are mutually uncorrelated random variables with zero mean and unit covariance. Particularly, when $f_j(\zeta; x_1)$ is a stationary Gaussian process, ξ_{j_0}, $\xi_{m,c}$ and $\xi_{m,s}$ are independent and identically distributed Gaussian random variables with zero mean and unit covariance.

A finite term Karhunen–Loève expansion is used in practical computations since $\{\lambda_{jm}\}_{j=0}^{\infty}$ converge to 0 exponentially when $c(x)$ is smooth. Therefore, for simplicity, here we use a finite term approximation of (2.33). By letting $\lambda_{jm} = \left(\alpha_j^{(1)}\right)^2 \overline{\lambda}_{jm}$ where $\overline{\lambda}_{jm} = \dfrac{\Lambda \hat{c}_{jm}}{2}$, we may express the profile of the random surface by

$$f_j(\zeta; x_1) = f_j^a + \alpha_j^{(1)} \cdot \bar{f}_j(\zeta; x_1), \tag{2.34}$$

where

$$\begin{aligned} \bar{f}_j(\zeta; x_1) =& \sqrt{\overline{\lambda}_{j0}}\xi_{j0}(\zeta)\sqrt{\frac{1}{\Lambda}} \\ &+ \sum_{m=1}^{M} \sqrt{\overline{\lambda}_{jm}} \left[\xi_{m,s}(\zeta)\sqrt{\frac{2}{\Lambda}} \sin\left(\frac{2m\pi x_1}{\Lambda}\right) + \xi_{m,c}(\zeta)\sqrt{\frac{2}{\Lambda}} \cos\left(\frac{2m\pi x_1}{\Lambda}\right) \right]. \end{aligned}$$

Chapter 3

Optimal design of random surfaces

3.1 Optimal design problem for transverse electric polarization

For each sample ζ, in light of the Rayleigh expansion (2.24), the diffracted field can be rewritten as

$$u^s(\zeta;\cdot) = \sum_{n=-\infty}^{\infty} r_n(\zeta)\, e^{i\kappa_n x_1 + i\eta_n x_2},$$

where the reflection coefficient $r_n(\zeta) = \hat{u}_n^s(\zeta; b)e^{-i\eta_n b}$, and $\hat{u}_n^s$ are the Fourier coefficients of the diffracted field u^s as defined in (2.26). Since $u = u^i + u^s$, $r_n(\zeta)$ can also be written as

$$r_n(\zeta) = \begin{cases} \hat{u}_n(\zeta; b)e^{-i\eta_n b}, & n \neq 0 \\ \\ \hat{u}_n(\zeta; b)e^{-i\rho b} - e^{-2ik_\ell b}, & n = 0, \end{cases} \tag{3.1}$$

where $\hat{u}_n(\zeta; b)$ are the Fourier coefficients of the total field $u(\zeta;\cdot)$ on $x_2 = b$.

Let $\mathcal{N} := \{n \in \mathbb{Z} \mid k_\ell^2 - \kappa_n^2 > 0\}$ be the set of indices for all propagating modes in the Rayleigh expansion. The goal is to trap the energy in the structure as much as possible. In other words, we hope to minimize the energy that propagates away. Denote $\boldsymbol{\alpha} = (\alpha_1, \cdots, \alpha_\ell)^\top$, where $\alpha_j = (\alpha_j^{(1)}, \alpha_j^{(2)})$, for $j = 1, \cdots, \ell$. $\alpha_j^{(1)}$ is the root mean square height of the surface and $\alpha_j^{(2)}$ is the correlation length corresponding to Γ_j. Let $R(\zeta;\alpha)$ be the reflectivity of the structure. For each sample ζ, the reflectivity associated with this structure is given by

$$R((\zeta;\boldsymbol{\alpha})) = \sum_{n\in\mathcal{N}} \frac{\eta_n}{\eta_0} \left|r_n(\zeta)\right|^2,$$

where η_n is defined in (2.25). Thus the mean reflectivity is

$$E[R((\zeta;\boldsymbol{\alpha}))] := \int_\Omega \sum_{n\in\mathcal{N}} \frac{\eta_n}{\eta_0} \left|r_n(\zeta)\right|^2 \, dP(\zeta),$$

where Ω and P denotes the random sample space and the probability measure, respectively.

Let $Q(\boldsymbol{\alpha}) := E\left[R(\zeta;\boldsymbol{\alpha})\right]$ be the cost function. Then the optimal design problem is to minimize the mean reflectivity $Q(\alpha)$, or equivalently, to solve the optimization problem

$$\text{Problem(I)} \qquad \min_{\boldsymbol{\alpha}\in U_{\boldsymbol{\alpha}}} Q(\boldsymbol{\alpha}) \tag{3.2}$$

over an admissible set $U_{\boldsymbol{\alpha}}$.

Next, we consider the optimization with multiple frequencies. In this case, the refractive index $\varepsilon_r = \varepsilon_r(\lambda)$ is a function of the wavelength [46], The total field can be formulated as

$$\begin{cases} \Delta u(\zeta;\cdot) + k_0^2 \varepsilon_r(\lambda) u(\zeta;\cdot) = 0 \; in \; D \setminus \Gamma_2(\zeta), \\ u(\zeta;0,x_2) = u(\zeta;\Lambda,x_2), \\ u(\zeta;x_1,f_1(x_1)) = 0; \; 0 \le x_1 \le \Lambda, \\ \partial_{x_2} u(\zeta;x_1,b) = T(u(\zeta;x_1,b)) + g, \\ u_+(\zeta;\cdot) = u_-(\zeta;\cdot), \; on \; \Gamma_1, \\ \partial_\nu u_+(\zeta;\cdot) = \partial_\nu u_-(\zeta;\cdot), \; on \; \Gamma_1. \end{cases} \tag{3.3}$$

so does the total field u and the reflectivity $R(\zeta;\boldsymbol{\alpha},\lambda)$. When the wavelength for the incident wave is within $[\lambda_{min},\lambda_{max}]$, the optimization problem with multiple frequencies can be formulated as follows:

$$\text{Problem(II)} \qquad \min_{\boldsymbol{\alpha}\in U_{\boldsymbol{\alpha}}} Q(\boldsymbol{\alpha}), \text{ where } Q(\boldsymbol{\alpha}) := E\left[\int_{\lambda_{min}}^{\lambda_{max}} R(\zeta;\boldsymbol{\alpha},\lambda) d\lambda\right]. \tag{3.4}$$

For the solar cells, the incident angle is no longer constant when the sun moves during the daytime. It is reasonable to consider the incident angle θ as a variable. Total field u satisfies

equation

$$\begin{cases} \Delta u(\zeta;\cdot) + k_0^2 \varepsilon_r u(\zeta;\cdot) = 0 & \text{in } D(\zeta)\backslash\Gamma(\zeta)(\zeta), \\ u(\zeta;\Lambda,x_2) = e^{i\alpha\Lambda} u(\zeta;0,x_2), & 0 < x_2 < b, \\ u(\zeta;x_1,0) = 0, & 0 < x_1 < \Lambda \\ \dfrac{\partial u}{\partial x_2}(\zeta;x_1,b) = T(u(\zeta;x_1,b)) + g(\theta) & 0 < x_1 < \Lambda. \end{cases} \tag{3.5}$$

For the case that the incident angle is not constant, for a given sample ζ, the total field u is a function of the incident angle θ. Therefore, the reflectivity $R(\zeta;\boldsymbol{\alpha},\theta)$ is also a function of θ. For the multiple incident angles with $\theta \in [\theta_{min}, \theta_{max}]$, the corresponding optimization problem is formulated as follows:

$$\text{Problem(III)} \qquad \min_{\boldsymbol{\alpha}\in U_{\boldsymbol{\alpha}}} Q(\boldsymbol{\alpha}), \text{ where } Q(\boldsymbol{\alpha}) := E\left[\int_{\theta_{min}}^{\theta_{max}} R(\zeta;\boldsymbol{\alpha},\theta)d\theta\right]. \tag{3.6}$$

3.2 Optimal design problem for transverse magnetic polarization

The transverse magnetic (TM) polarization case works analogously with a small change in the continuous conditions along the interfaces, which is discussed below.We simply show the difference by a two layers structure to illustrate the difference, which showed in Figure (3.1).

Here we consider the magnetic field H under transverse magnetic polarization, that is, H is of the form of $(0,0,u)$. Assume that the normal incident wave is of the form $u^i = e^{-ik_0 q x_2}$, where k_0 is the free space wave number and q is the refractive index of the TCO layer. The total field u after the scattering is composed of incident wave u^i and scattered wave u^s, i.e. $u = u^i + u^s$.

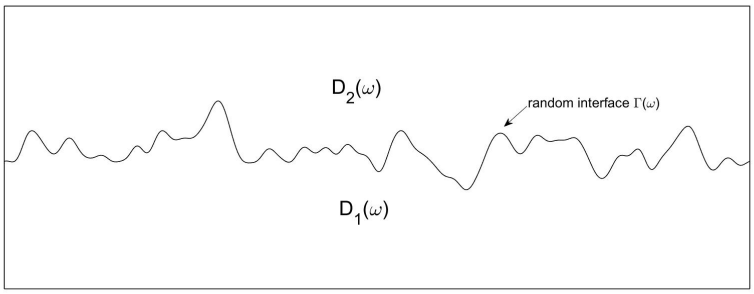

Figure 3.1: Scattering problem in the bounded domain D

The TCO and absorption layer are denoted as

$$D_1(\zeta) := \{(x_1, x_2) \mid x_1 \in (0, \Lambda), 0 < x_2 < h(\zeta; x_1)\}$$

and

$$D_2(\zeta) := \{(x_1, x_2) \mid x_1 \in (0, \Lambda), h(\zeta; x_1) < x_2 < \infty\}$$

For any simple ζ, the total field u satisfies

$$\begin{cases} \nabla \cdot (\varepsilon_r^{-1} \nabla u(\zeta; \cdot)) + k_0^2 u(\zeta; \cdot) = 0 \qquad \text{in } D(\zeta) \backslash \Gamma(\zeta), \\ u(\zeta; 0, x_2) = u(\zeta; \Lambda, x_2), \\ \partial_\nu u(\zeta; x_1, 0) = 0, \quad 0 < x_1 < \Lambda, \end{cases} \tag{3.7}$$

where

$$\varepsilon_r = \begin{cases} \varepsilon_{r,1}, & y < h(\zeta; x_1), \\ \varepsilon_{r,2}, & y > h(\zeta; x_1). \end{cases}$$

Here ν is the outer normal vector, ε_r is the relative permittivity value, $\varepsilon_{r,1}$ and$\varepsilon_{r,2}$ are the relative permittivity value of the absorption layer and the TCO layer, respectively. The permittivity of the solar cell is $\varepsilon = \varepsilon_r \cdot \varepsilon_0$, where ε_0 is the permittivity value in the vacuum. In addition, the continuity conditions are satisfied along the interface

$$u_+(\zeta; x_1, h(\zeta, x_1)) = u_-(\zeta; x_1, h(\zeta, x_1)), \tag{3.8}$$

$$\varepsilon_{r,2}^{-1} \partial_\nu u_+(\zeta; x_1, h(\zeta, x_1)) = \varepsilon_{r,1}^{-1} \partial_\nu u_-(\zeta; x_1, h(\omega, x_1)), \tag{3.9}$$

To formulate the scattering field in a bounded domain, consider $x_2 = b$ as a artificial upper boundary of the region, where $b > \max\limits_{0<x_1<\Lambda} h(\zeta; x_1)$. We will apply the DtN mapping condition for the scattered field u^s given by

$$u^s(x_1, x_2) = \sum_{n \in Z} \hat{u}_n^s(\zeta; x_2) e^{i\kappa_n x_1}$$

where $\kappa_n = \frac{2\pi n}{\Lambda}$, $\hat{u}_n^s(\zeta, x_2) = \frac{1}{\Lambda}\int_0^\Lambda u^s(\zeta; x_1, x_2)e^{-i\kappa_n x_1}dx_1$.

Denote $k = k_0\sqrt{\varepsilon_{r,2}}$. For a certain sample ζ , we can get the expression of the scattering field satisfies

$$\begin{cases} \nabla(\varepsilon_r^{-1}\nabla u(\zeta;\cdot) + k_0^2 u(\zeta;\cdot) = 0 & \text{in } D(\zeta)\backslash\Gamma(\zeta), \\ u(\zeta; 0, x_2) = u(\zeta; \Lambda, x_2), & 0 < x_2 < b, \\ \partial_\nu u(\zeta; x_1, 0) = 0, & 0 < x_1 < \Lambda, \\ \partial_{x_2} u(\omega; x_1, b) = T(u(\omega; x_1, b)) + g & 0 < x_1 < \Lambda, \end{cases} \tag{3.10}$$

where $g = -2ike^{-ikb}$ and T is the Dirichlet-to-Neumann map.

For each sample $\zeta \in \Omega$, the reflectivity can be defined as,

$$R(\zeta; h) = \sum_{n\in\mathcal{N}} \frac{\eta_n}{\eta_0}|r_n(\zeta)|^2, \tag{3.11}$$

where $\mathcal{N} := \{n \in N | k_0^2\varepsilon_{r,2} - \kappa_n^2 > 0\}$ is the index of propagating modes,

$$r_n(\zeta) = \begin{cases} \hat{u}_n(\zeta; b)e^{-i\eta_n b}, & n \neq 0 \\ \hat{u}_n(\zeta; b)e^{-ikb} - e^{-2ikb}, & n = 0, \end{cases} \tag{3.12}$$

which is inspired by

$$u^s(\zeta;\cdot) =: \sum_{n=-\infty}^{\infty} r_n(\zeta)e^{-i\kappa_n x_1 + i\eta_n x_2}$$

$$r_n = \hat{u}_n^s(\zeta; b)e^{-i\eta_n b},$$

where $\hat{u}_n^s$ is the fourier coefficient of the scatter wave u^s. The expectation of reflectivity is

$$E[R] := \int_\Omega \sum_{n\in\mathcal{N}} \frac{\eta_n}{\eta_0}|r_n(\zeta)|^2 dP(\zeta).$$

Here Ω and P denotes the random sample space and the probability measure respectively. We define the cost function

$$J(\alpha) := E(R(\zeta; h)),$$

where $\boldsymbol{\alpha} := (\sigma, l)$ is a vector consists of the root mean square σ and the correlation l of $h(\zeta, x_1)$. The optimal design problem is to minimize the mean $J(\boldsymbol{\alpha})$ of the reflectivity, in other words, to solve the following optimization problem.

$$\min_{\boldsymbol{\alpha} \in U_{\boldsymbol{\alpha}}} Q(\boldsymbol{\alpha}),$$

over an admissible set $U_{\boldsymbol{\alpha}}$.

We use the stochastic gradient method to solve the optimization problems. The gradient of the cost function R for a given sample ζ needs to be found during each iteration, which is discussed in the following section.

Chapter 4

The numerical algorithm

4.1 The stochastic gradient descent method

To minimize $Q(\boldsymbol{\alpha}) = E\left[R(\zeta;\boldsymbol{\alpha})\right]$, from certain initial guess, the full gradient decent method is defined by the iteration

$$\boldsymbol{\alpha}^{(n+1)} = \boldsymbol{\alpha}^{(n)} - h_n \cdot D_{\boldsymbol{\alpha}} Q(\boldsymbol{\alpha}^{(n)}), \tag{4.1}$$

where h_n is the step length [4]. If we use the Monte Carlo method to sample the probability space, we have $D_{\boldsymbol{\alpha}} Q(\boldsymbol{\alpha}^{(n)}) = E\left[D_{\boldsymbol{\alpha}} R(\zeta;\boldsymbol{\alpha}^{(n)})\right] = \frac{1}{M_C}\sum_{m=1}^{M_C} D_{\alpha} R(\zeta_m;\alpha^{(n)})$. M_C needs to be big enough to get a good approximation for the full gradient. Therefore, computing the gradient $D_{\boldsymbol{\alpha}} Q(\boldsymbol{\alpha}^{(n)})$ is very expensive.

The stochastic gradient descent method [40, 25, 3] is a widely used in solving stochastic optimization problems. The stochastic gradient decent method to minimize $Q(\boldsymbol{\alpha})$ is defined by

$$\boldsymbol{\alpha}^{(n+1)} = \boldsymbol{\alpha}^{(n)} - h_n \cdot D_{\boldsymbol{\alpha}} R(\zeta_n;\boldsymbol{\alpha}^{(n)}). \tag{4.2}$$

Here, for each $n \in N := \{1, 2, \cdots\}$, ζ_n is chosen randomly and h_n is a positive step size. Each iteration of stochastic gradient method is very cheap, involving only the computation of the gradient $D_{\boldsymbol{\alpha}} R(\zeta_n)$ for one sample. However the iterative sequence is not determined uniquely by the function $Q(\boldsymbol{\alpha})$, the starting point $\boldsymbol{\alpha}^{(1)}$, and the sequence of step size $\{h_n\}_{n=1}^{\infty}$. Rather, $\{\boldsymbol{\alpha}^{(n)}\}_{n=1}^{\infty}$ is a stochastic process whose behaviour is determined by the random sequence $\{\zeta_n\}_{n=1}^{\infty}$.

The stochastic gradient method and the full gradient method offer different trade-offs in terms of costs and expected improvement in each iteration for minimizing the cost function $Q(\boldsymbol{\alpha})$. Mini-batch stochastic gradient method is designed to combine the stochastic gradient method and the full gradient method, and is defined by

$$\boldsymbol{\alpha}^{(n+1)} = \boldsymbol{\alpha}^{(n)} - h_n \cdot G(\boldsymbol{\alpha}^{(n)}), \tag{4.3}$$

where $G(\boldsymbol{\alpha}^{(n)}) = \frac{1}{M_0} \sum_{m=1}^{M_0} D_\alpha R(\zeta_m; \alpha^{(n)})$ is the average gradient of a small randomly chosen sample subset $\{\zeta_m\}_{m=1}^{M_0}$.

There are several significant advantages of mini-batch stochastic gradient method. First, the mini-batch stochastic gradient method reduces the variance of the stochastic gradient, which produces more stable gradient than stochastic gradient. Second,The flexible choice for the size of the sample subset $\{\zeta_m\}_{m=1}^{M_0}$ can easily fits in the memory and it can benefit form vectorization and parallel computing. And third, if the iteration is stuck in a local minimum, some noisy steps can lead the way out of it.

Algorithm 1 The algorithm for GD method

1: Initialization $\alpha^{(0)}$
2: **for** iteration $n = 1, 2, \ldots$ **do**
- Choose sample $\{\zeta_m\}_{m=1}^{M}$, M is larger enough.
- Solve the scattered equation (3.10) and adjoint equation (4.27).
- Find gradient $D_\alpha Q(\alpha^{(n)}) \approx \frac{1}{M} \sum_{m=1}^{M} D_\alpha R(\zeta_m; \alpha^{(n)})$.
- $\alpha^{(n+1)} = \alpha^{(n)} - h_n \cdot D_\alpha Q(\alpha^{(n)})$ (where h_n is the step length).

3: **end for**

Algorithm 2 The algorithm for SGD method

1: Initialization $\alpha^{(0)}$
2: **for** iteration $n = 1, 2, \ldots$ **do**

- Choose random realization of ζ_n.
- Solve the scattered equation (3.10) and adjoint equation (4.27).
- Compute sample gradient $D_\alpha R(\zeta_n)$.
- Update $\alpha^{(n+1)} = \alpha^{(n)} - h_n \cdot D_\alpha R(\zeta_n; \alpha^{(n)})$ (where h_n is the step length).

3: **end for**

Algorithm 3 The algorithm for mini-batch SGD method

1: Choose initial guess $\boldsymbol{\alpha}^{(0)}$ and the sample size M_0
2: **while** The average gradient of the sample set $\|G(\boldsymbol{\alpha}^{(n)})\|_2 >$ tolerance **do**

- Choose a random samples subset $\{\zeta_m\}_{m=1}^{M_0}$.
- For each sample ζ_m, solve the boundary value problem (3.10) and the adjoint problem (4.27).
- Compute the gradient $D_{\boldsymbol{\alpha}} R(\zeta_m; \cdot)$ by formula (4.4) and (4.5)
- $G(\boldsymbol{\alpha}^{(n)}) = \frac{1}{M_0} \sum_{m=1}^{M_0} D_{\boldsymbol{\alpha}} R(\zeta_m; \boldsymbol{\alpha}^{(n)})$.
- $\boldsymbol{\alpha}^{(n+1)} = \boldsymbol{\alpha}^{(n)} - h_n \cdot G(\boldsymbol{\alpha}^{(n)})$ (where h_n is the step length).

3: **end while**

4.2 Computation of the gradient for transverse electric polarization

The shape derivative $D_{\boldsymbol{\alpha}}R$ can be evaluated by the adjoint state approach [22, 34] and its formula is given in the following theorem.

Theorem 4.2.1 *Denote* $D_{\alpha_j} := \left(\dfrac{\partial}{\partial\alpha_j^{(1)}}, \dfrac{\partial}{\partial\alpha_j^{(2)}}\right), j = 1, 2, \cdots, \ell$. *For each sample* ζ,

$$D_{\alpha_1}R(\zeta) = \frac{2}{\Lambda}\sum_{n\in\mathcal{N}}\frac{\eta_n}{\eta_0}Re\Big[(\hat{u}_n(\zeta;b) - a_n e^{-2ik_\ell b + i\rho b})\cdot\int_0^\Lambda(\frac{\partial\bar{u}}{\partial\nu}\cdot\frac{\partial u_n^*}{\partial\nu}\nu_2)\cdot\nabla_{\alpha_1}f_1 dx_1\Big] \tag{4.4}$$

$$\begin{aligned} D_{\alpha_j}R(\zeta) = \frac{2k_0^2}{\Lambda}\sum_{n\in\mathcal{N}}\frac{\eta_n}{\eta_0}Re\Big[&(\hat{u}_n(\zeta;b) - a_n e^{-2ik_\ell b + i\rho b})\cdot\overline{(\varepsilon_{r,j} - \varepsilon_{r,j-1})} \\ &\cdot\int_0^\Lambda[\bar{u}u_n^*]|_{(x_1,f_j)}\cdot\nabla_{\alpha_j}f_j dx_1\Big],\ j = 2,\cdots,\ell. \end{aligned} \tag{4.5}$$

where $a_0 = 1$ *and* $a_n = 0$ *if* $n \neq 0$, *and* $\nu = (\nu_1, \nu_2)^\top$ *is the normal vector pointing inside* D *along* Γ_1. u *is the solution to the forward problem* (3.10)*, and* u_n^* *solves the adjoint problem*

$$\begin{cases} \Delta u_n^*(\zeta;\cdot) + k_0^2\overline{\varepsilon_r}u_n^*(\zeta;\cdot) = 0\ in\ D(\zeta)\setminus\Gamma(\zeta) \\ u_n^*(\zeta;\Lambda,x_2) = e^{i\tau\Lambda}u_n^*(\zeta;0,x_2), \\ u_n^*(\zeta;x_1,f_1(x_1)) = 0;\ 0\le x_1\le\Lambda, \\ \partial_{x_2}u_n^*(\zeta;x_1,b) = T^*(u(\zeta;x_1,b)) + e^{i\kappa_n x_1}, \end{cases} \tag{4.6}$$

In the above theorem, $[u_n^*\bar{u}]|_{(x_1,f_j)}$ denotes the restriction of $u_n^*\bar{u}$ to the surface $\Gamma_j(\zeta)$. T^* is the adjoint operator of T such that

$$\langle Tu, v\rangle = \langle u, T^*v\rangle,$$

where $\langle\cdot,\cdot\rangle$ stands for the inner product over the function space $L^2(0,\Lambda)$. The proof of the theorem is shown in next section.

Let $H_0^1(D) = \{u\in H^1(D) | u = 0\ on\ \Gamma_1, u(\Lambda,x_2) = e^{i\tau\Lambda}u(0,x_2)\}$, where

$$H^1(D) = \{f(x) | \left(\int_D |f(x)|^2dx\right)^{\frac{1}{2}} < \infty,\ \left(\int_D |\nabla f(x)|^2dx\right)^{\frac{1}{2}} < \infty\}.$$

The bilinear form for (3.10) is

$$a(u(\zeta;\cdot),w)=\int_D \nabla u(\zeta;\cdot)\cdot\nabla\bar{w}-k_0^2\varepsilon_r u(\zeta;\cdot)\bar{w}dx-\langle Tu(\zeta;\cdot),w\rangle.$$

The weak solution $u\in H_0^1(D)$ for (3.10) satisfies

$$a(u(\zeta;\cdot),w)=\langle g,w\rangle \tag{4.7}$$

for all $w\in H_0^1(D)$.

Define $S:\alpha_1=\left(\alpha_1^{(1)},\alpha_1^{(2)}\right)\to u(x_1,b)$ where u is the solution of boundary value problem (3.10). $\Gamma_1^{\delta_i}$ denotes the perturbed interface Γ_1 due to the small perturbation δ_i of $\alpha^i,\ i=1,2$. The shape derivative is defined as $D_{\alpha_1}S:=\left(\frac{\partial S}{\partial\alpha_1^{(1)}}\frac{\partial S}{\partial\alpha_1^{(2)}}\right)$, in which $\frac{\partial S}{\partial\alpha_1^{(i)}}=\lim\limits_{\delta\to0}\frac{S(\Gamma_1^{\delta_i})-S(\Gamma_1)}{\delta_i},\ i=1,2.$

Lemma 4.2.2 *The shape derivative $D_{\alpha_1}S$ exits and $\frac{\partial S}{\partial\alpha_1^{(i)}}=u_{0i}(x_1,b),\ i=1,2$, where u_{0i} solves*

$$\begin{cases}\Delta u_{0i}(\zeta;\cdot)+k_0^2\varepsilon_r u_{0i}(\zeta;\cdot)=0 \text{ in } D(\zeta)\setminus\Gamma(\zeta)\\ u_{0i}(\zeta;0,x_2)=e^{i\tau\Lambda}u_{0i}(\zeta;\Lambda,x_2),\\ u_{0i}(\zeta;x_1,f_1(x_1))=-\frac{\partial f_1}{\partial_{\alpha_1^{(i)}}}\frac{\partial u}{\partial\nu}\nu_2;\ 0\le x_1\le\Lambda,\\ \partial_{x_2}u_{0i}(\zeta;x_1,b)=T(u_{0i}(\zeta;x_1,b)),\end{cases} \tag{4.8}$$

$\nu=(\nu_1,\nu_2)^\top$ is the normal vector pointing inside D along Γ_1, u is the solution of boundary value problem (3.10)*.*

Proof. Without loss of generality, we provide the proof for $\frac{\partial S}{\partial\alpha_1^{(1)}}$. When $\alpha_1^{(1)}$ is perturbed by a small number δ, the new root mean square is $(\alpha_1^{(1)})^\delta:=\alpha_1^{(1)}+\delta$ and the new boundary is $\Gamma_1^\delta:=\{(x_1,x_2)|x_2=f_1^\delta(\zeta;x_1)\}$, where $f_1^\delta=f_1+\delta\cdot\frac{\partial f_1}{\partial\alpha_1^{(1)}}+O(\delta^2)$. Let $W(x):=\delta\cdot V(x)+$

$O(\delta^2)\cdot(0,1)^\top$ and $V(x) := [0, \frac{\partial f_1}{\partial \alpha_1^{(1)}}]^\top$, then the perturbed boundary is given by

$$\Gamma_1^\delta = \{x + W(x) | x \in \Gamma_1\} = \{x + \delta \cdot V(x) + O(\delta^2)\cdot(0,1)^\top | x \in \Gamma_1\}.$$

When Γ_1 is perturbed to be Γ_1^δ, the region D_1 becomes D_1^δ. In the new domain $D^\delta = \cup_{j=2}^{\ell} D_j \bigcup D_1^\delta$, the total field u^δ satisfies

$$\begin{cases} \Delta u^\delta(\zeta;\cdot) + k_0^2 \varepsilon_r u^\delta(\zeta;\cdot) = 0 \ in \ D^\delta \setminus \Gamma \\ u^\delta(\zeta;\Lambda, x_2) = e^{i\tau\Lambda} u^\delta(\zeta;0,x_2), \\ u^\delta(\zeta;x_1, f_1(x_1)) = 0; \ 0 \le x_1 \le \Lambda, \\ \partial_{x_2} u^\delta(\zeta;x_1,b) = T(u^\delta(\zeta;x_1,b)) + g, \end{cases} \tag{4.9}$$

By definition, we have $\dfrac{\partial S}{\partial \alpha_1^{(1)}} = \lim\limits_{\delta\to 0} \dfrac{S(\Gamma_1^\delta) - S(\Gamma_1)}{\delta}$. Denote

$$H_0^1(D^\delta) = \{u \in H^1(D^\delta) | u = 0 \ on \ \Gamma_1^\delta, u(\Lambda, x_2) = e^{i\tau\Lambda} u(0,x_2)\}.$$

The weak solution u^δ for (4.9) satisfies

$$a^\delta(u^\delta(\zeta;\cdot), w^\delta) = \langle g, w^\delta \rangle \tag{4.10}$$

for all $w^\delta \in H_0^1(D^\delta)$, where

$$a^\delta(u^\delta(\zeta;\cdot), w^\delta) = \int_{D^\delta} \nabla u^\delta(\zeta;\cdot)\cdot\nabla \bar{w}^\delta - k_0^2 \varepsilon_r u^\delta(\zeta;\cdot)\overline{w^\delta} dx - \langle T u^\delta(\zeta;\cdot), w^\delta\rangle.$$

Let us extend the definition of $W(x)$ to the closure of D_1 such that $W(x)$ is zero away from Γ_1. Then we can obtain a continuous C^2 map ψ from D to D^δ: $x = \psi(y) = x + \delta\cdot V(y) + O(\delta^2), y \in D$. Denote the inverse map of ψ as $\phi(x)$, which maps D^δ to D. Let $\tilde{u}^\delta = u^\delta(\psi(y))$, $\tilde{w}^\delta = w^\delta(\psi(y))$, then $\tilde{u}^\delta$ and $\tilde{w}$ are defined on D. It is easy to get that $\frac{\partial u^\delta}{\partial x_1} = \sum_{m=1}^2 \frac{\partial \tilde{u}^\delta}{\partial y_m}\frac{\partial \phi_m}{\partial x_1}$ where ϕ_1, ϕ_2 are the two components of ϕ. By change of variables, we

have

$$a^\delta(u^\delta(\zeta;\cdot),w^\delta)=\int_D\Big[\sum_{m,n=1}^{2}b_{mn}\frac{\partial\tilde{u}^\delta(\zeta;\cdot)}{\partial y_m}\frac{\partial\overline{\tilde{w}^\delta}}{\partial y_n}-k_0^2\varepsilon_r\tilde{u}^\delta(\zeta;\cdot)\overline{\tilde{w}^\delta}\Big]Jdy-\langle T\tilde{u}^\delta(\zeta;\cdot),\tilde{w}^\delta\rangle$$

where $J=detD\psi,\ b_{mn}=\sum_{i=1}^{2}\frac{\partial\phi_m}{\partial x_i}\frac{\partial\phi_n}{\partial x_i}$. Define a new bilinear form

$$\tilde{a}^\delta(\tilde{u}^\delta(\zeta;\cdot),w)=\int_D\Big[\sum_{m,n=1}^{2}b_{mn}\frac{\partial\tilde{u}^\delta(\zeta;\cdot)}{\partial y_m}\frac{\partial\overline{w}}{\partial y_n}-k_0^2\varepsilon_r\tilde{u}^\delta(\zeta;\cdot)\overline{w}\Big]Jdy-\langle T\tilde{u}^\delta(\zeta;\cdot),w\rangle$$

for $\tilde{u}^\delta,w\in H_0^1(D)$. Then (4.10) is equivalent to finding $\tilde{u}^\delta\in H_0^1(D)$ such that

$$\tilde{a}(\tilde{u}^\delta(\zeta;\cdot),w)=\langle g,w\rangle \tag{4.11}$$

for all $w\in H_0^1(D)$.

From (4.7) and (4.11), it is easily seen that $\tilde{u}^\delta(\zeta;\cdot)-u(\zeta;\cdot)$ satisfies

$$a(\tilde{u}^\delta(\zeta;\cdot)-u(\zeta;\cdot),w)=-(\tilde{a}^\delta(\tilde{u}^\delta(\zeta;\cdot),w)-a(\tilde{u}^\delta(\zeta;\cdot),w)). \tag{4.12}$$

For the right-hand side,

$$\begin{aligned}\tilde{a}^\delta(\tilde{u}^\delta(\zeta;\cdot),w)-a(\tilde{u}^\delta(\zeta;\cdot),w)=&\int_D\Big[\sum_{m,n=1}^{2}b_{mn}\frac{\partial\tilde{u}^\delta(\zeta;\cdot)}{\partial y_m}\frac{\partial\overline{w}}{\partial y_n}-k_0^2\varepsilon_r\tilde{u}^\delta(\zeta;\cdot)\overline{w}\Big]Jdy\\&-\int_D\nabla\tilde{u}^\delta(\zeta;\cdot)\cdot\nabla\bar{w}-k_0^2\varepsilon_r\tilde{u}^\delta(\zeta;\cdot)\bar{w}dy\end{aligned} \tag{4.13}$$

where the Jacobian matrix $J=1+\delta\nabla\cdot V+O(\delta^2)$. By direct calculation we have $(b_{mn})J=I-\delta(\tilde{b}_{mn})+O(\delta^2)$, where I is he 2×2 identity matrix. We also have

$$\tilde{b}_{mn}=\nabla V+(\nabla V)^T-(\nabla\cdot V)I. \tag{4.14}$$

Therefore we have

$$a(\tilde{u}^\delta(\zeta;\cdot)-u(\zeta;\cdot),w)=\delta\int_D\sum_{m,n=1}^{2}\tilde{b}_{mn}\frac{\partial\tilde{u}^\delta(\zeta;\cdot)}{\partial y_m}\frac{\partial\overline{w}}{\partial y_n}+k_0^2\varepsilon_r(\nabla\cdot V)u(\zeta;\cdot)\overline{w}dy+O(\delta^2). \tag{4.15}$$

Denote $u'(\zeta;\cdot) = \lim_{\delta\to 0} \dfrac{\tilde{u}^{\delta}(\zeta;\cdot) - u(\zeta;\cdot)}{\delta}$. Then $u'(\zeta;\cdot)$ satisfies the following equations on D:

$$a(u'(\zeta;\cdot), w) = \int_D \sum_{m,n=1}^{2} b_{mn} \frac{\partial \tilde{u}^{\delta}(\zeta;\cdot)}{\partial y_m} \frac{\partial \overline{w}}{\partial y_n} + k_0^2 \varepsilon_r (\nabla \cdot V) u(\zeta;\cdot)\overline{w} dy. \tag{4.16}$$

By the formula (4.14), we have

$$\begin{aligned}\sum_{m,n=1}^{2} \tilde{b}_{mn} \frac{\partial u(\zeta;\cdot)}{\partial y_m} \frac{\partial \overline{w}}{\partial y_n} =& \nabla(V \cdot \nabla \bar{w}) \cdot \nabla u(\zeta;\cdot) + \nabla(V \cdot \nabla u(\zeta;\cdot)) \cdot \nabla \bar{w} \\ & - \nabla \cdot [(\nabla u(\zeta;\cdot) \cdot \nabla \bar{w}) V].\end{aligned}$$

By Green's formula and the boundary condition $u(\zeta;\cdot) = w = 0$ on Γ_1, it is easy to get that

$$\int_{\Gamma_1} (V \cdot \nabla \bar{w}) \frac{\partial u(\zeta;\cdot)}{\partial \nu} - (\nabla u(\zeta;\cdot) \cdot \nabla \bar{w})(V \cdot \nu) ds = 0.$$

Therefore, (4.16) can be reduced to

$$\begin{aligned} a(u'(\zeta;\cdot), w) =& \int_D -\nabla(V \cdot \nabla \bar{w}) \cdot \nabla u(\zeta;\cdot) + \nabla(V \cdot \nabla u(\zeta;\cdot)) \cdot \nabla \bar{w} + k_0^2 \varepsilon_r (\nabla \cdot V) u(\zeta;\cdot)\overline{w} dy \\ & + \int_{\Gamma_1} (V \cdot \nabla \bar{w}) \frac{\partial u(\zeta;\cdot)}{\partial \nu} - (\nabla u(\zeta;\cdot) \cdot \nabla \bar{w})(V \cdot \nu) ds \\ =& \int_D k_0^2 \varepsilon_r u(\zeta;\cdot)(V \cdot \nabla \bar{w}) + \nabla(V \cdot \nabla u(\zeta;\cdot)) \cdot \nabla \bar{w} + k_0^2 \varepsilon_r (\nabla \cdot V) u(\zeta;\cdot)\overline{w} dy \\ =& \int_D \nabla(V \cdot \nabla u(\zeta;\cdot)) \cdot \bar{w} - k_0^2 \varepsilon_r (V \cdot \nabla u(\zeta;\cdot))\bar{w} dy + \int_D k_0^2 \varepsilon_r \nabla \cdot (u(\zeta;\cdot)\bar{w} V) dy. \end{aligned} \tag{4.17}$$

We obtain

$$a(u'(\zeta;\cdot), w) = \int_D \nabla(V \cdot \nabla u(\zeta;\cdot)) \cdot \nabla \bar{w} - k_0^2 \varepsilon_r (V \cdot \nabla \bar{u}(\zeta;\cdot))\bar{w} dy \text{ for any } w \in H_0^1(D) \cap H^2(D)$$

since $\int_D k_0^2 \varepsilon_r \nabla \cdot (u(\zeta;\cdot)\bar{w} V) dy = 0$ by the divergence theorem. Then u' satisfies the following boundary value problem,

$$\begin{cases} \Delta u'(\zeta;\cdot) + k_0^2 \varepsilon_r u'(\zeta;\cdot) = (\Delta + k_0^2\varepsilon_r)(V - \nabla u) \text{ in } D(\zeta) \setminus \Gamma(\zeta) \\ u'(\zeta; 0, x_2) = e^{i\tau\Lambda} u'(\zeta; \Lambda, x_2), \\ u'(\zeta; x_1, f_1(x_1)) = 0;\ 0 \le x_1 \le \Lambda, \\ \partial_{x_2} u'(\zeta; x_1, b) = T(u'(\zeta; x_1, b)). \end{cases}$$

Let $u_{01} = u' - V \cdot \nabla u$, then $u_{01} = u'$ on $x_2 = b$, and u_{01} satisfies

$$\begin{cases} \Delta u_{01}(\zeta;\cdot) + k_0^2 \varepsilon_r u_{01}(\zeta;\cdot) = 0 \text{ in } D(\zeta) \setminus \Gamma(\zeta) \\ u_{01}(\zeta; 0, x_2) = e^{i\tau\Lambda} u_{01}(\zeta; \Lambda, x_2), \\ u_{01}(\zeta; x_1, f_1(x_1)) - \frac{\partial f_1}{\partial \alpha_1^{(i)}} \frac{\partial u}{\partial \nu} \nu_2;\ 0 \le x_1 \le \Lambda, \\ \partial_{x_2} u_{01}(\zeta; x_1, b) = T(u_{01}(\zeta; x_1, b)). \end{cases}$$

With this step we finish the proof of Lemma 4.2.2. Next, let us prove formula (4.4).

From the definition of the reflectivity $R(\zeta) = \sum\limits_{n\in\mathcal{N}} \frac{\eta_n}{\eta_0} |r_n(\zeta)|^2$, we have

$$\frac{\partial R(\zeta)}{\partial \alpha_1^{(1)}} = 2 \sum_{n\in\mathcal{N}} \frac{\eta_n}{\eta_0} \Re\Big[r_n \frac{\partial \bar{r}_n}{\partial \alpha_1^{(1)}} \Big],$$

where

$$r_n(\zeta) = \begin{cases} \hat{u}_n(\zeta; b) e^{-i\eta_n b}, & n \neq 0 \\ \hat{u}_n(\zeta; b) e^{-i\rho b} - e^{-2ik_0 q_\ell b}, & n = 0. \end{cases}$$

By direct calculation, we have

$$\frac{\partial r_n(\zeta)}{\partial \alpha_1^{(1)}} = \frac{\partial \hat{u}_n(\zeta; b)}{\partial \alpha_1^{(1)}} e^{-i\eta_n b}.$$

Applying Lemma 4.2.2, we have $\dfrac{\partial u(\zeta;b)}{\partial \alpha_1^{(1)}} = \lim\limits_{\delta\to 0} \dfrac{u^{\delta}(\zeta;b) - u(\zeta;b)}{\delta} = u_0(\zeta;b)$. It follows that

$$r_n \frac{\partial \bar{r}_n}{\partial \alpha_1^{(1)}} = \begin{cases} \hat{u}_n(\zeta;b) \cdot \dfrac{1}{\Lambda} \displaystyle\int_0^{\Lambda} e^{i\kappa_n x_1} \, \overline{u_0(\zeta;x_1,b)} \, dx_1, & n \neq 0 \\ \left(\hat{u}_n(\zeta;b) - e^{-2ik_0 q_\ell b + i\rho b}\right) \cdot \dfrac{1}{\Lambda} \displaystyle\int_0^{\Lambda} e^{i\kappa_n x_1} \, \overline{u_0(\zeta;x_1,b)} \, dx_1, & n = 0. \end{cases} \tag{4.18}$$

By multiplying the partial differential equation in the adjoint problem (4.27) by $\overline{u_0(\zeta;\cdot)}$ and multiplying the complex conjugate of partial differential equation in problem (4.8) by $u_n^*(\zeta;\cdot)$, then integrating over the domain $D_j, j = 1, \cdots, \ell$ respectively. it follows that

$$\int_{D_j} (\Delta u_n^*(\zeta;\cdot) + k_0^2 \overline{\varepsilon_r} u_n^*(\zeta;\cdot)) \overline{u_0(\zeta;\cdot)} - u_n^*(\zeta;\cdot) \overline{(\Delta u_0(\zeta;\cdot) + k_0^2 \varepsilon_r u_0(\zeta;\cdot))} \, dx = 0;$$

By applying Green's formula on each $D_j,\ j = 1, .., \ell$ and adding the obtained equations together, we have

$$\begin{aligned} &- \int_0^{\Lambda} ([0, \frac{\partial f_1}{\partial \alpha_1^{(1)}}]^{\top} \cdot \nu) \left[\frac{\partial \overline{u(\zeta;\cdot)}}{\partial \nu} \cdot \frac{\partial u_n^*(\zeta;\cdot)}{\partial \nu} \right] dx_1 \\ &+ \int_0^{\Lambda} \overline{u_0(\zeta;\cdot)} \left(T^*(u_n^*(\zeta;\cdot) + e^{i\kappa_n x_1}) \right) - u_n^*(\zeta;\cdot) T(u_0(\zeta;\cdot)) dx_1 = 0. \end{aligned}$$

where we have used the boundary conditions in boundary value problem (4.27) and (4.8).

Since T^* is the adjoint operator of T, we can get

$$\int_0^{\Lambda} e^{i\kappa_n x_1} \, \overline{u_0(\zeta;x_1,b)} \, dx_1 = \int_0^{\Lambda} \frac{\partial \overline{u(\zeta;\cdot)}}{\partial \nu} \cdot \frac{\partial u_n^*(\zeta;\cdot)}{\partial \nu} \nu_2 \frac{\partial f_1}{\partial \alpha_1^{(1)}} dx_1.$$

By substituting into (4.18), we have

$$\frac{\partial R}{\partial \alpha_1^{(1)}} = \frac{2}{\Lambda} \sum_{n \in \mathcal{N}} \frac{\eta_n}{\eta_0} Re\Big[(\hat{u}_n(\zeta;b) - a_n e^{-2ik_0 q_\ell b + i\rho b}) \cdot \int_0^{\Lambda} \frac{\partial \overline{u(\zeta;\cdot)}}{\partial \nu} \cdot \frac{\partial u_n^*(\zeta;\cdot)}{\partial \nu} \nu_2 \frac{\partial f_1}{\partial \alpha_1^{(1)}} dx_1 \Big].$$

Therefore,

$$D_{\alpha_1}R = \frac{2}{\Lambda}\sum_{n\in\mathcal{N}}\frac{\eta_n}{\eta_0}Re\Big[(\hat{u}_n(\zeta;b) - a_n e^{-2ik_0q_\ell b+i\rho b})\cdot\int_0^\Lambda(\frac{\partial\overline{u(\zeta;\cdot)}}{\partial\nu}\cdot\frac{\partial u_n^*(\zeta;\cdot)}{\partial\nu}\nu_2)\cdot\nabla_{\alpha_1}f_1dx_1\Big].$$

To prove (4.5), we need to derive the perturbation of the reflectivity δR due to the perturbation of the interface by δf_j caused by the small perturbation of $\alpha_j^{(1)}$ or $\alpha_j^{(2)}$, $j = 2,\cdots,\ell$. When the interface Γ_j is perturbed to be $f_j^\delta := f_j+\delta f_j$, the permittivity becomes $\varepsilon_r^\delta := \varepsilon_r+\delta\varepsilon_r$. It is observed that for any test function $v \in L^2(D)$, the inner product

$$(v,\delta\varepsilon_r) := \int_D v(x)\,\overline{\delta\varepsilon_r}(x)\,dx = \int_{\text{symdiff}(D_j,D_j^\delta)} v(x)\,\overline{\delta\varepsilon_r}(x)\,dx.$$

Here D_j and D_j^δ are the corresponding layers with the interfaces f_j and f_2^δ, respectively, and the symmetric difference of the two sets D_2 and D_j^δ is given by

$$\text{symdiff}(D_j,D_j^\delta) = (D_j\cup D_j^\delta)\backslash(D_j\cap D_j^\delta).$$

Since the relative permittivity of the domain D_{j-1} and D_j are $\varepsilon_{r,j-1}$ and $\varepsilon_{r,j}$, respectively, the above inner product can be simplified as

$$(v,\delta\varepsilon_r) = \int_0^\Lambda v(x_1,f_j(x_1))\,\overline{(\varepsilon_{r,1}-\varepsilon_{r,2})}\cdot\delta f_j\,dx \tag{4.19}$$

for an infinitesimal δf.

Let δu denote the perturbation of the total field. As a result of perturbation analysis, δu satisfies the following equations:

$$
\begin{cases}
\Delta\delta u(\zeta;\cdot) + k_0^2\varepsilon_r\delta u(\zeta;\cdot) = -k_0^2\delta\varepsilon_r u(\zeta;\cdot) & \text{in } D(\zeta)\setminus\Gamma(\zeta) \\
\delta u(\zeta;\Lambda,x_2) = e^{i\tau\Lambda}\delta u(\zeta;0,x_2), & 0<x_2<b, \\
\delta u(\zeta;x_1,f_1(x_1)) = 0, & 0<x_1<\Lambda \\
\dfrac{\partial\delta u}{\partial x_2}(\zeta;x_1,b) = T(\delta u(\zeta;x_1,b)) & 0<x_1<\Lambda, \\
\delta u_+(\zeta;x_1,f_j(\zeta,x_1)) = \delta u_-(\zeta;x_1,f_j(\zeta,x_1)) & 0<x_1<\Lambda, \\
\partial_\nu\delta u_+(\zeta;x_1,f_j(\zeta,x_1)) = \partial_\nu\delta u_-(\zeta;x_1,f_j(\zeta,x_1)) & 0<x_1<\Lambda.
\end{cases}
\tag{4.20}
$$

By multiplying the partial differential equation in the adjoint problem (4.27) by $\overline{\delta u(\zeta;\cdot)}$ and partial differential equation in (4.20) by $\overline{u_n^*(\zeta;\cdot)}$, and integrating over the domain $D_j, j = 1,\cdots,\ell$, respectively, it follows that

$$
\begin{aligned}
&\int_{D_j} (\Delta u_n^*(\zeta;\cdot) + k_0^2\overline{\varepsilon_r}u_n^*(\zeta;\cdot))\,\overline{\delta u(\zeta;\cdot)} - u_n^*(\zeta;\cdot)\,\overline{(\Delta\delta u(\zeta;\cdot) + k_0^2\varepsilon_r\delta u(\zeta;\cdot))}\,dx \\
&= \int_{D_j} u_n^*(\zeta;\cdot)k_0^2\overline{\delta\varepsilon_r u(\zeta;\cdot)}\,dx, \quad j = 1,\cdots,\ell.
\end{aligned}
$$

Applying the Green's second identity on the left-hand sides and adding the above equations together yields

$$
\begin{aligned}
&\int_{\Gamma_j(\zeta)} (\partial_\nu u_n^*(\zeta;\cdot))_-\overline{(\delta u(\zeta;\cdot))}_- - (u_n^*(\zeta;\cdot))_-\overline{(\partial_\nu\delta u(\zeta;\cdot))}_- ds \\
&+ \int_{\Gamma_j(\zeta)} (u_n^*(\zeta;\cdot))_+\overline{(\partial_\nu\delta u(\zeta;\cdot))}_+ - (\partial_\nu u_n^*(\zeta;\cdot))_+\overline{(\delta u(\zeta;\cdot))}_+ ds \\
&+ \int_0^\Lambda e^{i\kappa_n x}\,\overline{\delta u(\zeta;x_1,b)}\,dx_1 = k_0^2\int_D \bar{\delta\varepsilon}_r u(\bar{\zeta};\cdot)u_n^*(\zeta;\cdot)\,dx,
\end{aligned}
$$

where we have used the boundary conditions in (4.27) and (4.20). By the continuity conditions along the interface $\Gamma_j(\zeta)$, this can be further reduced to the following:

$$
\int_0^\Lambda e^{i\kappa_n x}\,\overline{\delta u(\zeta;x_1,b)}\,dx_1 = k_0^2\int_D \bar{\delta\varepsilon}_r u(\bar{\zeta};\cdot)u_n^*(\zeta;\cdot)\,dx. \tag{4.21}
$$

For the cost function after perturbation $R^\delta(\zeta)$, we have

$$\begin{aligned} R^\delta(\zeta) &= \sum_{n\in\mathcal{N}} \frac{\eta_n}{\eta_0} |r_n + \delta r_n|^2 \\ &= \sum_{n\in\mathcal{N}} \frac{\eta_n}{\eta_0} \Big\{ |r_n|^2 + 2\Re[r_n \overline{\delta r_n}] + |\delta r_n|^2 \Big\} \\ &= R(\zeta, f_i) + 2\sum_{n\in\mathcal{N}} \frac{\eta_n}{\eta_0} \Re[r_n \overline{\delta r_n}] + O((\delta f_i)^2). \end{aligned}$$

The perturbation of the cost function $\delta R := R^\delta - R$ is given by

$$\delta R = 2\sum_{n\in\mathcal{N}} \frac{\eta_n}{\eta_0} \Re[r_n \overline{\delta r_n}] + O((\delta f_i)^2). \tag{4.22}$$

For each term $r_n\overline{\delta r_n}$, by virtue of (3.12), it follows that

$$r_n\overline{\delta r_n} = \begin{cases} \hat{u}_n(\zeta; b) \cdot \dfrac{1}{\Lambda}\displaystyle\int_0^\Lambda e^{i\kappa_n x_1}\, \overline{\delta u(\zeta; x_1, b)}\, dx_1, & n \neq 0 \\ \big(\hat{u}_n(\zeta; b) - e^{-2ik_0 q_\ell b + i\rho b}\big) \cdot \dfrac{1}{\Lambda}\displaystyle\int_0^\Lambda e^{i\kappa_n x_1}\, \overline{\delta u(\zeta; x_1, b)}\, dx_1, & n = 0. \end{cases} \tag{4.23}$$

Therefore, by substituting (4.21), we have

$$r_n\overline{\delta r_n} = \begin{cases} \hat{u}_n(\zeta; b) \cdot \dfrac{k_0^2}{\Lambda}\displaystyle\int_D \bar{\delta\varepsilon}_r \bar{u} u_n^*\, dx, & n \neq 0, \\ \big(\hat{u}_n(\zeta; b) - e^{-2ik_0 q_\ell b + i\rho b}\big) \cdot \dfrac{k_0^2}{\Lambda}\displaystyle\int_D \bar{\delta\varepsilon}_r \bar{u} u_n^*\, dx, & n = 0. \end{cases} \tag{4.24}$$

The perturbation of the reflectivity is expressed by

$$\delta R = \frac{2k_0^2}{\Lambda} \sum_{n\in\mathcal{N}} \frac{\eta_n}{\eta_0} \Re\Big[(\hat{u}_n(\zeta; b) - \alpha_n e^{-2ik_0 q_\ell b + i\rho b}) \cdot \int_D \bar{\delta\varepsilon}_r \bar{u} u_n^*\, dx \Big] + O(\delta f^2).$$

Due to equation (4.19), we get

$$\delta R = \frac{2k_0^2}{\Lambda} \sum_{n\in\mathcal{N}} \frac{\eta_n}{\eta_0} \Re\Big[(\hat{u}_n(\zeta; b) - \alpha_n e^{-2ik_0 q_\ell b + i\rho b}) \cdot \overline{(\varepsilon_{r,1} - \varepsilon_{r,2})} \cdot \int_0^\Lambda [\bar{u} u_n^*]|_{(x_1, f_j)} \cdot \delta f_j\, dx_1 \Big] + O(\delta f^2).$$

The desired formula (4.4) for $\nabla_{\alpha_j} R,\ j = 2, \cdots, \ell$ then follows by the chain rule.

4.3 Computation of the gradient for transverse magnetic polarization

The gradient of the interface for transverse magnetic polarization can be obtained analogously with the change of the continuity condition with transverse electric polarization. For simplicity, we assume the domain D has two layers D_1 on bottom and D_2 on top. We restrict the discussion of the optimal design under the normal incidence. The random structure is illuminated by an incident time-harmonic plane wave $u^i = e^{ik_0 q_2 d\cdot x}$, where k_0 is the free-space wavenumber, $q_2\,(:=\sqrt{\varepsilon_{r,2}})$ is the refractive index of the D_2 layer. Denote the interface between D_1 and D_2 as $\Gamma(\zeta) = \{(x_1, x_2)|x_2 = h(\zeta; x_1)\}$.

Theorem 4.3.1 *For each sample ζ, the gradient $\nabla_\alpha R$ for the formula defined in* (3.11) *can be expressed as*

$$\nabla_\alpha R = \frac{2}{\Lambda}\sum_{n\in N}\frac{\eta_n}{\eta_0}\mathbf{Re}[(\hat{u}_n(\zeta;b) - a_n e^{-ikb})\overline{(\varepsilon_{r,j-1}^{-1} - \varepsilon_{r,j}^{-1})}\cdot\int_0^\Lambda [W(x_1, h(x_1))\cdot\nabla_\alpha h dx_1]. \quad (4.25)$$

where

$$W(x, h(x)) := \begin{cases} \lim\limits_{\substack{(x_1,x_2)\to(x_1,h(x_1)),\\ (x_1,x_2)\in D_2}} \nabla u(x_1, x_2)\bar{u_n^*}(x_1, x_2),\ \nabla_\alpha h \textit{ point to } D_2 \\ \lim\limits_{\substack{(x_1,x_2)\to(x_1,h(x_1)),\\ (x_1,x_2)\in D_1}} \nabla u(x_1, x_2)\bar{u_n^*}(x_1, x_2),\ \nabla_\alpha h \textit{ point to } D_1 \end{cases} \quad (4.26)$$

$a_0 = 1$ and $a_n = 0 (n \neq 0)$, u is the solution of the scattering problem (3.10)*, and u_n^* is the solution of the following adjoint problem*

$$\begin{cases} \nabla(\varepsilon_r^{-1}\nabla u_n^*(\zeta;\cdot) + k_0^2 u_n^*(\zeta;\cdot) = 0 & \textit{in } D(\zeta)\backslash\Gamma(\zeta), \\ u_n^*(\zeta; 0, x_2) = u_n^*(\zeta; \Lambda, x_2), & 0 < x_2 < b, \\ \partial_\nu u_n^*(\zeta; x_1, 0) = 0, & 0 < x_1 < \Lambda, \\ \dfrac{\partial u_n^*}{\partial x_2}(\omega; x_1, b) = T^*(u_n^*(\omega; x_1, b)) + e^{i\kappa_n x} & 0 < x_1 < \Lambda, \\ (u_n^*)_+(\zeta; x_1, h(\zeta, x_1)) = (u_n^*)_-(\zeta; x_1, h(\zeta, x_1)) & 0 < x_1 < \Lambda, \\ \varepsilon_{r,2}^{-1}(\partial_\nu u_n^*)_+(\zeta; x_1, h(\zeta, x_1)) = \varepsilon_{r,1}^{-1}(\partial_\nu u_n^*)_-(\zeta; x_1, h(\zeta, x_1)) & 0 < x_1 < \Lambda. \end{cases} \quad (4.27)$$

Where T^* is the adjoint operator of T,

$$\langle Tu, v\rangle = \langle u, T^*v\rangle$$

Note that both ε_r and $\nabla u \nabla u_n^*$ attain jumps across the interface $\Gamma(\zeta)$. Denote $\nabla_\alpha h$ is the gradient of h with respect to α.

Denote $H^1(D) = \{u(x,y) | (\int_D |f(x)|^2 dx)^{\frac{1}{2}} < \infty,\ (\int_D |f'(x)|^2 dx)^{\frac{1}{2}} < \infty$ and $u(0,y) = u(\Lambda, y)\}$. The variational formula for (3.10) is $a(u,v) := \langle g, v\rangle,\ \forall v \in H^1(D)$, where

$$a(u,v) = \int_D \varepsilon_r^{-1} \nabla u \cdot \nabla \bar{v} - k_0^2 u \bar{v} d\mathbf{x} - \langle Tu, v\rangle. \tag{4.28}$$

Similarly, the variational formulation for (4.27) is denoted as $a^*(u_n^*, v) := \langle e^{i\kappa_n x}, v\rangle,\ \forall v \in H^1(D)$, where

$$a^*(u_n^*, v) = \int_D \varepsilon_r^{-1} \nabla u_n^* \cdot \nabla \bar{v} - k_0^2 u \bar{v} d\mathbf{x} - \langle T^* u_n^*, v\rangle. \tag{4.29}$$

With regard to the shape derivative $\nabla_\alpha R$, we know that the change of the reflectivity δR is caused by the change δh of the random surface h. If the interface $\Gamma = (x_1, h(x_1))$ is perturbed to be $\Gamma^\delta = (x_1, h^\delta(x_1))$. For the perturbed interface $\Gamma^\delta = (x_1, h^\delta(x_1))$, denote the total field as u^δ and the relative permittivity as ε_r^δ. The corresponding variation problem is $a^\delta(u^\delta, v) := \langle g, v\rangle,\ \forall v \in H^1(D)$, where

$$a^\delta(u,v) = \int_D (\varepsilon_r^\delta)^{-1} \nabla u^\delta \cdot \nabla \bar{v} - k_0^2 u^\delta \bar{v} d\mathbf{x} - \langle Tu^\delta, v\rangle. \tag{4.30}$$

Let $\delta u = u^\delta - u$ and $(\delta\varepsilon_r)^{-1} = (\varepsilon_r^\delta)^{-1} - \varepsilon_r^{-1}$, form (4.28) and (4.30) we have

$$\int_D \varepsilon_r^{-1} \nabla \delta u \cdot \nabla \bar{v} - k_0^2 \delta u \bar{v} d\mathbf{x} - \langle T\delta u, v\rangle = -\int_D (\delta\varepsilon_r)^{-1} \nabla u^\delta \nabla \bar{v} d\mathbf{x} \tag{4.31}$$

Setting $v = \delta u$ in (4.29) and $v = u_n^*$ in (4.31) leads to

$$\begin{cases} \int_D \varepsilon_r^{-1} \nabla u_n^* \nabla \overline{\delta u} - k_0^2 u_n^* \delta u d\mathbf{x} - \langle T^* u_n^*, \delta u\rangle = \langle e^{i\kappa_n x}, \delta u\rangle \\ \int_D \varepsilon_r^{-1} \nabla \delta u \nabla \overline{u_n^*} - k_0^2 \delta u \overline{u_n^*} d\mathbf{x} - \langle T\delta u, u_n^*\rangle = -\int_D (\delta\varepsilon_r)^{-1} \nabla u^\delta \nabla \overline{u_n^*} d\mathbf{x} \end{cases} \tag{4.32}$$

Therefore, we have

$$\langle e^{i\kappa_n x}, \delta u\rangle = -\int_D (\overline{\delta\varepsilon_r})^{-1}\nabla u^\delta \nabla \overline{u_n^*} d\mathbf{x} \tag{4.33}$$

$$= -\int_D (\overline{\delta\varepsilon_r})^{-1}\nabla u \nabla \overline{u_n^*} d\mathbf{x} + O(\|(\delta\varepsilon_r)^{-1}\| \cdot \|\delta u\|) \tag{4.34}$$

For any test function $v \in H^1(D)$, there is an inner product,

$$(v, (\delta\varepsilon_r)^{-1}) := \int_D v(x)\overline{(\delta\varepsilon_r(x_1))^{-1}} = \int_{\text{symdiff}(D_1, D_1^\delta)} v(x_1)\overline{(\delta\varepsilon_r(x_1))^{-1}} dx_1 \tag{4.35}$$

Here D_1 and D_1^δ are the absorbing layers corresponding to the interface h and h^δ, respectively, and the symmetric difference between the two regions can be expressed as,

$$\text{symdiff}(D_1, D_1^\delta) = (D_1 \cup D_1^\delta) \setminus (D_1 \cap D_1^\delta).$$

It is known that the relative permittivity value of the absorption layer and the TCO layer are $\varepsilon_{r,1}$ and $\varepsilon_{r,2}$,respectively. For an infinitesimal interface disturbance δh, the inner product can be simplified to

$$(v, (\delta\varepsilon_r)^{-1}) = \int_0^\Lambda v(x_1, h(x_1))(\overline{\varepsilon_{r,1}^{-1} - \varepsilon_{r,2}^{-1}})\delta h dx \tag{4.36}$$

For the new interface h^δ, the reflectivity at the sample ω is

$$\begin{aligned} R^\delta(\omega, h) &= \sum_{n\in\mathcal{N}} \frac{\eta_n}{\eta_0}\|r_n + \delta r_n\|^2 \\ &= \sum_{n\in\mathcal{N}} \frac{\eta_n}{\eta_0}\Big\{\|r_n\|^2 + 2Re[r_n\overline{\delta r_n}] + \|\delta r_n\|^2\Big\} \\ &= R(\omega, h) + 2\sum_{n\in\mathcal{N}} \frac{\eta_n}{\eta_0} Re[r_n\overline{\delta r_n}] + O(\delta h^2). \end{aligned}$$

We can get the influence of the disturbance $\delta R := R^\delta - R$ of the random surface h on the scattering rate is,

$$\delta R = 2\sum_{n\in N} \frac{\eta_n}{\eta_0} Re[r_n\overline{\delta r_n}] + o(\delta h^2)$$

With regard to the item $r_n\overline{\delta r_n}$ can be expressed as,

$$r_n\overline{\delta r_n} = \begin{cases} \hat{u}_n(\omega;b)\cdot\dfrac{1}{\Lambda}\displaystyle\int_0^\Lambda e^{i\kappa_n x}\,\overline{\delta u(\omega;x,b)}\,dx, & n\neq 0 \\ \left(\hat{u}_n(\omega;b)-e^{-ikb}\right)\cdot\dfrac{1}{\Lambda}\displaystyle\int_0^\Lambda e^{i\kappa_n x}\,\overline{\delta u(\omega;x,b)}\,dx, & n=0. \end{cases}$$

Since

$$\int_0^\Lambda e^{i\kappa_n x}\,\overline{\delta u(\zeta;x,b)} = -\int_D \overline{(\delta\varepsilon_r)^{-1}\nabla u\nabla\overline{u_n^*}}d\mathbf{x} + O(\|(\delta\varepsilon_r)^{-1}\|\cdot\|\delta u\|)$$

Substitute formula (4.36), it can be obtained by calculation from (4.33)

$$r_n\overline{\delta r_n} = \hat{u}_n(\zeta;b)\cdot\frac{1}{\Lambda}\overline{(\varepsilon_{r,1}^{-1}-\varepsilon_{r,2}^{-1})}\cdot\int_0^\Lambda[W(x_1,h(x_1))\cdot\delta h dx_1] + O(\|(\delta\varepsilon_r)^{-1}\|\cdot\|\delta u\|), n\neq 0;$$

$$\begin{aligned} r_n\overline{\delta r_n} =&(\hat{u}_n(\zeta;b)-e^{-ikb})\cdot\frac{1}{\Lambda}\overline{(\varepsilon_{r,1}^{-1}-\varepsilon_{r,2}^{-1})}\cdot\int_0^\Lambda[W(x_1,h(x_1))\cdot\delta h dx_1] \\ &+O(\|(\delta\varepsilon_r)^{-1}\|\cdot\|\delta u\|),\ n=0. \end{aligned}$$

where

$$W(x_1,h(x_1)) := \begin{cases} \lim\limits_{(x_1,x_2)\to(x_1,h(x_1))}\nabla u(x_1,x_2)\bar{u}_n^*(x_1,y_2),\ \delta h>0, \\ \lim\limits_{(x_1,x_2)\to(x_1,h(y_1))}\nabla u(x_1,y_1)\bar{u}_n^*(x_1,x_2),\ \delta h<0. \end{cases} \tag{4.37}$$

Finally, the disturbance of the scattering rate can be expressed as

$$\begin{aligned} \delta R =&\frac{2}{\Lambda}\sum\frac{\eta_n}{\eta_0}Re[(\hat{u_n}(\zeta;b)-a_n e^{-ikb})\cdot\overline{(\varepsilon_{r,1}^{-1}-\varepsilon_{r,2}^{-1})}\cdot\int_0^\Lambda[W(x_1,h(x_1))\cdot\delta h dx_1] \\ &+O(\|(\delta\varepsilon_r)^{-1}\|\cdot\|\delta u\|)], \end{aligned}$$

By chain rule, we have

$$\nabla_\alpha R = \frac{2}{\Lambda}\sum_{n\in\mathcal{N}}\frac{\eta_n}{\eta_0}\mathrm{Re}[(\hat{u}_n(\zeta;b)-a_n e^{-ikb})\overline{(\varepsilon_{r,1}^{-1}-\varepsilon_{r,2}^{-1})}\cdot\int_0^\Lambda[W(x_1,h(x_1))\cdot\nabla_\alpha h dx_1].$$

The proof for theorem (4.3.1) is done.

4.4 Convergence for the stochastic gradient descent algorithm

In what follows, we use ∇ and ∇^2 to denote the gradient and the Hessian of a function with respect to $\boldsymbol{\alpha}$, respectively. Let C denote generic constant. In this section, we examine the convergence of the stochastic gradient algorithm for solving the optimization problem (3.2). Let us focus the case when the random variables $\{\xi_{j,m}\}_{m=0}^{M}$ in the Karhunen–Loève expansion (2.34) are uniformly distributed over $[-0.5, 0.5]$. We also assume that the iteration sequence $\{\boldsymbol{\alpha}^{(n)}\}_{n=1}^{\infty}$ is bounded in the closed region $U_{\boldsymbol{\alpha}} = \Big([0, a] \times [b, \Lambda]\Big)^{\ell}$, where a, b are positive constants.

From (2.34) , we see that

$$\frac{\partial f_j(\zeta; x_1)}{\partial \alpha_j^{(1)}} = \bar{f}_j(\zeta; x_1), \tag{4.38}$$

which is bounded when $\alpha^{(1)} \in [0, a]$. Since $f_j(x_1)$ is smooth, it can be shown that

$$\begin{aligned}\frac{\partial f_j(\zeta; x_1)}{\partial \alpha_j^{(2)}} =& \frac{\lambda_0'}{2\sqrt{\lambda_0}}\xi_{j_0}(\zeta)\sqrt{\frac{1}{\Lambda}} \\ &+ \sum_{m=1}^{M} \frac{\lambda_{jm}'}{2\sqrt{\lambda_{jm}}}\left[\xi_{m,s}(\zeta)\sqrt{\frac{2}{\Lambda}}\sin\left(\frac{2m\pi x_1}{\Lambda}\right) + \xi_{m,c}(\zeta)\sqrt{\frac{2}{\Lambda}}\cos\left(\frac{2m\pi x_1}{\Lambda}\right)\right],\end{aligned} \tag{4.39}$$

where $\lambda_{jm}' = \dfrac{\partial \lambda_{jm}}{\partial \alpha_j^{(2)}}$ and $\lambda_{jm}' = \dfrac{(\alpha^{(1)})^2 \Lambda \widehat{c_{jm}'}}{2}, \quad m = 0, 1, 2, \cdots$, and $\widehat{c_{jm}'}$ is the Fourier cosine expansion coefficients of the covariance operator

$$K'\varphi(x_1) := \int_0^{\Lambda} \frac{\partial c_j(x_1 - \tilde{x}_1)}{\partial \alpha_j^{(2)}}\, \varphi(\tilde{x}_1) d\tilde{x}_1.$$

By direct calculation, we have $\dfrac{\partial c_j(x_1)}{\partial \alpha_j^{(2)}} = \dfrac{2}{(\alpha_j^{(2)})^3} x_1^2 exp\Big(-\dfrac{x_1^2}{(\alpha_j^{(2)})^2}\Big)$. Since $\dfrac{\partial c_j(x_1)}{\partial \alpha_j^{(2)}}$ is smooth and bounded when $\alpha_j^{(2)} \in [b, \Lambda]$, we have $\dfrac{\lambda_{j_m}'}{\sqrt{\lambda_{j_m}}}$ converges to 0 exponentially. $\dfrac{\partial f_j(\zeta; x_1)}{\partial \alpha_j^{(2)}}$ is bounded since the right hand of (4.39) convergent. In the same way, we have $\dfrac{\partial^2 f_j}{\partial (\alpha_j^{(1)})^2}$ and $\dfrac{\partial^2 f_j}{\partial (\alpha_j^{(2)})^2}$ are also bounded.

Lemma 4.4.1 *For fixed sample ζ, $\dfrac{\partial^2 R(\zeta;\alpha)}{\partial(\alpha_j^{(1)})^2}$, $\dfrac{\partial^2 R(\zeta;\alpha)}{\partial\alpha_j^{(2)}\partial\alpha_j^{(1)}}$ and $\dfrac{\partial^2 R(\zeta;\alpha)}{\partial(\alpha_j^{(2)})^2}$ are uniformly bounded on $U_{\boldsymbol{\alpha}}$, $j=1,\cdots,\ell$.*

Proof. Let $\delta u := u^\delta - u$ denote the perturbation of the total field due to the perturbation of the interface $f_j^\delta = f_j + \delta f_j,\ j=2,\cdots,\ell$. By the perturbation analysis, δu satisfies (4.20). Recall that for $j=2,\cdots,\ell$,

$$\begin{aligned}\partial_{\alpha_j^{(1)}} R(\zeta;\alpha) = \frac{2k_0^2}{\Lambda}\sum_{n\in\mathcal{N}}\frac{\eta_n}{\eta_0} Re\big[(\hat{u}_n(\zeta;b) - a_n e^{-ik_0 q_\ell b})\cdot\overline{(\varepsilon_{r,j}-\varepsilon_{r,j-1})} \\ \cdot\int_0^\Lambda [\bar{u}u_n^*]|_{(x_1,f_j)}\cdot\partial_{\alpha_j^{(1)}} f_j dx_1\big],\ j=2,3,\cdots,\ell.\end{aligned} \tag{4.40}$$

By the chain rule, we have

$$\begin{aligned}\frac{\partial^2 R(\zeta;\alpha)}{\partial(\alpha_j^{(1)})^2} =& \frac{2k_0^2}{\Lambda}\sum_{n\in\mathcal{N}}\frac{\eta_n}{\eta_0} Re[\partial_{\alpha_j^{(1)}}\hat{u}_n(\zeta;b)\cdot\overline{(\varepsilon_{r,j}-\varepsilon_{r,j-1})}\cdot\int_0^\Lambda [\bar{u}u_n^*]|_{(x_1,f_j)}\cdot\partial_{\alpha_j^{(1)}} f_j dx_1 \\ &+ (\hat{u}_n(\zeta;b) - a_n e^{-ik_0 q_\ell b})\cdot\overline{(\varepsilon_{r,j}-\varepsilon_{r,j-1})}\cdot\partial_{\alpha_j^{(1)}}\int_0^\Lambda [\bar{u}u_n^*]|_{(x_1,f_j)}\cdot\partial_{\alpha_j^{(1)}} f_j dx_1.\end{aligned} \tag{4.41}$$

We have that $\partial_{\alpha_j^{(1)}}\hat{u}_n(\zeta;b)\cdot\overline{(\varepsilon_{r,j}-\varepsilon_{r,j-1})}\cdot\int_0^\Lambda[\bar{u}u_n^*]|_{(x_1,f_j)}\cdot\partial_{\alpha_j^{(1)}} f_j dx_1$ is uniformly bounded since $\partial_{\alpha_j^{(1)}} f_j$ and $\partial_{\alpha_j^{(1)}}\hat{u}_n(\zeta;b)$ are uniformly bounded. On the other hand,

$$\begin{aligned}&\partial_{\alpha_j^{(1)}}\int_0^\Lambda [\bar{u}u_n^*]|_{(x_1,f_j)}\cdot\partial_{\alpha_j^{(1)}} f_j dx_1 \\ =&\lim_{\delta\to0}\frac{1}{\delta}\Big[\int_0^\Lambda [\bar{u}^\delta u_n^{*\delta}]|_{(x_1,f_j^\delta)}\cdot\partial_{\alpha_j^{(1)}} f_j^\delta dx_1 - \int_0^\Lambda [\bar{u}u_n^*]|_{(x_1,f_j)}\cdot\partial_{\alpha_j^{(1)}} f_j dx_1\Big] \\ =&\lim_{\delta\to0}\frac{1}{\delta}\Big[\int_0^\Lambda [\bar{u}^\delta u_n^{*\delta}]|_{(x_1,f_j^\delta)}\cdot\partial_{\alpha_i^{(1)}} f_i^\delta dx_1 - \int_0^\Lambda [\bar{u}u_n^*]|_{(x_1,f_j)}\cdot\partial_{\alpha_j^{(1)}} f_j^\delta dx_1\Big] \\ &+\lim_{\delta\to0}\frac{1}{\delta}\Big[\int_0^\Lambda [\bar{u}u_n^*]|_{(x_1,f_j)}\cdot\partial_{\alpha_j^{(1)}} f_j^\delta dx_1 - \int_0^\Lambda [\bar{u}u_n^*]|_{(x_1,f_j)}\cdot\partial_{\alpha_j^{(1)}} f_j dx_1\Big].\end{aligned}$$

For the first limit above, we have

$$\begin{aligned}
&\lim_{\delta\to 0}\frac{1}{\delta}\Big[\int_0^{\Lambda}[\bar{u}^{\delta}u_n^{*\delta}]|_{(x_1,f_j^{\delta})}\cdot\partial_{\alpha_j^{(1)}}f_j^{\delta}dx_1-\int_0^{\Lambda}[\bar{u}u_n^{*}]|_{(x_1,f_j)}\cdot\partial_{\alpha_j^{(1)}}f_j^{\delta}dx_1\Big]\\
=&\lim_{\delta\to 0}\frac{1}{\delta}\Big[\int_0^{\Lambda}([\bar{u}^{\delta}u_n^{*\delta}]|_{(x_1,f_j^{\delta})}-[\bar{u}u_n^{*}]|_{(x_1,f_j)})\cdot\partial_{\alpha_j^{(1)}}f_j^{\delta}dx_1\Big]\\
=&\lim_{\delta\to 0}\frac{1}{\delta}\Big[\int_0^{\Lambda}([\bar{u}^{\delta}u_n^{*\delta}]|_{(x_1,f_j^{\delta})}-[\bar{u}u_n^{*\delta}]|_{(x_1,f_j)}+[\bar{u}u_n^{*\delta}]|_{(x_1,f_j)}-[\bar{u}u_n^{*}]|_{(x_1,f_j)})\cdot\partial_{\alpha_j^{(1)}}f_j^{\delta}dx_1\Big].
\end{aligned}$$

By definition of δu, we have

$$\lim_{\delta\to 0}\frac{1}{\delta}\Big[\int_0^{\Lambda}([\bar{u}^{\delta}u_n^{*\delta}]|_{(x_1,f_j^{\delta})}-[\bar{u}u_n^{*\delta}]|_{(x_1,f_j)})\partial_{\alpha_j^{(1)}}f_j^{\delta}dx_1\Big]=\lim_{\delta\to 0}\frac{1}{\delta}\int_0^{\Lambda}[\bar{\delta u}u_n^{*\delta}]|_{(x_1,f_j^{\delta})}\partial_{\alpha_j^{(1)}}f_j^{\delta}dx_1].$$

From equation (4.20), there exists a constant C such that $\|\delta u\|_{L^2(D)}<C\|k_0^2\delta\varepsilon_r u(\zeta;\cdot)\|_{L^2(D)}$.

$$\begin{aligned}
\|\delta\varepsilon_r u(\zeta;\cdot)\|_{L^2(D)}&=\Big[\int_D|\delta\varepsilon_r u|^2dx\Big]^{1/2}=\Big[\int_{\text{symdiff}(D_j,D_j^{\delta})}|\delta\varepsilon_r u|^2dx\Big]^{1/2}\\
&\le|\delta|\Big[\int_0^{\Lambda}|u(x_1,f_j(x_1))|^2|\varepsilon_{r,j}-\varepsilon_{r,j-1}|^2\|\max(\nabla f_j(x_1))dx_1\Big]^{1/2}.
\end{aligned}$$

Since f_j is smooth, there exists a constant C such that

$$\Big|\lim_{\delta\to 0}\frac{1}{\delta}\Big[\int_0^{\Lambda}[\bar{\delta u}u_n^{*\delta}]|_{(x_1,f_j^{\delta})}\partial_{\alpha_j^{(1)}}f_j^{\delta}dx_1\Big]\Big|<C,$$

Then, it follows,

$$\Big|\int_0^{\Lambda}([\bar{u}^{\delta}u_n^{*\delta}]|_{(x_1,f_j^{\delta})}-[\bar{u}u_n^{*\delta}]|_{(x_1,f_j)})\partial_{\alpha_i^{(1)}}f_j^{\delta}dx_1\Big|<C$$

In the same way, we have that

$$\Big|\lim_{\delta\to 0}\frac{1}{\delta}\Big[\int_0^{\Lambda}([\bar{u}u_n^{*\delta}]|_{(x_1,f_j)}-[\bar{u}u_n^{*}]|_{(x_1,f_j)})\cdot\partial_{\alpha_j^{(1)}}f_j^{\delta}dx_1\Big]\Big|<C.$$

Then we have

$$\left|\partial_{\alpha_j^{(1)}}\int_0^{\Lambda}[\bar{u}u_n^*]|_{(x_1,f_j)}\cdot\partial_{\alpha_i^{(1)}}f_j dx_1\right|<C. \tag{4.42}$$

From equation (4.41) and the inequalities above, we see that $\dfrac{\partial^2 R}{\partial(\alpha_j^{(1)})^2}$ is bounded. Similarly, we can prove that $\dfrac{\partial^2 R(\zeta;\alpha)}{\partial(\alpha_j^{(2)})^2}$, $\dfrac{\partial^2 R(\zeta;\alpha)}{\partial\alpha_j^{(2)}\partial\alpha_j^{(1)}}$ are bounded when $(\alpha_j^{(1)},\alpha_j^{(2)})\in[0,\sigma]\times[\ell,\Lambda]$ $j=2,3,\cdots,l$.

The derivative on along the bottom Γ_1 also exists:

$$\partial_{\alpha_1^{(1)}}R(\zeta;\alpha)=\frac{2}{\Lambda}\sum_{n\in\mathcal{N}}\frac{\eta_n}{\eta_0}Re[(\hat{u}_n(\zeta;b)-a_n e^{-2ik_0q_\ell b+i\rho b})\cdot\int_0^{\Lambda}\frac{\partial\bar{u}}{\partial\nu}\frac{\partial u_n^*}{\partial\nu}\cdot\partial_{\alpha_1^{(1)}}f_1(x_1)\nu_2 dx_1]. \tag{4.43}$$

By chain rule, we have

$$\begin{aligned}\frac{\partial^2 R(\zeta;\alpha)}{\partial(\alpha_1^{(1)})^2}=&\frac{2}{\Lambda}\sum_{n\in\mathcal{N}}\frac{\eta_n}{\eta_0}Re[\frac{\partial}{\partial\alpha_1^{(1)}}\hat{u}_n(\zeta;b)\cdot\int_0^{\Lambda}\frac{\partial\bar{u}}{\partial\nu}\frac{\partial u_n^*}{\partial\nu}\cdot\partial_{\alpha_1^{(1)}}f_1(x_1)\nu_2 dx_1\\&+(\hat{u}_n(\zeta;b)-a_n e^{-2ik_0q_\ell b+i\rho b})\cdot\int_0^{\Lambda}\frac{\partial\bar{u}}{\partial\nu}\frac{\partial u_n^*}{\partial\nu}\cdot\frac{\partial^2}{\partial(\alpha_1^{(1)})^2}f_1(x_1)\nu_2 dx_1\\&+(\hat{u}_n(\zeta;b)-a_n e^{-2ik_0q_\ell b+i\rho b})\cdot\int_0^{\Lambda}\frac{\partial}{\partial\alpha_1^{(1)}}(\frac{\partial\bar{u}}{\partial\nu}\frac{\partial u_n^*}{\partial\nu})\cdot\partial_{\alpha_1^{(1)}}f_1(x_1)\nu_2 dx_1].\end{aligned}$$

Since $\dfrac{\partial u}{\partial\nu}$, $\dfrac{\partial u_n^*}{\partial\nu}$, $\partial_{\alpha_1^{(1)}}f_1$ are continuous with respect to $\alpha_1^{(1)}$ when $\alpha_j^{(1)}\in[0,a]$ and $\dfrac{\partial\hat{u}_n}{\partial\alpha_1^{(1)}}$ is bounded, we have $\dfrac{\partial^2 R(\zeta;\alpha)}{\partial(\alpha_1^{(1)})^2}$ is bounded. Similarly, $\dfrac{\partial^2 R(\zeta;\alpha)}{\partial(\alpha_1^{(2)})^2}$, $\dfrac{\partial^2 R(\zeta;\alpha)}{\partial\alpha_1^{(2)}\partial\alpha_1^{(1)}}$ are bounded.

Theorem 4.4.2 *Assume that the sequence $\{\alpha^{(n)}\}_{n=1}^{\infty}$ is uniformly bounded in the closed region $U_{\boldsymbol{\alpha}}$. For the iteration, $\alpha^{(n+1)}=\alpha^{(n)}-h_n\nabla R(\alpha^{(n)},\zeta_n)$ with the diminishing step size, that is, $\sum_{n=1}^{\infty}h_n=\infty$ and $\sum_{n=1}^{\infty}h_n^2<\infty$. We have $E[\|\nabla Q(\alpha^{(n)})\|_2^2]\to 0$ as $n\to\infty$,*

Proof. From (4.38) and (4.39), it follows that

$$E\left[\|\frac{\partial f_j(\zeta;x_1)}{\partial\alpha_j^{(1)}}\|^2_{L^2([0,\lambda])}\right]<C\sum_{m=0}^{M}\|\overline{\Lambda}_{jm}\|^2<C, \tag{4.44}$$

$$E\left[\|\frac{\partial f_j(\zeta;x_1)}{\partial \alpha_j^{(2)}}\|^2_{L^2([0,\lambda])}\right] < C\sum_{m=1}^{M}\|\frac{\Lambda'_{j_m}}{2\sqrt{\lambda_{j_m}}}\|^2 < C. \tag{4.45}$$

Therefore, $E\left[\|\nabla_{\alpha_j} f_j(\zeta;x_1)\|_2^2\right] < C,\ j=1,\cdots,\ell$. Let $p(y_1,\cdots,y_M)$ be the joint probability density function of the multivariate random variable $(\xi_1,\cdots,\xi_M)$. Therefore, from the continuous dependence of the solution of the boundary value problem (3.10) on the interfaces, u can be viewed as a continuous function of random variables $(\xi_1,\cdots,\xi_M)$. Therefore,

$$\begin{aligned}
&E\left[\|u(\xi_1,\cdots,\xi_M)\|^2_{L^2(D)}\right]\\
=&\int_\Omega \|u(\xi_1,\cdots,\xi_M)\|^2_{L^2(D)}dP(\xi_1,\cdots,\xi_M)\\
=&\int_{R^M} \|u(y_1,\cdots,y_M)\|^2_{L^2(D)}p(y_1,\cdots,y_M)dx_1\cdots dy_M\\
=&\int_{[-0.5,0.5]^M} \|u(y_1,\cdots,y_M)\|^2_{L^2(D)}p(y_1,\cdots,y_M)dy_1\cdots dy_M\\
<&C.
\end{aligned} \tag{4.46}$$

Similarly, we have

$$E\left[\|u_n^*\|^2_{L^2(D)}\right] < C,\ E\left[\|\frac{\partial u}{\partial \nu}\|^2_{L^2(\Gamma_1)}\right] < C \text{ and } E\left[\|\frac{\partial u_n^*}{\partial \nu}\|^2_{L^2(\Gamma_1)}\right] < C. \tag{4.47}$$

From Theorem 4.2.1, we have

$$\begin{aligned}
E\left[\|D_{\alpha_1}R(\zeta)\|_2^2\right] &\le C\max_{n\in\mathcal{N}} E\left[\|\hat{u}_n(\zeta;b)+\int_0^\Lambda(\frac{\partial\bar{u}}{\partial\nu}\cdot\frac{\partial u_n^*}{\partial\nu}\nu_2)\cdot\nabla_{\alpha_1}f_1dx_1\|_2^2\right]\\
&\le C\max_{n\in\mathcal{N}}\left[E\left[|\hat{u}_n(\zeta;b)|^2\right]+E\big[\|\int_0^\Lambda(\frac{\partial\bar{u}}{\partial\nu}\frac{\partial u_n^*}{\partial\nu}\nu_2)\cdot\nabla_{\alpha_1}f_1dx_1\|_2^2\big]\right]
\end{aligned}$$

By (4.45)(4.46)(4.47), and the Cauchy Schwartz inequality, we have $E\left[\|D_{\alpha_1}R(\zeta)\|_2^2\right] \le C$. Similarly,

$$\begin{aligned}
E\left[\|D_{\alpha_j}R(\zeta)\|_2^2\right] &\le C\max_{n\in\mathcal{N}} E\left[\|\hat{u}_n(\zeta;b)+\int_0^\Lambda[\bar{u}u_n^*]|_{(x_1,f_j)}\cdot\nabla_{\alpha_j}f_jdx_1\|_2^2\right]\\
&\le C\max_{n\in\mathcal{N}}\left[E\left[|\hat{u}_n(\zeta;b)|^2\right]+E\big[\|\int_0^\Lambda[\bar{u}u_n^*]|_{(x_1,f_j)}\cdot\nabla_{\alpha_j}f_jdx_1\|_2^2\big]\right]\\
&\le C,\ j=2,\cdots,\ell.
\end{aligned}$$

From Lemma 4.4.1, for any fixed sample ζ, ∇R and $\nabla^2 R$ is bounded.

$$
\begin{aligned}
&\|\nabla^2 Q(\boldsymbol{\alpha})\|_2^2 \\
=&\left\|E[\nabla^2 R(\boldsymbol{\alpha})]\right\|_2^2 \\
\leq& E\left[\|\nabla^2 R(\boldsymbol{\alpha})\|_2^2\right] \\
=& E\left[\|\nabla^2 R(\xi_1, \cdots, \xi_M)\|_2^2\right] \\
=& \int_\Omega \|\nabla^2 R(\xi_1, \cdots, \xi_M)\|_2^2 dP(\xi_1, \cdots, \xi_M) \\
=& \int_{R^M} \|\nabla^2 R(y_1, \cdots, y_M)\|_2^2 p(y_1, \cdots, y_M) dx_1 \cdots dy_M \\
=& \int_{[-0.5,0.5]^M} \|\nabla^2 R(y_1, \cdots, y_M)\|_2^2 p(y_1, \cdots, y_M) dy_1 \cdots dy_M \\
<& C.
\end{aligned}
\tag{4.48}
$$

Therefore,

$$
\begin{aligned}
Q(\boldsymbol{\alpha}^{(n+1)}) - Q(\boldsymbol{\alpha}^{(n)}) \leq\leq& \nabla Q(\alpha^{(n)})^T(\boldsymbol{\alpha}^{(n+1)} - \boldsymbol{\alpha}^{(n)}) + \frac{1}{2}\|\nabla^2 Q(\boldsymbol{\alpha})\|_2^2 |\boldsymbol{\alpha}^{(n+1)} - \boldsymbol{\alpha}^{(n)}\|^2 \\
\leq& \nabla Q(\boldsymbol{\alpha}^{(n)})^T(\boldsymbol{\alpha}^{(n+1)} - \boldsymbol{\alpha}^{(n)}) + \frac{1}{2} C\|\boldsymbol{\alpha}^{(n+1)} - \boldsymbol{\alpha}^{(n)}\|^2 \\
\leq& -h_n \nabla Q(\boldsymbol{\alpha}^{(n)})^T \nabla R(\boldsymbol{\alpha}^{(n)}, \zeta_n) + \frac{1}{2} h_n^2 C\|\nabla R(\boldsymbol{\alpha}^{(n)}, \zeta_n)\|_2^2
\end{aligned}
\tag{4.49}
$$

Let us take conditional expectation with respect to ζ_n. Since $E_{\zeta_n}[\|\nabla R(\boldsymbol{\alpha}^{(n)}, \zeta_n)\|^2 < C$, we have

$$
\begin{aligned}
E_{\zeta_n}[Q(\boldsymbol{\alpha}^{(n+1)})] - Q(\boldsymbol{\alpha}^{(n)}) &\leq -h_n \nabla Q(\boldsymbol{\alpha}^{(n)})^T E_{\zeta_n}[\nabla R(\boldsymbol{\alpha}^{(n)}, \zeta_n)] + \frac{1}{2} h_n^2 C^2 \\
&\leq -h_n \|\nabla Q(\boldsymbol{\alpha}^{(n)})\|_2^2 + \frac{1}{2} h_n^2 C^2.
\end{aligned}
$$

By taking total expectation, we get

$$
E[Q(\boldsymbol{\alpha}^{(n+1)})] - E[Q(\boldsymbol{\alpha}^{(n)})] \leq -h_n E[\|\nabla Q(\boldsymbol{\alpha}^{(n)})\|_2^2] + \frac{1}{2} h_n^2 C^2 \tag{4.50}
$$

Denote $Q_\infty := \lim_{n\to\infty} Q_n$, the reflectivity is positive, then $Q_\infty > 0$. By adding the equations above from 1 to n, we get

$$Q_\infty - E[Q(\boldsymbol{\alpha}^{(1)})] \leq E[Q(\boldsymbol{\alpha}^{(n+1)})] - E[Q(\boldsymbol{\alpha}(1)] \leq -\sum_{j=1}^{(n)} h_j E[\|\nabla Q(\boldsymbol{\alpha}^{(j)})\|_2^2] + \frac{1}{2}C^2 \sum_{j=1}^{(n)} h_j^2$$

We have

$$\sum_{j=1}^{n} h_j E[\|\nabla Q(\boldsymbol{\alpha}^{(n)})\|_2^2] \leq E[Q(\boldsymbol{\alpha}^{(1)})] - Q_\infty + \frac{1}{2}C^2 \sum_{j=1}^{n} h_j^2$$

Since $\sum_{n=1}^{\infty} h_n^2 < \infty$, we have $\lim_{n\to\infty} \sum_{j=1}^{n} h_j E[\|\nabla Q(\boldsymbol{\alpha}^{(j)})\|_2^2] < \infty$. Due to $\sum_{n=1}^{\infty} h_n = \infty$, we have

$$\lim_{n\to\infty} \inf E[\|\nabla Q(\boldsymbol{\alpha}^{(n)})\|_2^2] = 0.$$

Define $G(\boldsymbol{\alpha}) := \|\nabla Q(\boldsymbol{\alpha})\|_2^2$. $\nabla G(\boldsymbol{\alpha})$ is Lipschitz continuous since $\|\nabla^2 Q(\alpha)\|_2^2 < C$ on the closed region $U_{\boldsymbol{\alpha}}$ and let L_G be the Lipschitz constant of $\nabla G(\boldsymbol{\alpha}) = 2\nabla^2 Q(\boldsymbol{\alpha})\nabla Q(\boldsymbol{\alpha})$. Then,

$$\begin{aligned} G(\boldsymbol{\alpha}^{(n+1)}) - G(\boldsymbol{\alpha}^{(n)}) &\leq \nabla G(\boldsymbol{\alpha}^{(n)})^\top (\boldsymbol{\alpha}^{(n+1)} - \boldsymbol{\alpha}^{(n)}) + \frac{1}{2} L_G \|\boldsymbol{\alpha}^{(n+1)} - \boldsymbol{\alpha}^{(n)}\|_2^2 \\ &\leq -h_n \nabla G(\boldsymbol{\alpha}^{(n)})^\top \nabla R(\boldsymbol{\alpha}^{(n)}, \zeta_n) + \frac{1}{2} h_n^2 L_G \|\nabla R(\boldsymbol{\alpha}^{(n)}, \zeta_n)\|_2^2 \end{aligned}$$

Taking the expectation with respect to the distribution of ζ_n,

$$\begin{aligned} & E_{\zeta_k}[G(\boldsymbol{\alpha}^{(n+1)})] - G(\boldsymbol{\alpha}^{(n)}) \\ \leq & -2h_n \nabla Q(\boldsymbol{\alpha}^{(n)})^\top \nabla^2 Q(\boldsymbol{\alpha}^{(n)})^\top E_{\zeta_n}[\nabla R(\boldsymbol{\alpha}^{(n)}, \zeta_n)] + \frac{1}{2} h_n^2 L_G E_{\zeta_n} \|\nabla R(\alpha^{(n)}, \zeta_n)\|_2^2 \\ \leq & 2h_n \|\nabla Q(\boldsymbol{\alpha}^{(n)})\|_2 \|\nabla^2 Q(\boldsymbol{\alpha}^{(n)})\|_2 \|\nabla Q(\boldsymbol{\alpha}^{(n)})\|_2 + \frac{1}{2} h_n^2 L_G E_{\zeta_n} \|\nabla R(\boldsymbol{\alpha}^{(n)}, \zeta_n)\|_2^2 \\ \leq & 2h_n L \|\nabla Q(\boldsymbol{\alpha}^{(n)})\|_2^2 + \frac{1}{2} h_n^2 L_G \|\nabla Q(\boldsymbol{\alpha}^{(n)})\|_2^2 \end{aligned}$$

By taking the total expectation, it yields

$$E[G(\boldsymbol{\alpha}^{(n+1)})] - E[G(\boldsymbol{\alpha}^{(n)})] \leq 2h_n C E[\|\nabla Q(\boldsymbol{\alpha}^{(n)})\|_2^2] + \frac{1}{2} h_n^2 L_G E[\|\nabla Q(\boldsymbol{\alpha}^{(n)})\|_2^2] \quad (4.51)$$

By adding the equations above from 1 to n, we get

$$\begin{aligned}\lim_{n\to\infty} G(\boldsymbol{\alpha}^{(n)}) - E[G(\boldsymbol{\alpha}^{(1)})] &\leq E[G(\boldsymbol{\alpha}^{(n+1)})] - E[G(\boldsymbol{\alpha}^{(1)})] \\ &\leq -\sum_{j=1}^{n} h_j E[\|\nabla G(\boldsymbol{\alpha}^{j})\|_2^2] + \frac{1}{2} L_G C \sum_{j=1}^{n} h_j^2\end{aligned}$$

Since the first term on the right hand above is bounded

$$\begin{aligned}\sum_{j=1}^{n} h_j E[\|\nabla G(\boldsymbol{\alpha}^{(j)})\|_2^2] &\leq \lim_{n\to\infty} G(\boldsymbol{\alpha}^{(n)}) - E[G(\boldsymbol{\alpha}^{(1)})] \\ &\leq E[G(\boldsymbol{\alpha}^{(n+1)})] - E[G(\boldsymbol{\alpha}^{(1)})] + \frac{1}{2} L_G C \sum_{j=1}^{n} h_j^2\end{aligned}$$

the right-hand side above is the term of a convergent sum. Therefore $\lim_{n\to\infty} \inf E[G(\alpha)] = 0$.

Define

$$S_n^+ = \sum_{j=1}^{n} \max(0, E[G(\boldsymbol{\alpha}^{(j+1)})] - E[G(\boldsymbol{\alpha}^{(j)})]),$$

$$S_n^- = \sum_{j=1}^{n} \max(0, E[G(\boldsymbol{\alpha}^{(j)})] - E[G(\boldsymbol{\alpha}^{(j+1)})]).$$

S_n^+ and S_n^- are both nondecreasing and upper bounded, therefore they converge.

$$G(\boldsymbol{\alpha}^{(n)}) = G(\boldsymbol{\alpha}^{(0)}) + S_n^+ - S_n^- \geq 0$$

Then $G(\boldsymbol{\alpha}^{(n)})$ converges and $\lim_{n\to\infty} E[G(\boldsymbol{\alpha}^{(n)})] = 0$.

Chapter 5

Numerical experiments

In this section, we present several numerical examples to demonstrate the efficiency of the numerical algorithms for solving the optimal design problems. The Monte Carlo method will be used to choose the samples when we apply the full gradient method. In all examples, we use $\tilde{R} := \frac{1}{M_0}\sum_{m=1}^{M_0} R(\zeta_m; \boldsymbol{\alpha}^{(n)})$ and $\|\tilde{G}\| := \frac{1}{M_0}\|\sum_{m=1}^{M_0} D_{\boldsymbol{\alpha}} R(\zeta_m; \boldsymbol{\alpha}^{(n)})\|_2$ to denote the average reflectivity and the amplitude of gradient. For all examples, the average thickness of the each layer is set as $a = 300$ nm, and the size of the periodic cell $\Lambda = 1500$ nm.

5.1 Transverse electric polarization

Example 5.1.1

In this example, we use the transverse magnetic polarization case to verify the accuracy of the numerical solver for solving scattering problems. Assume that the wave length $\Lambda_0 = 500nm$ in free space has a refractive index of $q_1 = 2.0$ and $q_2 = 1.2$ in regions D_1 and D_2, respectively.

In order to verify the accuracy of the numerical algorithm, consider the model when the interface is flat. We use the finite element method [10] to solve the boundary value problem numerically. Assuming that the normal incident wave is time-harmonic plane wave $u^i = e^{-ik_0 q_2 x_2}$, where k_0 is the wave number in free space, the analytical solution of the scattering problem u can be obtained in the following way:

$$u(x) = \begin{cases} e^{-ik_0 q_2 x_2} + c_2 e^{ik_0 q_2 x_2}, \\ c_1(e^{ik_0 q_1 x_2} + e^{-ik_0 q_1 x_2}). \end{cases}$$

Take the derivative of the above equation,

$$\nabla u(x) = \begin{cases} -ik_0q_2e^{-ik_0q_2x_2} + ik_0q_2c_2e^{ik_0q_2x_2}, \\ c_1(ik_0q_1e^{ik_0q_1x_2} - ik_0q_1e^{-ik_0q_1x_2}). \end{cases}$$

Apply the continuity of the electric field and magnetic field, we have

$$e^{-ik_0q_2x_2} + c_2e^{ik_0q_2x_2} = c_1(e^{ik_0q_1x_2} + e^{-ik_0q_1x_2}),$$

$$q_1^2(-ik_0q_2e^{-ik_0q_2x_2} + ik_0q_2c_2e^{ik_0q_2x_2}) = q_2^2c_1(ik_0q_1e^{ik_0q_1x_2} - ik_0q_1e^{-ik_0q_1x_2}).$$

It can be obtained by direct calculation,

$$c_2 = \frac{c_1(e^{ik_0q_1} + e^{-ik_0q_1})}{e^{ik_0q_2} - e^{-2ik_0q_2}},$$

$$c_2 = \frac{c_1q_2(e^{ik_0q_1} - e^{-ik_0q_1})}{q_1e^{ik_0q_2} + e^{-2ik_0q_2}}.$$

Therefore, we can get

$$c_1 = \frac{2q_1e^{-ik_0q_2}}{q_1(e^{ik_0q_1} + e^{-ik_0q_1}) - q_2(e^{ik_0q_1} - e^{-ik_0q_1})}.$$

Then we apply the linear finite element method to solve the scattering problem. We set the mesh size $\Delta = 12nm, 6nm, 3nm, 1.5nm$, and we give the corresponding $L^2 - norm$ form numerical error in Table 5.1. From Table 5.1, we can see that the convergence order of the numerical method is about 2, which is consistent with the numerical convergence theory of the linear finite element method.

Table 5.1: L^2-norm of the error for the numerical solution at various mesh size and the corresponding convergence order.

Δ	12 nm	6 nm	3 nm	1.5 nm
$\|\|\tilde{u} - u_\Delta\|\|_{L^2}$	0.23134	0.0428	0.0136	0.00294
convergence order		2.01	2.03	1.98

Next we consider a sample of Gaussian random interface with the root mean square (RMS) height $\sigma = 30nm$ and the correlation length $l = 24nm$. The regions are divided according to the mesh size $\Delta = 12nm, 6nm, 3nm, 1.5nm$. In order to test the convergence of the numerical solution of the partial differential equation, we choose the numerical solution u of the mesh size $\Delta = 0.6nm$ as the reference solution, and calculate the $L^\infty - norm$ error $\|u - u_\Delta\|_L^\infty$ of the numerical solution on the boundary $\Delta = 3nm$ in the case of the above four different triangulations. We can clearly see the convergence of the finite element method. In order to illustrate the scattering effect of rough surfaces, we also draw the total field of the scattering problem(figure 5.2 and figure 5.3). When the mesh size is $\Delta = 3nm$. Figure 5.1 is the mesh for the chosen sample when we apple the finite element method.

Table 5.2: $||\tilde{u} - u_\Delta||_{L^\infty}$ for various mesh sizes along the boundary $x_2 = b$, where $\tilde{u}$ is the reference solution obtained with $\Delta = 0.06nm$

Δ	12 nm	6 nm	3 nm	1.5 nm
$\|\|\tilde{u} - u_\Delta\|\|_{L^\infty}$	0.2918	0.0692	0.0125	0.0049

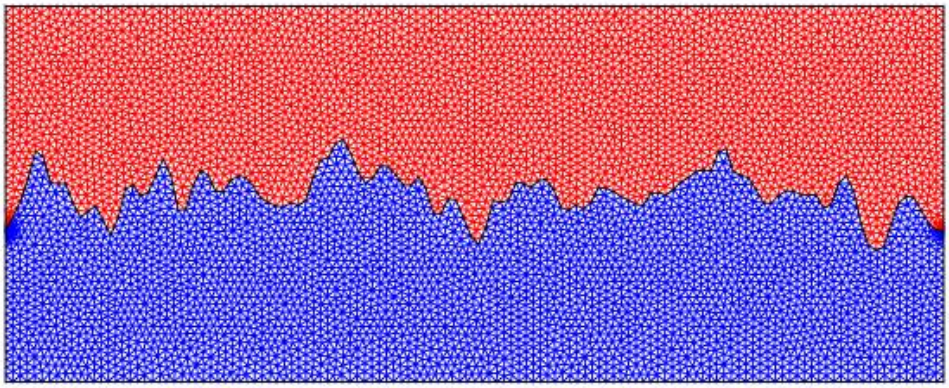

Figure 5.1: A mesh for a chosen sample

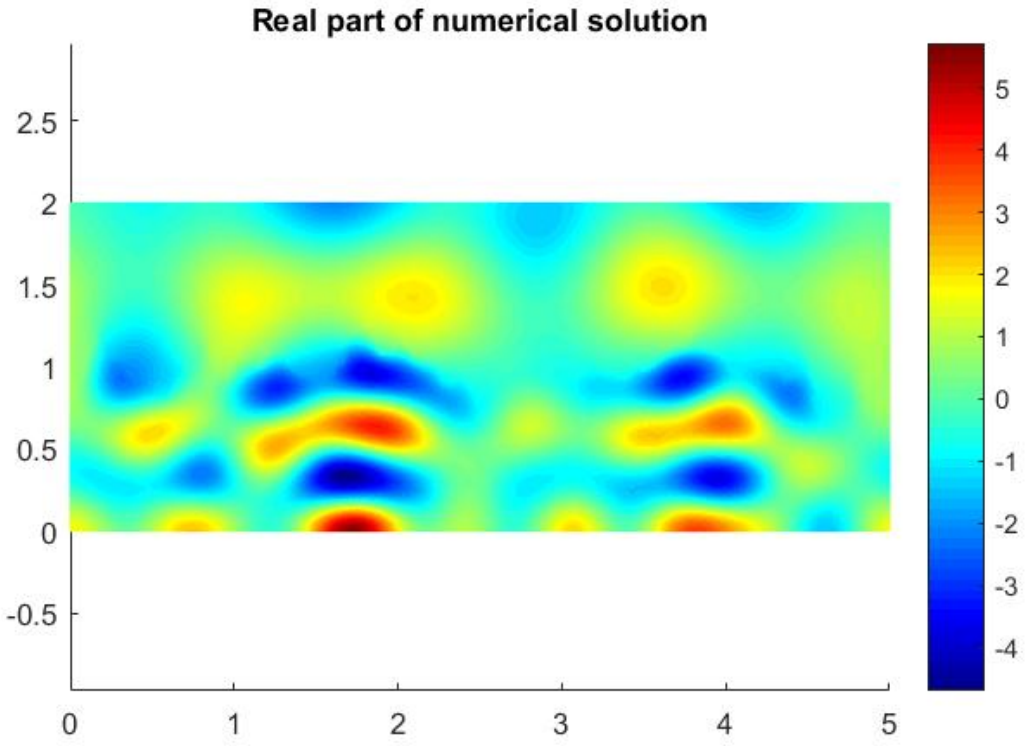

Figure 5.2: Real part of the total field with $\Delta = 3nm$

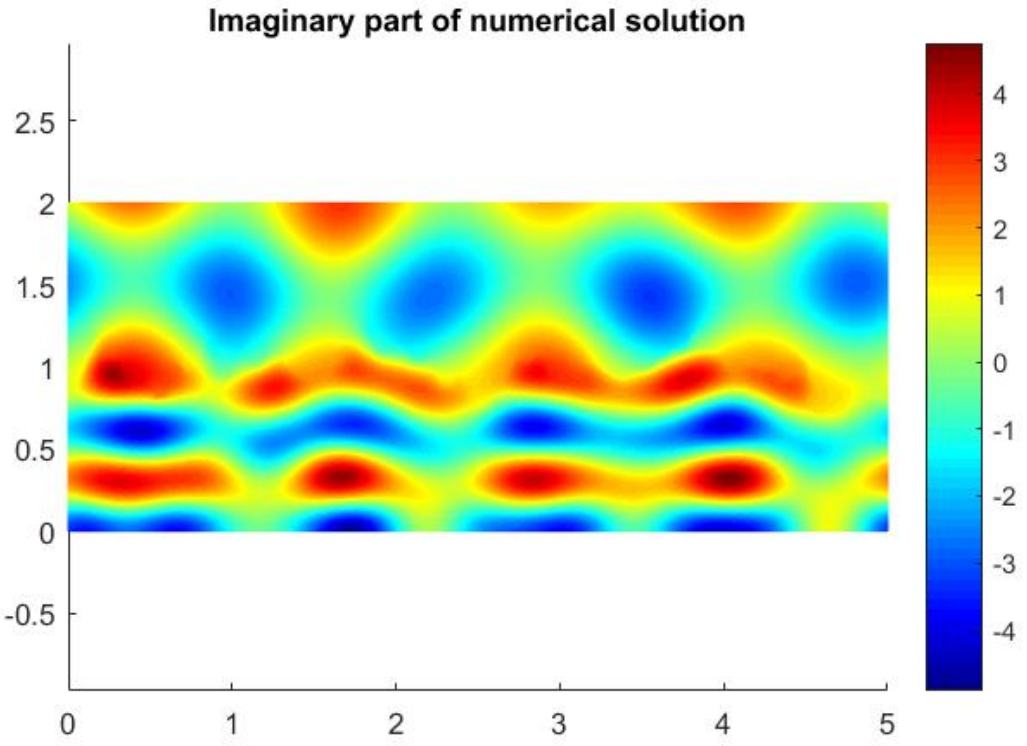

Figure 5.3: Imaginary part of the total field with $\Delta = 3nm$

Example 5.2.2

In this example, we still consider a transverse magnetic polarization case. We assume that the wavelength in the vacuum is $\Lambda_0 = 650nm$. The refractive index of TCO layer is 1.915, or its relative permittivity $\varepsilon_{r1} = 3.667$; refractive index of the absorbing layer is $4.2 + 0.045i$ when $\Lambda_0 = 650nm$. This means that the relative index value of the absorbing layer is $\varepsilon_{r,2} = 17.6380 + 0.3780i$ [15, 23, 38]. Figure 5.4 shows an iterative diagram of the objective function $Q(\boldsymbol{\alpha})$ using the full gradient method. The iteration point (σ, l) corresponding to each iteration is given in table 5.3.

Table 5.3: The value of σ and l for all iterations.

Iteration	0	1	2	3	...	10	11	12	13	14
σ	21	24.04	27.29	30.57	...	48.70	49.73	49.74	50.57	51.24
l	36	36.03	36.02	35.87	...	35.56	35.43	35.43	35.74	35.85

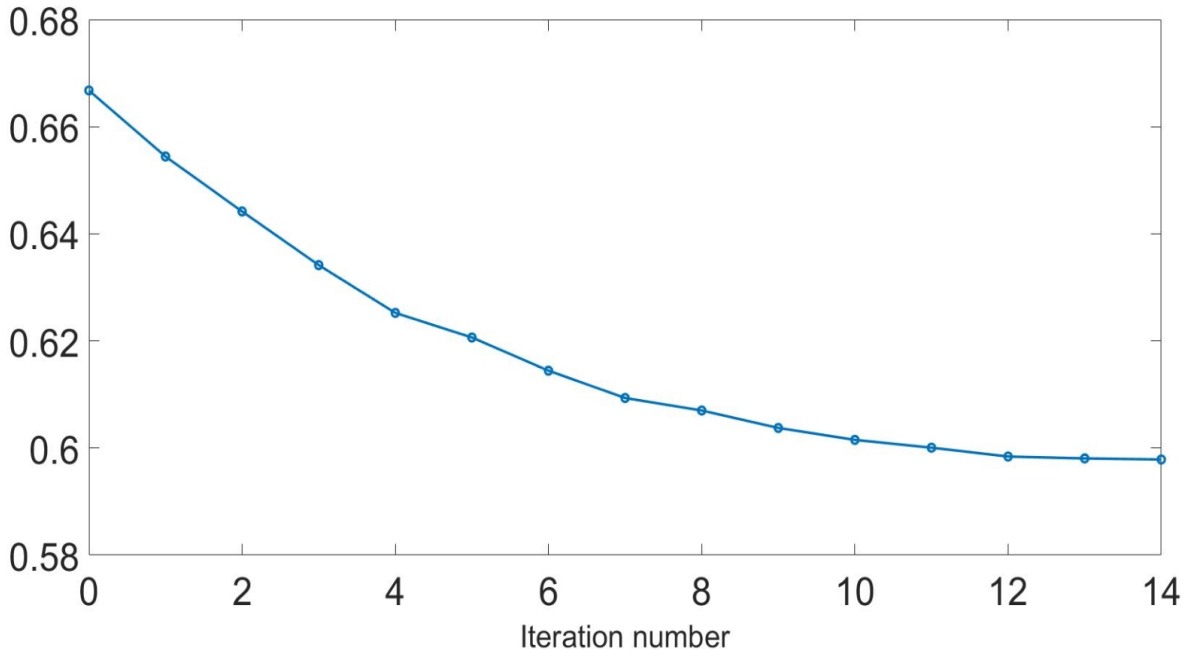

Figure 5.4: The cost function $Q(\alpha)$ for all iterations

Figure 5.5 shows the iterative diagram of the stochastic gradient descent algorithm applied to the objective function $\tilde{R}(\boldsymbol{\alpha})$. We note that the stochastic gradient method only needs 150 numerical solutions for u and u_n^*, whereas, for the gradient decent method, it requires 15000

solves for the boundary value problems and the adjoint problem when we set the number of Monte Carlo sample to be 1000 for each step. It is obvious that the stochastic gradient method is far more efficient than the full gradient method. Figure 5.6 shows one sample realization for the initial parameters. Figure 5.7 shows one realization of the random surface under the optimal statistical parameters. In Figure 5.8 and Figure 5.9, we show one sample of total field at the optimal parameters.

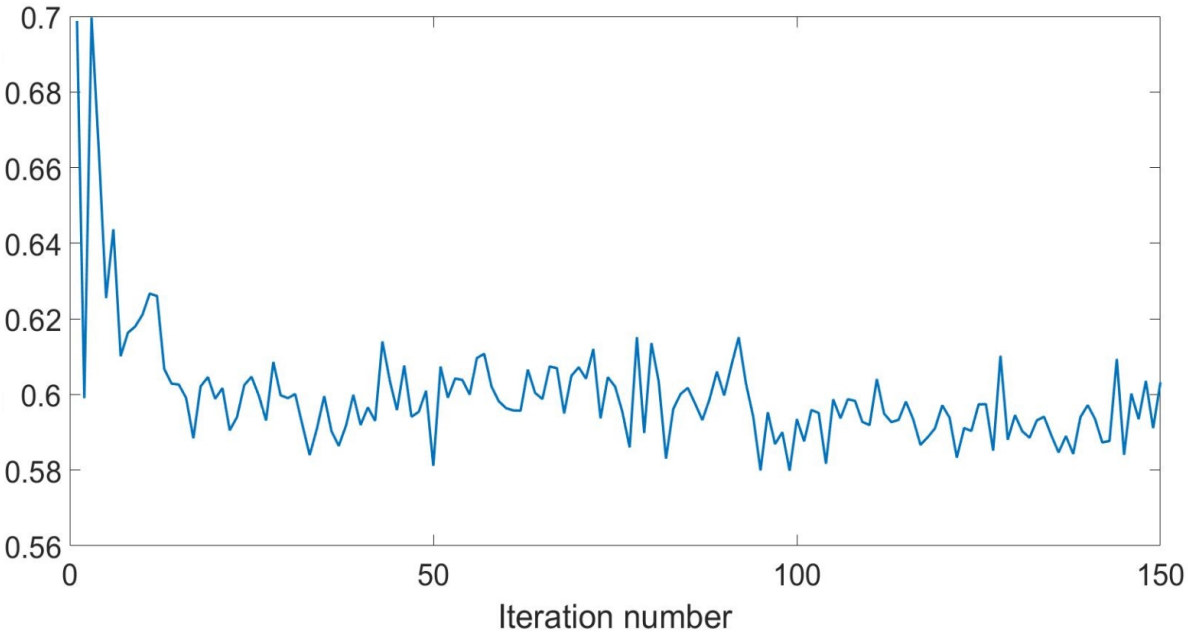

Figure 5.5: The cost function $\tilde{R}\boldsymbol{\alpha}$ for all iterations with stochastic gradient method

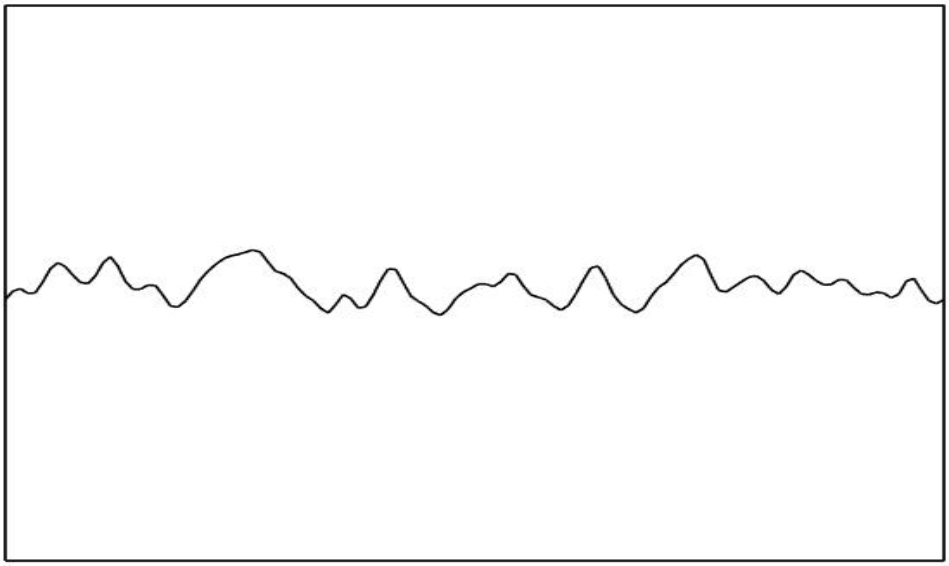

Figure 5.6: One random sample at initial parameter

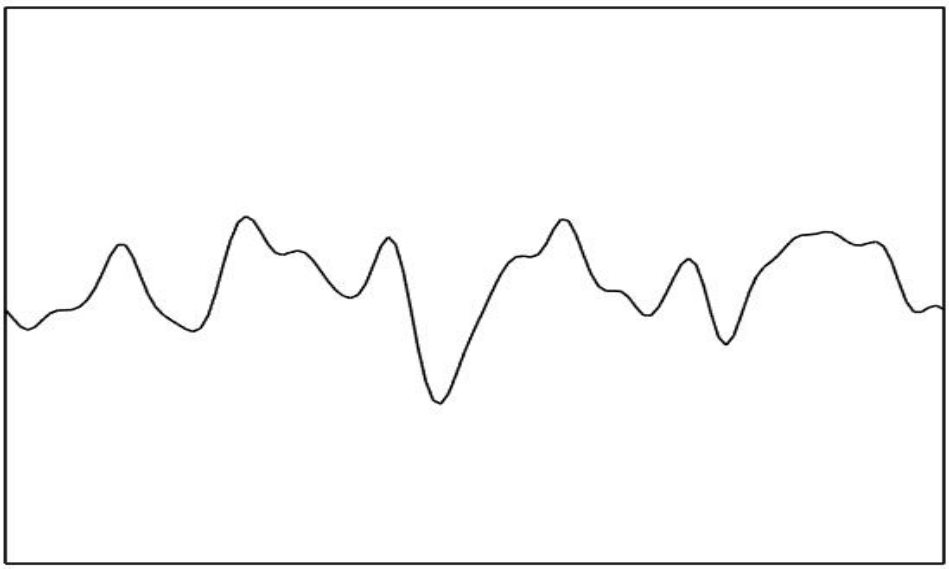

Figure 5.7: One random sample at optimal parameter

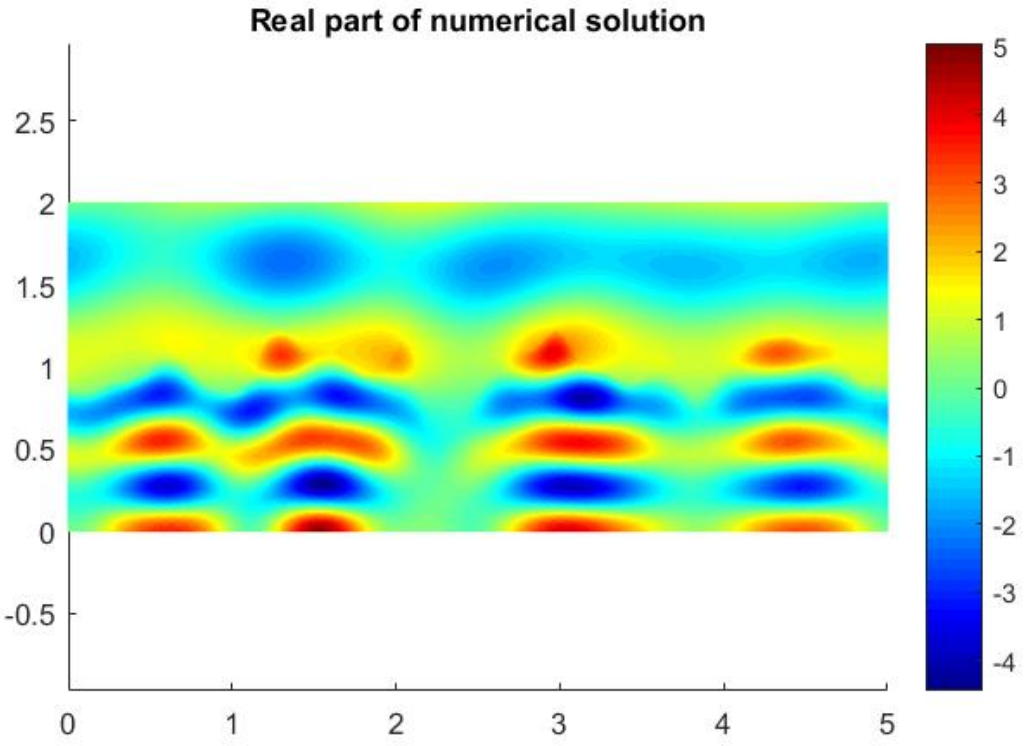

Figure 5.8: Real part of the total field of one sample after optimal design

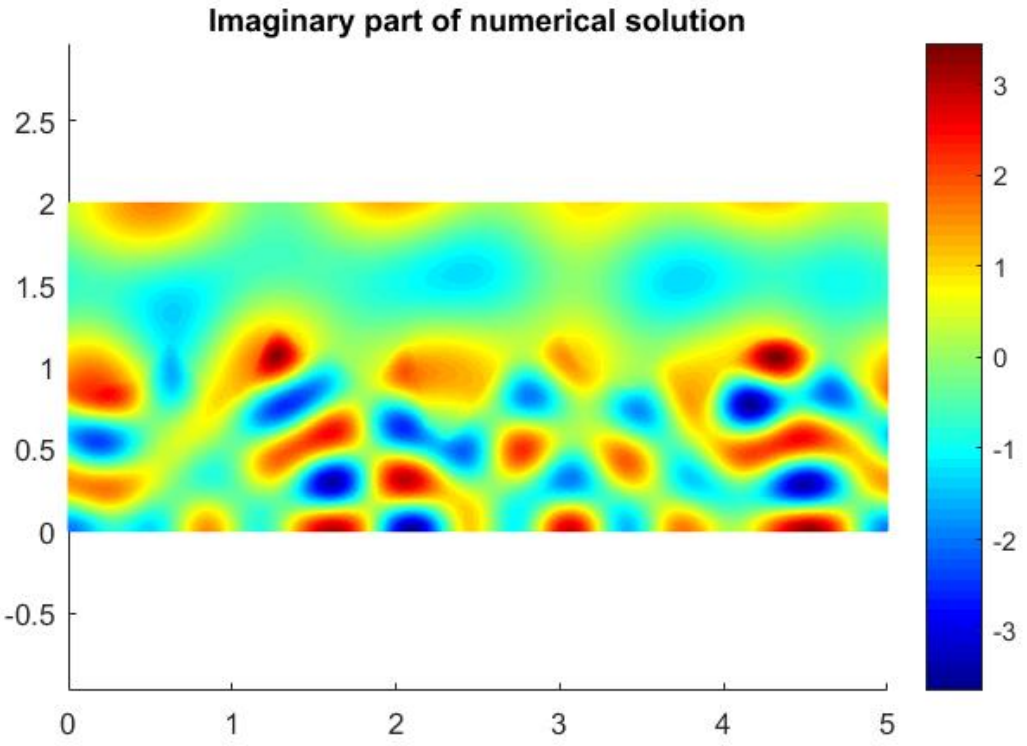

Figure 5.9: Imaginary part of the total field of one sample after optimal design

We also calculate the absorptivity of solar cells with flat surface and the optimal random surface. It can be calculated that when the optimal random surface texture is obtained, the average absorptivity E of solar cells is about 0.392. The absorptance with a flat surface is 0.231. Thus the optimal design model significantly improves the efficiency of solar cells.

Table 5.4: The absorptances of solar cells with different types of surfaces

	flat surface	optimal surface
σ(nm)	0	51.24
l(nm)		35.85
E[A]	0.231	0.402

Example 5.2.1

In this example we consider the transverse electric polarization case. Assume that the cell consists of two layers only, that is, an absorbing layer (e.g., a-Si:H) sits at the bottom and a transparent conducting oxide (TCO) layer lies on the top. Assume that the free space wavelength $\lambda_0 = 650$ nm. The refractive index of the TCO layer is 1.915, or equivalently, its relative permittivity $\varepsilon_{r,1} = 3.667$ [15, 23, 38]. The refractive index of the absorbing layer is set to $4.2 + 0.045i$ when $\lambda_0 = 650$ nm [46]. This implies that the relative permittivity $\varepsilon_{r,2} = 17.6380 + 0.3780i$, the incident angle $\theta = 0$. We consider the interface and the bottom as Gaussian random processes which are approximated by formula 2.34. The initial guess is chosen to be $\alpha_1 = \left(\alpha_1^{(1)}, \alpha_1^{(2)}\right) = (35nm, 20nm),\ \alpha_2 = \left(\alpha_2^{(1)}, \alpha_2^{(2)}\right) = (35nm, 20nm)$ for the interface and the bottom, respectivly. We apply both the stochastic gradient decent algorithm and the gradient decent method to solve the optimization problem (3.2), where the gradient is computed via formulas (4.4) and (4.5). We stop the optimization iterations when the gradient is less than 0.05.

Figure 5.10 and Figure 5.12 shows the optimal result for the stochastic gradient decent method and gradient decent method, respectively. Figure 5.10 shows the reflectivity decrease at the beginning and then oscillates near the minimum. When the cost function is far away form the minimum, the gradient dominate the iteration. The gradient leads the iteration to its minimum. When the cost function approach the minimum, the randomness dominate the iteration, therefore the cost function oscillates near the minimum. These are the results that two methods start with the same initial guess converge to the similar optimal parameters and the minimal reflectivity they attains are almost the same(see Table 5.5).

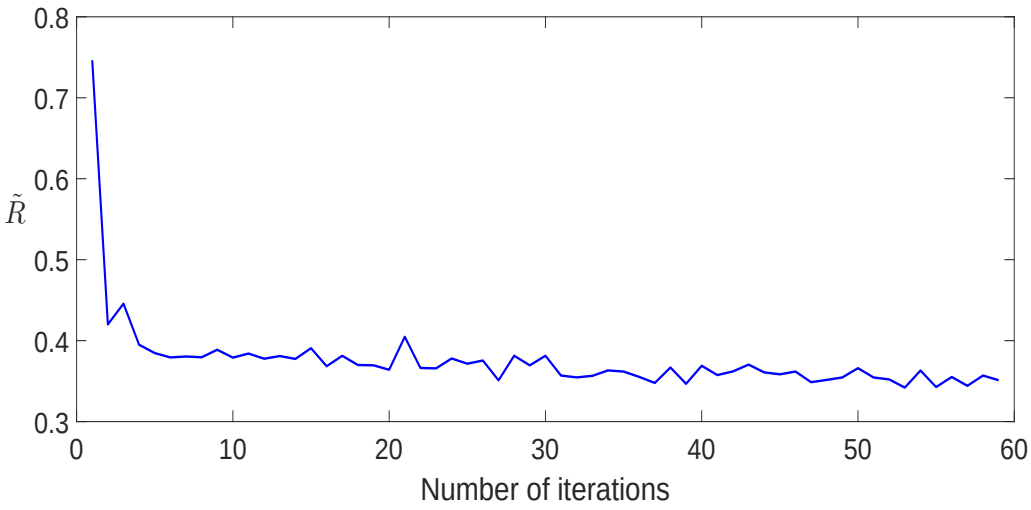

Figure 5.10: The average of reflectivity for all iterations using stochastic gradient method.

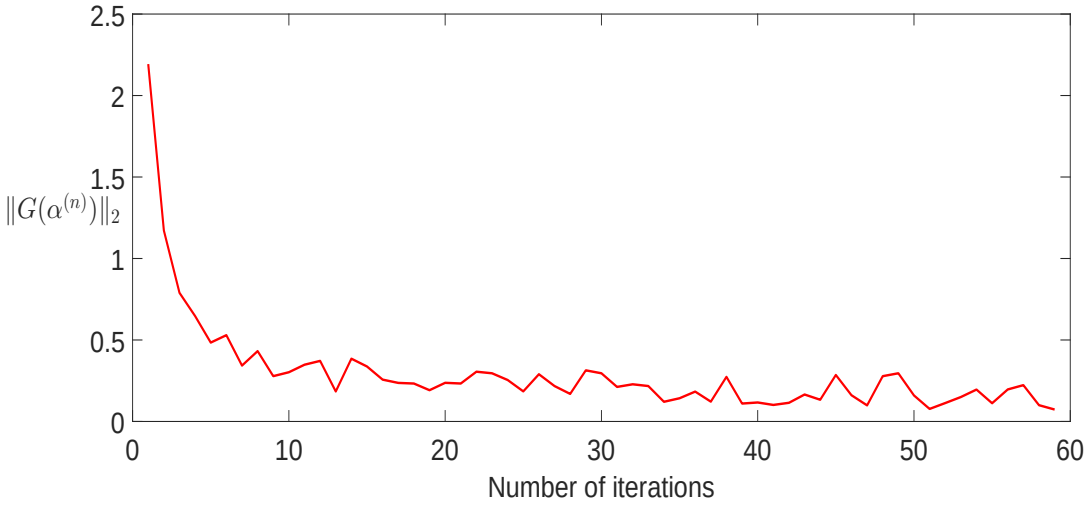

Figure 5.11: The norm of average gradient for all iterations using stochastic gradient method.

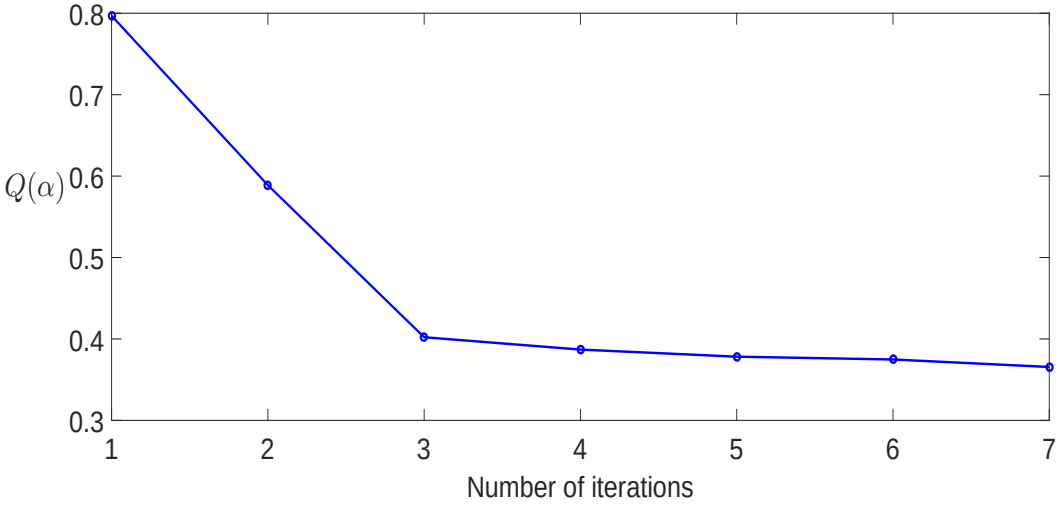

Figure 5.12: The cost function $Q(\boldsymbol{\alpha})$ for all iterations using full gradient method.

Table 5.5: The values of $\alpha^{(1)}$ and $\alpha^{(2)}$ for full gradient method and stochastic gradient method.

optimal result(nm)	$\alpha_1^{(1)}$	$\alpha_1^{(2)}$	$\alpha_2^{(1)}$	$\alpha_2^{(2)}$	reflectivity
Full gradient method	55	67	40	17	0.364
Stochastic gradient method	57	63	42	15	0.352

We also consider the optimization when the free space wavelength $\lambda_0 = 720$ nm. In this case, the reflectivity is larger since the wavelength is larger. The refractive index of the absorbing layer is $4 + 0.0035i$. The results obtained from stochastic gradient method (Figure 5.13) is also very close to the result obtained from GD method (Figure 5.15).

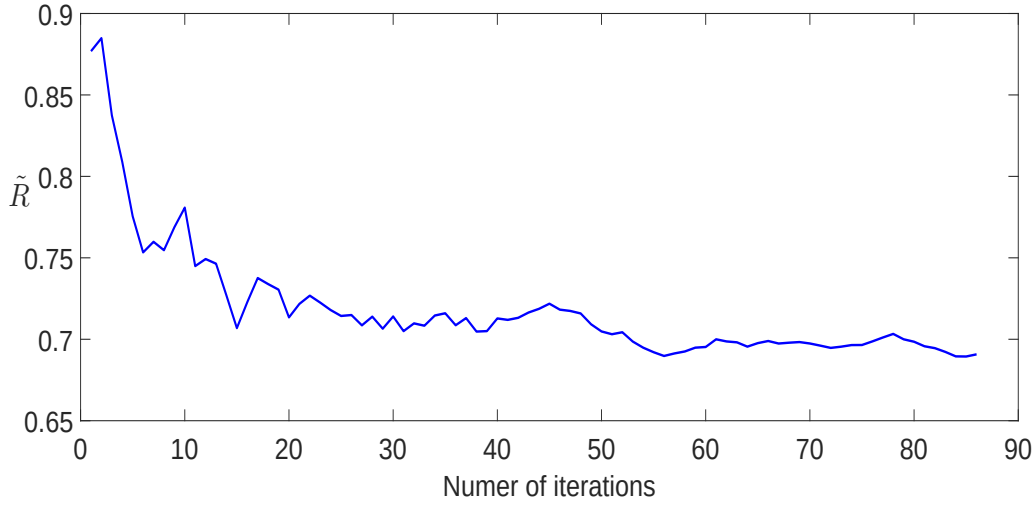

Figure 5.13: The average of $R(\boldsymbol{\alpha})$ for all iterations using stochastic gradient method.

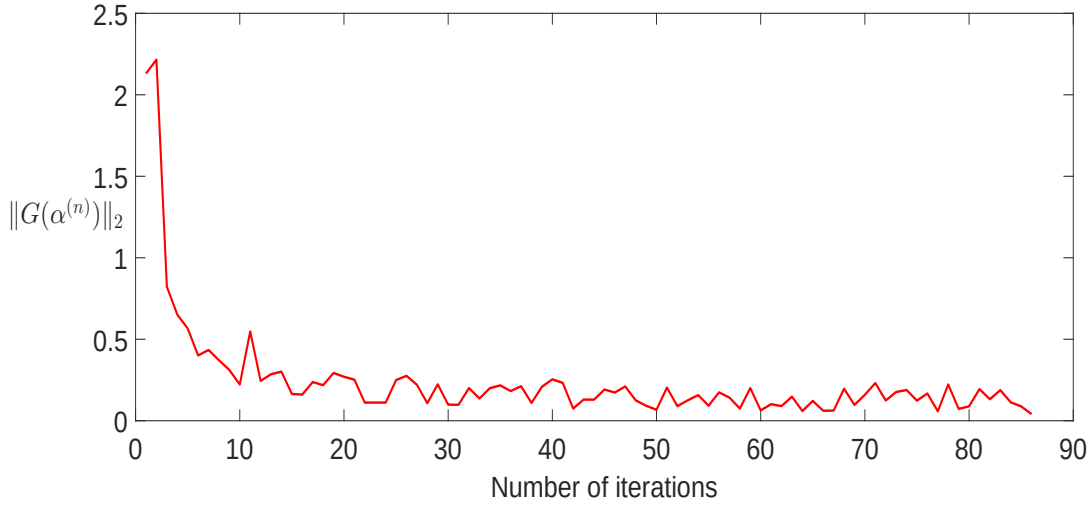

Figure 5.14: The norm of average gradient for all iterations using stochastic gradient method.

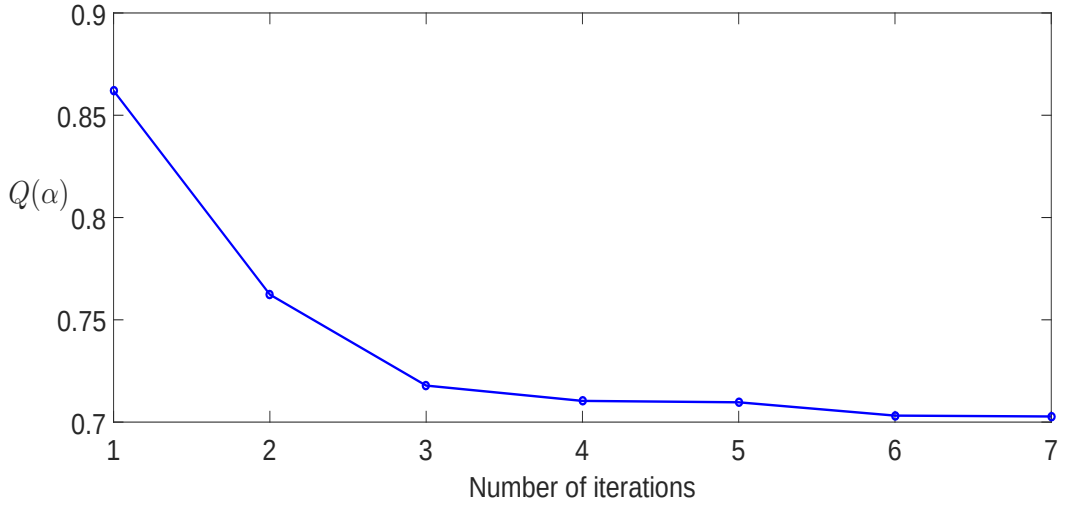

Figure 5.15: The cost function $Q(\alpha)$ for all iterations using full gradient method.

The mini-batch stochastic gradient decent method lowers the computational cost dramatically. For the full gradient method algorithm, we choose the Monte-Carlo sample size to be 1000. Then we need to solve 7000 boundary value problems (3.10) and the corresponding adjoint problems (4.27) in the optimal algorithm. When we employ the stochastic gradient method algorithm 4.1, no more than 100 boundary value problems and the corresponding

Table 5.6: The values of $\alpha^{(1)}$ and $\alpha^{(2)}$ for full gradient method and stochastic gradient method.

optimal result(nm)	$\alpha_1^{(1)}$	$\alpha_1^{(2)}$	$\alpha_2^{(1)}$	$\alpha_2^{(2)}$	reflectivity
Full gradient method	40	37	38	27	0.703
Stochastic gradient method	44	33	41	24	0.695

adjoint problems need to be solved. Figure 5.11 and 5.14 shows that the gradient decreases as the iteration increasing. So for the rest of the examples, the stochastic gradient method is employed.

Example 5.2.2

In this example, we consider the transverse electric polarization case. We compare the differences between the optimal results for the random process is of uniform type with Example 4. For simplicity we do not explicitly consider glass substrate and assume that the cell consists of two layers only, that is, an absorbing layer (e.g., a-Si:H) at the bottom and a transparent conducting oxide (TCO) layer on the top. Assume that the free space wavelength $\lambda_0 = 650$ nm. The relative permittivity of the TCO layer is $\varepsilon_{r,1} = 3.667$, and the relative permittivity for the absorbing layer is $\varepsilon_{r,2} = 17.6380 + 0.3780i$ [15, 23, 38]. The incident angle $\theta = 0$.

First, we consider interfaces $\Gamma_j,\ j = 1, 2$ that are random processes with the covariance function $c_j(x_1 - \tilde{x}_1) = \left(\alpha_j^{(1)}\right)^2 \exp\left(-|x_1 - \tilde{x}_1|^2 / \left(\alpha_j^{(2)}\right)^2\right),\ 0 < \alpha_j^{(2)} \ll \Lambda$. The initial guess is chosen to be $\alpha_1 = \left(\alpha_1^{(1)}, \alpha_1^{(2)}\right) = (35nm, 20nm)$ and $\alpha_2 = \left(\alpha_2^{(1)}, \alpha_2^{(2)}\right) = (35nm, 20nm)$. We apply both the stochastic gradient decent algorithm and the gradient decent method to solve the optimization problem (3.2), where the gradient is computed via formulas (4.4) and (4.5). The stopping criteria is set as the amplitude of the gradient $\|\tilde{G}\|$ is less than 0.05.

Figure 5.16 shows the value of $\tilde{R}$ at each iteration for the mini-batch stochastic gradient method when the interfaces are of uniform type. We see that the reflectivity decrease at the beginning and then vibrates near the minimum. Figure 5.17 shows the amplitude of the gradient $\|\tilde{G}\|$ for each iteration. The gradient decreases as iteration goes. Figure 5.18 is the reflectivity Q for each iteration when the full gradient method is applied. Here, the Monte Carlo method is used for sampling the random space. Table 5.7 is the optimal solutions obtained by the stochastic gradient decent method and the full gradient decent method.

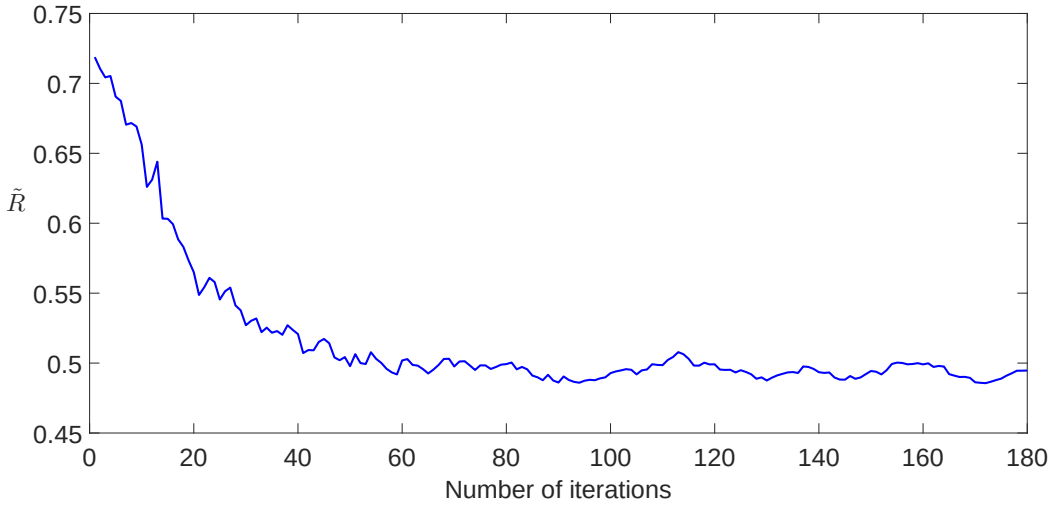

Figure 5.16: The reflectivity value $\tilde{R}(\boldsymbol{\alpha})$ during the stochastic gradient iterations when $\{\xi_0, \xi_{m,s}, \xi_{m,c}\}$ are uniform random variables.

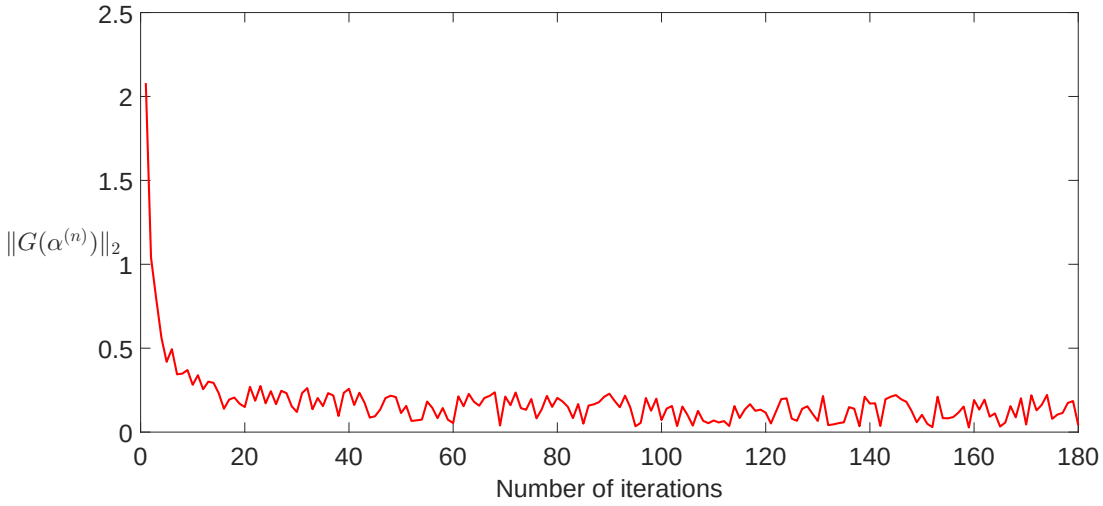

Figure 5.17: The norm of the average gradient $\|\tilde{G}\|$ during the stochastic gradient iterations when $\{\xi_0, \xi_{m,s}, \xi_{m,c}\}$ are uniform random variables.

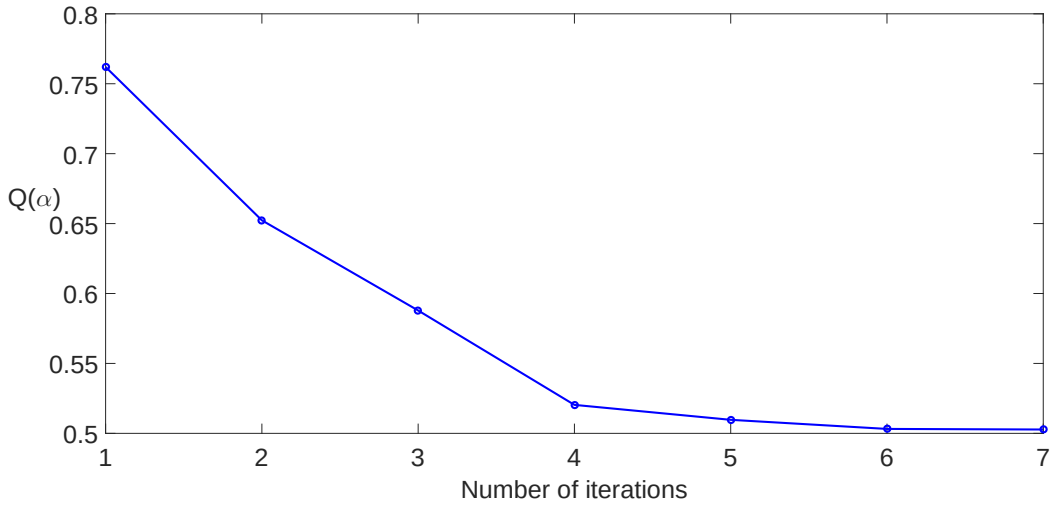

Figure 5.18: The reflectivity value $Q(\boldsymbol{\alpha})$ during the stochastic gradient iterations when $\{\xi_0, \xi_{m,s}, \xi_{m,c}\}$ are uniform random variables.

Table 5.7: The optimal values of $\alpha^{(1)}$ and $\alpha^{(2)}$ obtained by the full gradient method and stochastic gradient method for uniform random variable.

optimal result(nm)	$\alpha_1^{(1)}$	$\alpha_1^{(2)}$	$\alpha_2^{(1)}$	$\alpha_2^{(2)}$	reflectivity
Full gradient method	41	30	38	26	0.503
Stochastic gradient method	44	33	35	24	0.495

Though the optimal solution obtained by the full gradient and the stochastic gradient methods are close, their computational cost is significantly different. When we Monte Carlo method to sample the probability space, the sample size need to be big enough. We choose the Monte Carlo sample size is 1000 for each iteration. The algorithm stops after 7 steps. In this 7 iterations we need to solve 7000 boundary value problems (3.10) and the corresponding adjoint problem (4.27). On the other hand the stochastic gradient method only requires solving no more than 100 boundary value problems and the corresponding adjoint problem. Therefore the mini-batch stochastic gradient decent method reduces the computational cost dramatically compared to the full gradient method.

Example 5.2.3

In this example we consider the transverse electric polarization case and assume the random process is Gaussian random process. Consider the multiple-layer solar cell structure as shown in Figure 5.19, which consists of the glass, absorbing layer, the TCO layers and metal. The refractive index of the TCO, the absorbing layer and the glass substrate are 1.915, $4.2 + 0.045i$ and 1.4, respectively. Let the incident angle $\theta = 0$ and the wavelength $\lambda_0 = 650$ nm. Assume that all the interfaces are Gaussian random processes.

When the stochastic gradient method in Algorithm 3 is applied, the average reflectivity $\tilde{R}$ for each iterations is shown in Figure 5.20. The reflectivity for the optimal random structure is around 0.37 and the absoptance is 0.63. As a comparison, we compute the absorptance of the structure with flat interfaces and its value is only 0.13. Figure 5.21 and Figure 5.22 show the wave field for a realization of random structure with the optimal result, Figure 5.23 and Figure 5.24 show the wave field for the structure with flat interfaces.

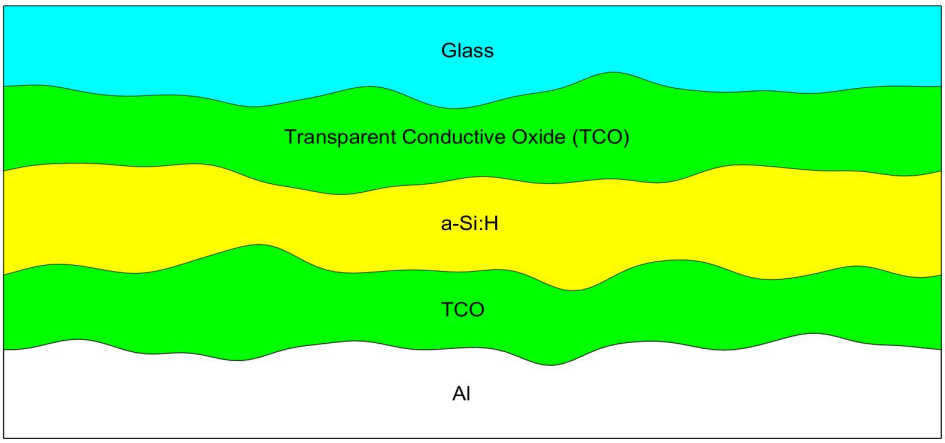

Figure 5.19: Random structure with 5 layers.

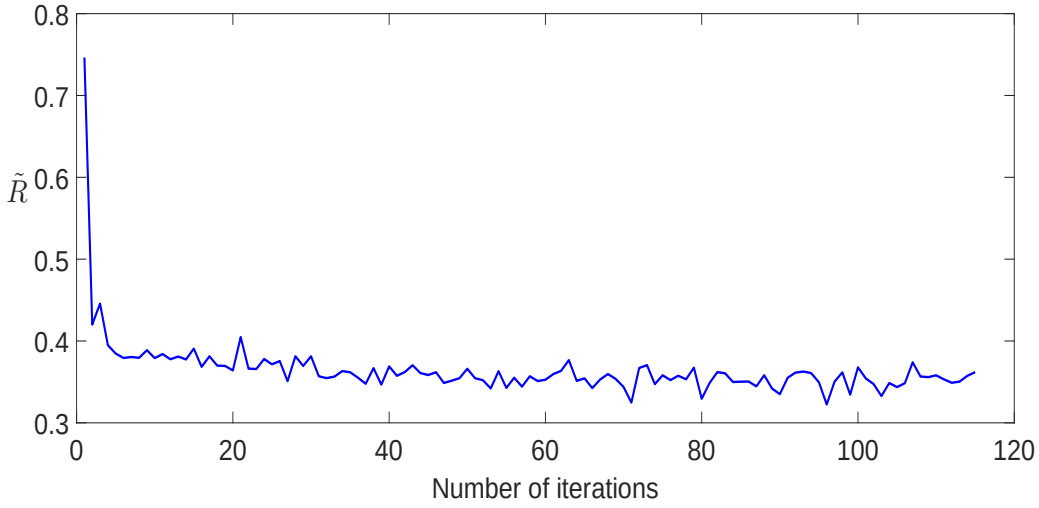

Figure 5.20: The reflectivity value $\tilde{R}(\boldsymbol{\alpha})$ during the stochastic gradient iterations of the structure with five layers for Problem(I).

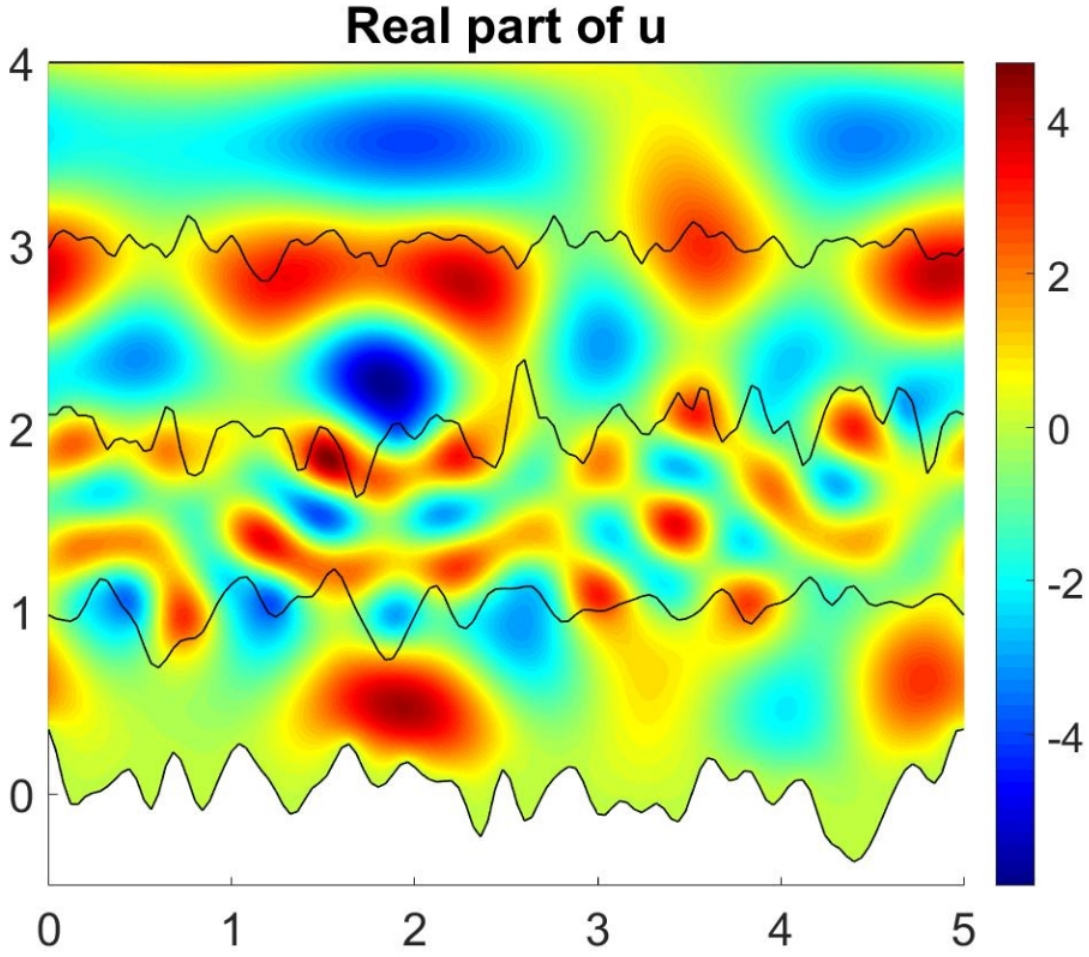

Figure 5.21: Numerical solution of u for a chosen random structure with optimal result.

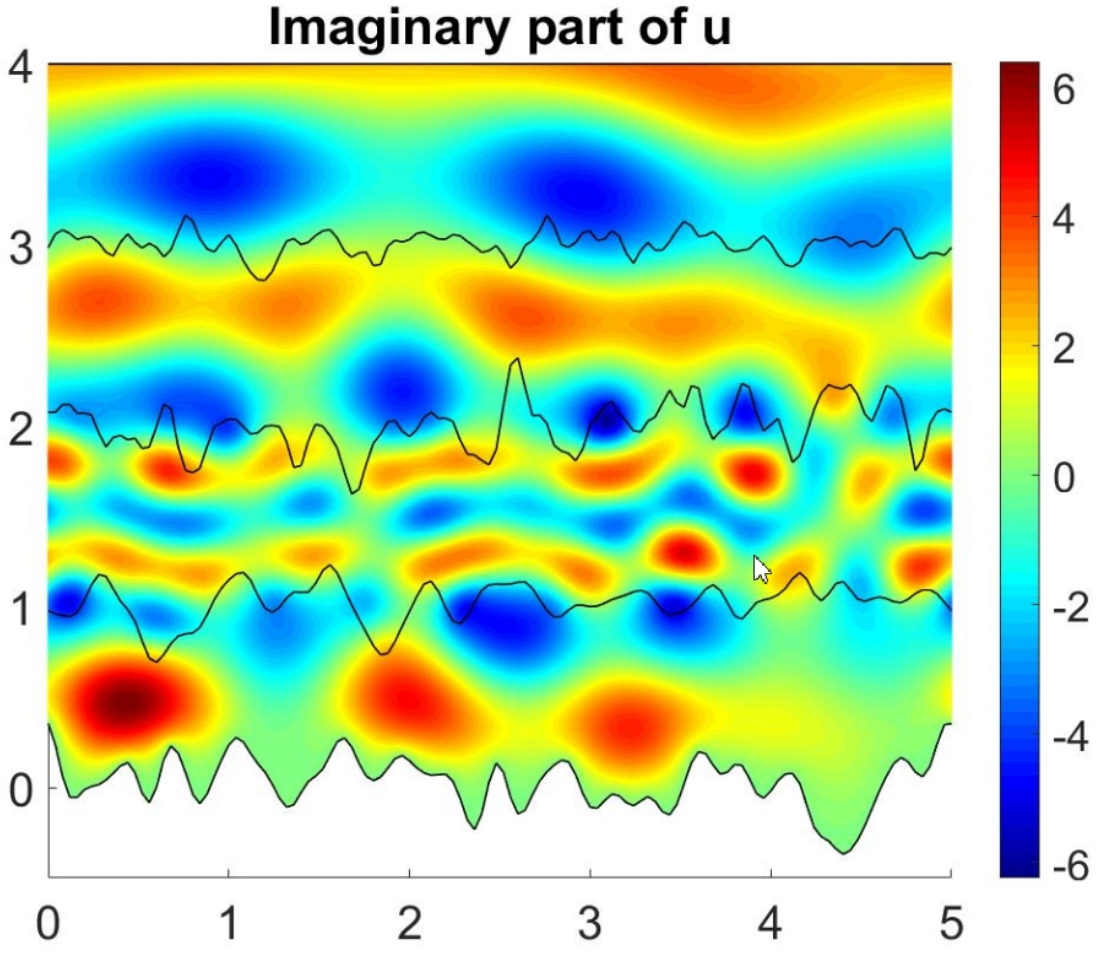

Figure 5.22: Numerical solution of u for a chosen random structure with optimal result.

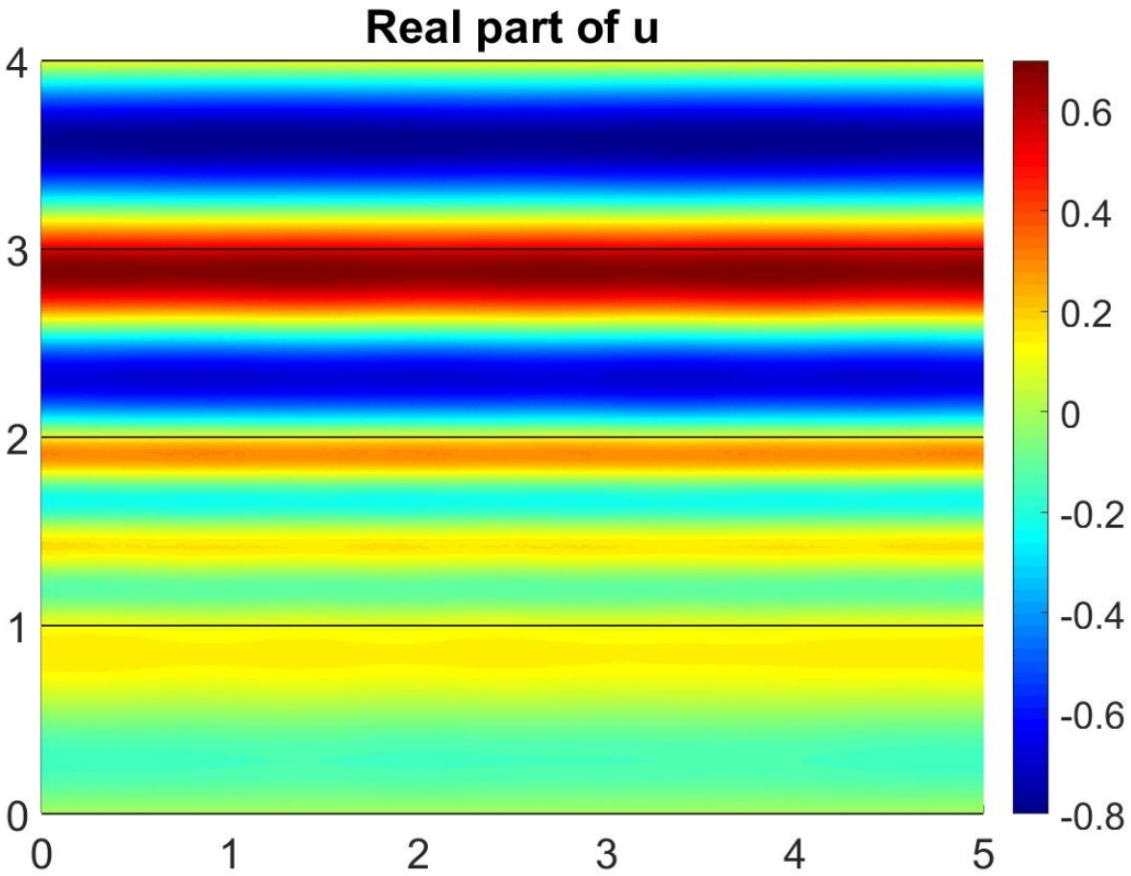

Figure 5.23: Real part of u for the structure with flat interfaces.

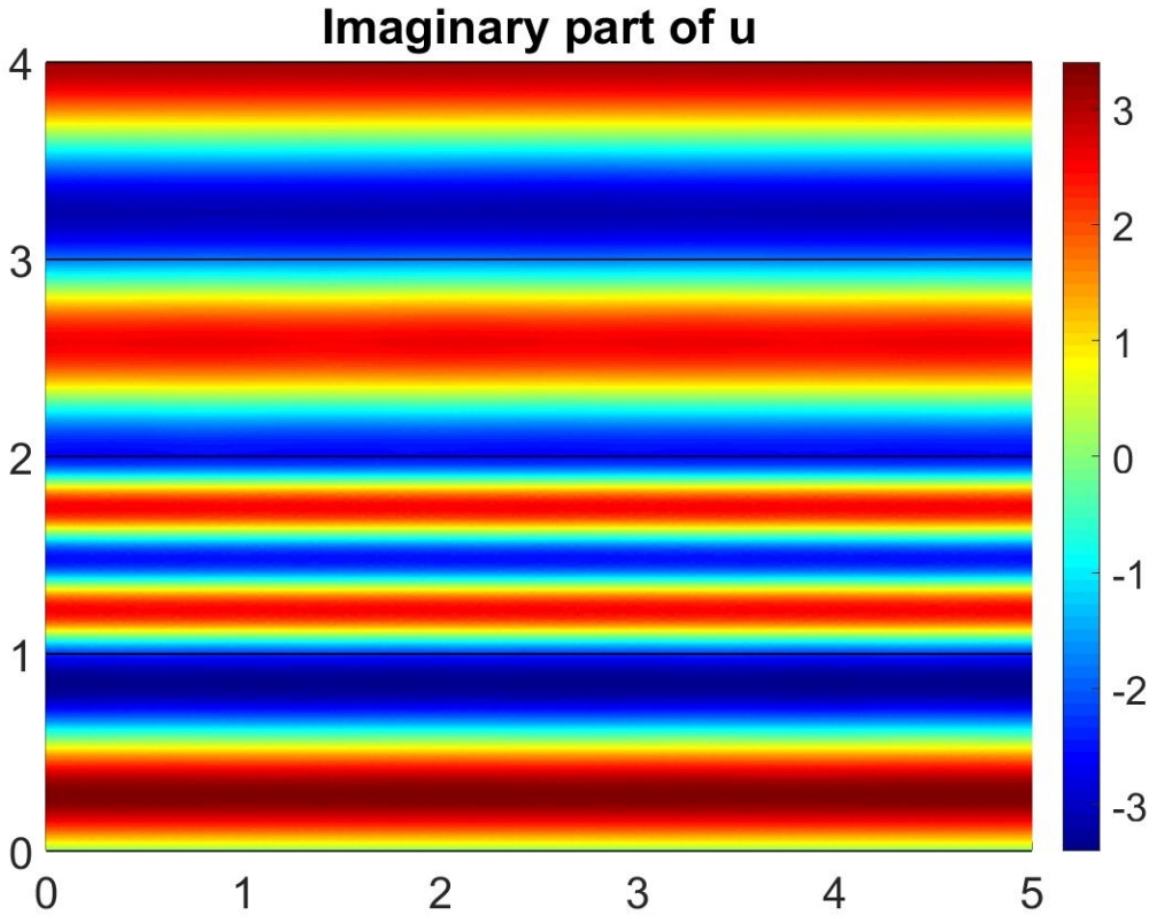

Figure 5.24: Imaginary part of u for the structure with flat interfaces.

Example 5.2.4

In this example, we consider the more challenging optimization problem with multiple frequencies, which is formulated in problem (3.4). Let us still use the multi-layer structure as shown in Figure 5.19. We consider the transverse electric polarization case and assume the random process is Gaussian random process. Assume that the interfaces are Gaussian random processes. The refractive index of the absorbing layer is set as $4.5 + 0.12i$ and $4.2 + 0.045i$ when $\lambda_{min} = 600$ nm and $\lambda_{max} = 650$ nm, respectively. For simplicity, we assume it is a linear function of the wavelength between λ_{min} and λ_{max}. The computational cost for this problem is higher than the problem considered in Example 3. We simply use the summation $\frac{1}{M_\lambda}\sum_{m=1}^{M_\lambda} R(\zeta;\boldsymbol{\alpha},\lambda_m)$ to approximate the integral $\int_{\lambda_{min}}^{\lambda_{max}} R(\zeta;\boldsymbol{\alpha},\lambda)d\lambda$ in problem (3.4), where $\lambda_m = \lambda_{min} + \frac{\lambda_{max}-\lambda_{min}}{M_\lambda - 1}(m-1)$. We consider the normal incidence with the incident angle $\theta = 0$.

The reflectivity at each iteration for the mini-batch stochastic gradient approach is shown in Figure 5.25. The reflectivity of the optimal structure is about 0.28 and its absorptance is about 0.72. The absorptance is significantly enhanced compared to the absorptance for the structure with flat surface, which is 0.24.

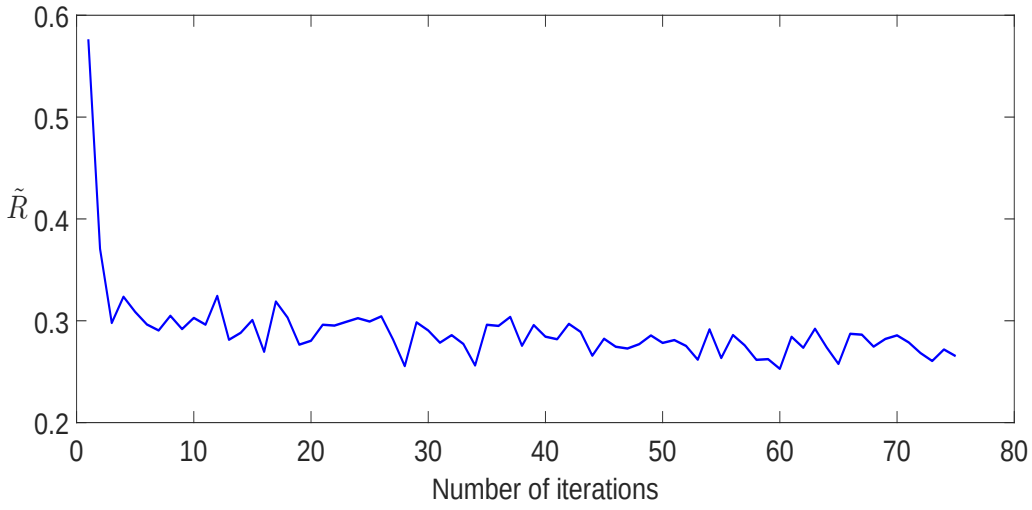

Figure 5.25: The reflectivity value $\tilde{R}(\boldsymbol{\alpha})$ during the stochastic gradient iterations of the structure with five layers for Problem(II).

Example 5.2.5

In this example we consider the transverse electric polarization case and assume the random process is Gaussian random process. Consider the optimization problem with multiple incident angle for the structure as shown in Figure 5.19. In this example we consider the transverse electric polarization case and assume the random process is Gaussian random process. This is formulated in Problem (3.6). We still consider the interfaces are Gaussian random processes and solve the problem with the stochastic gradient method. We need to evaluate a integral with respect to the incident angle and use the summation $\frac{1}{M_\lambda}\sum_{m=1}^{M_\lambda} R(\zeta;\boldsymbol{\alpha},\theta_m)$ to approximate the integral $\int_{\theta_{min}}^{\theta_{max}} R(\zeta;\boldsymbol{\alpha},\theta)d\lambda$ in problem (3.6), where $\theta_m = \theta_{min} + \frac{\theta_{max}-\theta_{min}}{M_\theta - 1}(m-1)$.

Let the range of the incident angel from $\theta_{min} = -\frac{\pi}{12}$ to $\theta_{max} = \frac{\pi}{12}$, the reflectivity at each iteration is shown in Figure 5.26. The reflectivity for the optimal structure is about 0.49 and the absorptance is about 0.51. The optimal structure enhances the absorptance since the absorptance for the structure with flat interface is about 0.11.

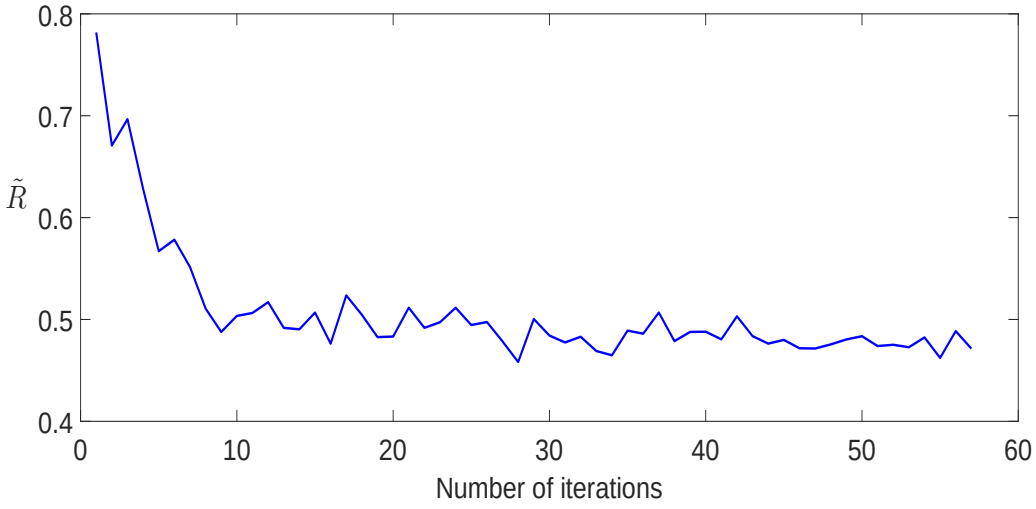

Figure 5.26: The reflectivity value $\tilde{R}(\boldsymbol{\alpha})$ during the stochastic gradient iterations for Problem(III).

Chapter 6

Conclusion and further work

In this work, we have formulated the optimal design problem for random surface and random bottom shape textures in thin-film solar cells and presented a gradient-based algorithm with the adjoint state method to solve the problem numerically. The stochastic gradient method is applied to solve the random optimization problem, this leads to significant savings in computational cost. The presented numerical results demonstrate the accuracy and convergence of the algorithm. It is shown that the optimal random textures obtained numerically would yield an absorption enhancement for the multiple frequency and multiple incident angle.

The mathematical and numerical investigation presented here is the rising field along this research direction and we are currently exploring further to answer the following questions. First, in terms of the formulation of the optimal design problems, since the optimal function only depends on the boundary, it may be possible to apply the boundary integral method instead of the finite element method. Additionally, the numerical simulations and the optimal design procedures will be carried out for the three-dimensional models.

References

[1] C. Battaglia, *et al.*, *Light trapping in solar cells: can periodic beat random?*, ACS Nano, **6** (2012): 2790-2797.

[2] C. R. Baraona and H.W. Brandhorst, *High Efficiency Silicon Solar Cell Review*. High Efficiency Silicon Solar Cell Review. **3326** (1975), 71.

[3] L. Bottou and F. E. Curtis and J. Nocedal, *Optimization Methods for Large-Scale Machine Learning*, SIAM Rev. Soc. Ind. Appl. Math, **60** (2018), 223-311.

[4] G. Bao, Y. Cao, J. Lin and H. W. Van Wyk, *Computational Optimal Design of Random Rough Surfaces in Thin-Film Solar Cells*, Commun. Comput. Phys., **88** (2019), 1815-2406.

[5] G. Bao, D. Dobson, and J. Cox, *Mathematical studies in rigorous grating theory*. J. Opt. Soc. Amer. A, **12** (1995), 1029-1042.

[6] G. Bao and J. Lin, *Imaging of Local Surface Displacement on an Infinite Ground Plane: The Multiple Frequency Case*, SIAM J. Appl. Math., **71** (2011), 17331752.

[7] G. Bao and Y. Wang, *Optimal design of antireflection coatings with different metrics*, J. Opt. Soc. Am. A, **30** (2013), 656-662.

[8] P. Bermel *et al.*, *Improving thin-film crystalline silicon solar cell efficiencies with photonic crystals*, Opt. Express **15** (2007), 16986.

[9] A. BONNET-BENDHIA AND F. STARLING, *Guided waves by electromagnetic gratings and non-uniqueness examples for the diffraction problem*, Math. Meth. Appl. Sci., **17** (1994), 305-338.

[10] S. Brenner and R. Scott, *The Mathematical Theory of Finite Element Methods*, Texts Applied Mathematics (Vol. 15), Springer Science & Business Media, 2007.

[11] A. Čampa, J. Krč, and M. Topič, *Analysis and optimisation of microcrystalline silicon solar cells with periodic sinusoidal textured interfaces by two-dimensional optical simulations*, J. Appl. Phys., **105** (2009), 083107.

[12] Y. Cao and D. Stanescu, *Shape optimization for noise radiation problems*, Comput. Math. Appl., **44** (2002), 1527-1537.

[13] Y. Cao, M. Y. Hussaini , and H. Yang, *Numerical optimization of radiated engine noise with uncertain wavenumbers*, Int. J. Numer. Anal. Mod., **4** (2007), 392-401.

[14] M. Delfour and and J. Zolésio, *Shapes and geometries: Metrics, analysis, differential calculus, and optimization*, Advances in Design and Control, SIAM, **22** (2011).

[15] S. Fahr, C. Rockstuhl, and F. Lederer, *Engineering the randomness for enhanced absorption in solar cells*, Appl. Phy. Lett. **92** (2008): 171114.

[16] V. Ferry, *et al.* ,*Optimized spatial correlations for broadband light trapping nanopatterns in high efficiency ultrathin film a-Si: H solar cells*, Nano Lett., **11** (2011), 4239-4245.

[17] R. G. Ghanem and P. D. Spanos. *Stochastic finite elements: a spectral approach.* Springer-Verlag New York, Inc., New York, NY, USA, (1991).

[18] I. Gohberg, S. Goldberg, and M. A. Kaashoek. *Basic classes of linear operators.* (2004).

[19] J. C. Goldschmidt *et al.*, *Increasing the efficiency of fluorescent concentrator systems*, Sol. Energy Mat. Sol. Cells, **93** (2009), 176-182.

[20] G. Gunzburger and H. Kim, *Existence of an optimal solution of a shape control problem for the stationary Navier-Stokes equations*, SIAM J. Control Optim., **36** (1998), 895-909.

[21] J. Haslinger and R. Mäkinen, *Introduction to Shape Optimization: Theory, Approximation, and Computation*, Society for Industrial and Applied Mathematics, 2003.

[22] M. Hinze *et al.*, *Optimization with PDE Constraints*, Mathematical Modeling: Theory and Applications (Vol. 23), Springer Science & Business Media, 2008.

[23] P. Kowalczewski, M. Liscidini, and L. Andreani, *Engineering Gaussian disorder at rough interfaces for light trapping in thin-film solar cells*, Opt. Lett., **37** (2012), 4868-4870.

[24] O. Kluth *et al.*, *Texture etched ZnO: Al coated glass substrates for silicon based thin film solar cells*, Thin Solid Films, **351** (1999), 247-253.

[25] J. Kiefer and J. Wolfowitz, *Stochastic Estimation of the Maximum of a Regression Function* Ann. Math. Statist. **3** (1952), 462-466.

[26] C. Lalau-Keraly, S. Bhargava, O. Miller, and E. Yablonovitch, *Adjoint shape optimization applied to electromagnetic design*, Opt. Exp., **21** (2013), 21693-21701.

[27] G. Lord, C. Powell, and T. Shardlow, *An Introduction to Computational Stochastic PDEs*, Cambridge University Press, 2014.

[28] G. J. Lord, C. E. Powell and T. Shardlow. *An Introduction to Computational Stochastic PDEs*. Cambridge University Press, (2014).

[29] O. P. Le Maitre and O. M. Knio. *Spectral Methods for Uncertainty Quantification With Applications to Computational Fluid Dynamics.* Scientific Computation. Springer, (2010).

[30] A.R. Manwell. *A uniqueness theorem for the moving medium reduced wave equation.* Applicable Analysis 12:3, (1981) pages 215-228.

[31] A. McEvoy et al., eds. *Practical Handbook of Photovoltaics: Fundamentals and Applications*, Elsevier, 2003.

[32] J. Müller, R. Bernd, J. Springer, and M. Vanecek, *TCO and light trapping in silicon thin film solar cells*, Solar Energy **77** (2004), 917-930.

[33] S. Nicolay *et al.*, *Control of LPCVD ZnO growth modes for improved light trapping in thin film silicon solar cells* Solar Energy Materials and Solar Cells, **95** (2011), 1031-1034.

[34] J. Nocedal and S. Wright, *Numerical Optimization* (Second edition), Springer New York, 2006.

[35] J. A. Ogilvy, *Theory of Wave Scattering from Random Rough Surfaces*, Adam Hilger, 1991.

[36] J. Poortmansand and V. Arkhipov, eds. *Thin film solar cells: fabrication, characterization and applications*, Vol. 5, John Wiley & Sons, 2006.

[37] R. Petit. *Electromagnetic Theory of Gratings. Springer*, (1980).

[38] C. Rockstuhl, et al., *Comparison and optimization of randomly textured surfaces in thin-film solar cells*, Opt. Exp., **18** (2010), A335-A341.

[39] C. Rockstuhl and F. Lederer, *Photon management by metallic nanodiscs in thin film solar cells*, Appl. Phys. Lett., **94** (2009), 213102.

[40] H. Robbins and S. Monro, *A Stochastic Approximation Method The Annals of Mathematical Statistics*, **22** (1951), 400-407.

[41] J. Sokolowski and J. P. Zolesio, *Introduction to Shape Optimization, Springer Berlin Heidelberg*, 1992.

[42] J. W. Strutt. *On the Dynamical Theory of Gratings.* Proceedings of the Royal Society of London. Series A, Containing Papers of a Mathematical and Physical Char- acter, vol. 79, no. 532, (1907), pp. 399-416.

[43] R.E.I. Schropp, *Nanostructured Materials for Solar Energy Conversion*, Solar Energy, **79**(2006): 131-166.

[44] X. Sheng, S. Johnson, J. Michel, and L. Kimerling, *Optimization-based design of surface textures for thin-film Si solar cells*, Opt. Exp., **19** (2011), A841-A850.

[45] E. Yablonovitch and G. Cody, *Intensity enhancement in textured optical sheets for solar cells*, IEEE Trans. Electron Devices, **29** (1982), 300-305.

[46] M. Zeman *et al.*, *Optical modeling of a-Si:H solar cells with rough interfaces: Effect of back contact and interface roughness*, J. Appl. Phys., **88** (2000), 6436-6443.